IN-SITU FABRICATION AND EVALUATION OF TI-6AL-4V META BIOMECHANISMS BASED ON SELECTIVE LASER MELTING

MARIA MORALIDOU
(4627644)
SUPERVISION
PROF. AMIR A. ZADPOOR
IR. ELINE (H.M.A.) KOLKEN
DR.IR. G. (GERWIN) SMIT

TU Delft

In-situ Fabrication and Evaluation of Ti-6Al-4V Meta-Biomechanisms based on Selective Laser Melting

Msc Thesis

by

Moralidou Maria

in partial fulfillment of the requirements for the degree of

Master of Science
Biomedical Engineering, Biomaterials and Tissue Biomechanics track at

,

to be defended publicly on Tuesday March 5, 2019 at 10:45 AM.

Student Number:	4627644
Supervisors:	Prof. Dr. Ir. A. Zadpoor
	Eline Kolken, ir. H.M.A.
	Dr.Ir. G. (Gerwin) Smit

March 1, 2019

Dedication

This thesis is dedicated to my parents Christos Moralidis and Eleni Ftaka as well my brother, George Moralidis and my aunt Maria Moralidou for their love, endless support and encouragement.

Abstract

Cavitary bone defects are common in orthopedic surgery and may be present after curettage of benign tumors or as tumor-like lesions. Bone graft substitutes, especially from biocompatible materials, can be used as a solution for filling up those defects. However, these cavitary bone defects differ in size and location. It would therefore be convenient to utilize an implant that can change its shape according to its surrounding 3D environment, meaning there is not need to customize the implant for every patient case.

In the last decade, additive manufacturing (AM) techniques have been the driving force behind the fabrication of complex three-dimensional objects. The various assets of these procedures enable the production of very complex designs with appropriate material properties. These materials that are engineered to exhibit certain properties are referred to as meta-materials. Functionalizing these materials on a nano-scale, to have certain biological or mass transport properties, brings us to a new class of materials better known as meta-biomaterials. In this regard, highly deformable implants with novel properties can be referred to as meta-biomechanisms, consisting of multiple interconnected joints.

The current research revolves around the direct fabrication of meta-biomechanisms using Selective Laser Melting (SLM). Subsequently, the general design recommendations and process constraints have been discussed briefly for the fabrication of mechanisms using SLM. In this regard, SLM poses an extra burden on the removal of supports especially for the vulnerable geometries and within the joints clearance.

Implementing a design approach, including both systematic and intuitive methods, was chosen as the main tool towards the accomplishment of the research aim. Consequently, new designs are proposed to minimize these undesirable events and the supports, with the subsequent challenge to obtain multi-joint mechanisms with increased Degrees of Freedom (DOF) and the least amount of supports. The first joints have been successfully printed, as well as meshes of multiple joints.

Surface Morphing Experiments were finally executed to classify them in terms of motion, taking into account the final application. According to the results, the majority of the proposed meta-biomechanisms approach well the reference acetabular model, with an absolute difference below 1, reassuring the possibility of the proposed meta-biomechanisms as potential implants in cavitary bone defects. Besides the evaluation in terms of mobility, the structures were mechanically tested to derive their behavior under compression loading. The force needed to induce a sharp break was lower than the average peak force reported in hip joints during daily activities. Subsequently, the experiments revealed that their mechanical strength depends on the fitting of the structures inside the acetabulum model. The bigger the gap between the structure and the acetabulum, the weaker the structure under compression loading. Overall, their scale and size should be optimized to sustain the average day-to-day forces joints are subjected to.

Contents

Acknowledgements

I would like to thank Professor Amir Zadpoor for his expert advice in this thesis project. Additionally, I really appreciate the assistance of Sander Leeflang, manager of the department lab. He helped me learning how to design efficiently parts that intend to be 3D-printed.
This project would be impossible without the support of the PH.D candidate, Eline Kolken. She was always there for me, answering my questions, guiding my work and learning me how to present my effort in a more academic way.
Moreover, I would like to express my many thanks to my friends Marianna Paresoglou, Victoria Mavrikopoulou, Su Guvenir, Liana Mitrakou and Virginia Casasnovas for their encouragement and endless support in this important and mutual step. Finally, I would like to thank my house mates Marianna Franco, Aya Mahgoub, Yamuna Sakthivel and Veronica Torri for their patience and their psychological help in this work.

Moralidou Maria,
Delft, March
2019

1. Introduction

Frequent pathogenic conditions encountered in orthopaedic surgery are cavitary bone defects, particularly in the pediatric patient population.[1,2] These are the result of benign tumours or relative injuries such as solitary and aneurysmal bone cysts as well as non-ossifying fibromas (Figure 1.1).[1] Current treatments include autologous bone grafts, with the sacrifice of considerable morbidity. Particularly, increased surgical and post-surgical time, as well 15.8-29.2% of complication rate (infection, hematoma, wound problems, fracture) are associated with them.[1,3] Allografts are also candidates for filling cavitary bone defects, without participating in the healing procedure though.[1,4] Additionally, they carry a high risk of disease transmission, being responsible for 1 out of 1.6 million 'viral transmission risk' cases.[3]

In response to the downsides of the above methods, bone substitutes from biocompatible materials gain popularity throughout the world. However, due to the poor osseointegration of orthopedic implants, they constitute a major concern in the biomedical field.[1] This is significant if one considers the 500.000 bone graft procedures that the United States perform each year, which cost around 1.5 billion dollars annually.[3]

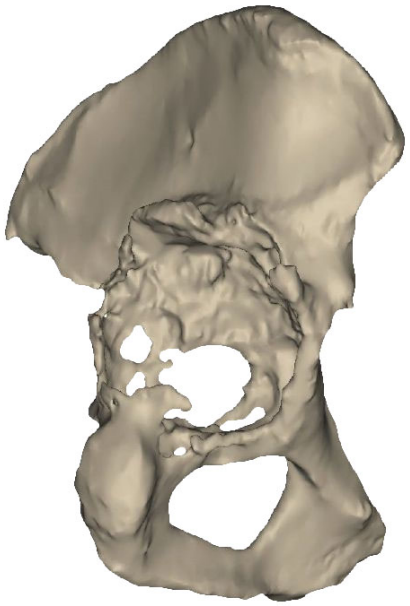

Figure 1.1: Illustrative demonstration of a massive bone defect.[1]

Sadly, massive bone defects usually vary in size and location, and this poses an additional burden to the fabrication of appropriate bone substitutes.[1] It would therefore be convenient to fill those bone defects with deformable bone substitutes that will enhance tissue regeneration. Moreover, they should

perform adequate structural integrity reassuring implant's longevity.

Among various types of materials, metals are preferable, due to their ability to sustain greater loads. A metal with good mechanical properties that can be further improved in terms of corrosion resistance and biocompatibility using post-processing techniques,[5] is Titanium (Ti), as well as its alloys.[5–7] Titanium alloys are also applicable in numerous structural implementations because they are characterized by a low density and a high strength to weight ratio.[8]

Even though material's selection meets the demands of biocompatibility and strength, manufacturing a bone substitute with motion remains a challenge. The materials used in the fabrication of bone graft substitutes can be engineered to exhibit novel mechanical properties. These materials are known as meta-materials or "designer" materials. Those that can be processed at a nano-scale, to have certain biological or mass transport properties, are referred to as meta-biomaterials. Meta-biomaterials are highly applicable in the medical field since they can be designed to stimulate tissue regeneration.[9,10]

In this regard, structures or meshes of metal joints, with mechanical properties not found in nature, can be referred to as Meta-Biomechanisms. These can form metallic structures with multiple Degrees of Freedom (DOF), which in their turn can enable the mobility of the implanted substitute.

Unfortunately, previous researches managed to print non-assembly joints with a limited range of motion, using other techniques rather than SLM. According to the literature, only 36% of reported efforts had to do with metals, whereas only 26% concerns SLM.

This research will revolve around the fabrication of non-assembly meshes of titanium joints with multiple DOF, using SLM. In this regard, design and process constraints of SLM will be analyzed to formulate the basic requirements of meta-biomechanisms. In addition, the final application will play a role to that, since increased range of motion is the key property. The basic goal of this study is designing metal meta-biomechanisms, which should:

- Include multiple joints, to form the so-called meshes of joints, that can behave like a metal clay.
- Be fabricated in-situ using SLM, without the presence of undesirable phenomena, such as supports.
- Present the ability of fitting to any irregular surface.

1.1 Background Information: "Direct Fabrication of Meta-Biomechanisms"

It is widely known, that over the last ten years, "freeform" fabrication procedures emerged to change the design procedure and the engineer's perspectives.[11–13] Additive Manufacturing (AM) techniques, a technical term attributed to the above procedures, is an economically feasible technique, with many assets. These include the absence of tools, uncomplicated file storage and the possibility to manufacture any design feature with geometrical complexities.[14,15]

Apart from the design freedom that 3D-Printing provides, it also enables the direct fabrication of multi-joint mechanisms or structures. It is therefore possible to directly print such a complex mesh of metal joints, since integrated parts can be fabricated effectively as fully functional assemblies.[16–18] In this regard, the designer has the ability to rapidly evaluate the final product and verify this with the customers.[19] This is extremely beneficial for the fabrication of mechanisms, and specifically non-assembly mechanisms, due to the potential assessment of uncertain configurations at any stage of the process.[20]

In contrast to the conventional procedures, in which each part of a multi-link system is independently manufactured and subsequently assembled, in-situ fabrication emerged to simplify the process and make it cost and time effective.[21] According to its description, in-situ fabrication is *the direct fabrication of 3D structures with distinct mating parts without requiring assembly.*[20] The parts are designed separately and then assembled digitally, in order to form the CAD file that is going to guide the printing procedure.[21] These structures are also known as non-assembly mechanisms and AM techniques are capable of producing multi-articulated systems in-situ.[22]

The designer can visualize and define the interference between parts or between parts and their environment. Furthermore, the designer is capable of acknowledging the joints DOF and integrate virtual control or actuating systems to understand the mechanisms kinematic behavior.[23] Consequently, through the elimination of mistakes and optimization of the procedure, non-assembled mechanisms can be fabricated in-situ. However, in-situ fabrication involves some issues like the determination of joint-clearance, definition of fabrication-direction, optimization of supports and the removal of them and residual material after printing.[22]

1.1.1 Constraints and Restrictions

SLM: A competitive procedure in Direct Fabrication of Metal Parts

Selective laser melting (SLM) is the most advantageous technology compared with other RP techniques in manufacturing of metallic products with certain mechanical properties.[16,20,21,24,25,27] SLM belongs to the group of Powder Bed Fusion (PBF) processes, in which a roller spreads the powder over a build-plate inside a gas-controlled chamber. The metallic powder is selectively consolidated by a laser source. Guided by an STL file, which slices the initial CAD model into layers, the laser builds the part layer by layer.[16] The STL file includes the slices, each of them containing a cross-section of the part. The distance between the consecutive slices is known as the layer thickness.[17] The substrate goes down a layer thickness and a newly formed layer is distributed by the roller. The machine performs the above steps iteratively to completely print the part.[16] An illustrative demonstration of the Selective Laser Melting process has been depicted in Figure 1.2.

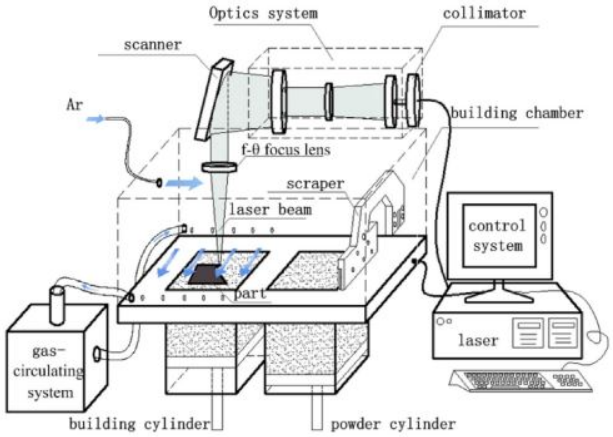

Figure 1.2: Illustrative demonstration of the Selective Laser Melting process.[34]

The binding mechanism of SLM is full melting, explaining the capability of SLM to produce metal end-use parts.[27,28] In addition, metal end-use parts with densities as high as 99.8% can be manufactured with the appropriate optimization of process parameters.[7,29–31] Thus, the designer can tune the process parameters to achieve fine mechanical properties. The aim of producing fully dense metal-based parts with fine metallurgical bonding, creates quite some challenges though.[16,16,20,24,25,27]

Process Constraints of SLM

SLM is a very complicated procedure where a lot of process parameters, as well as pre-fabrication procedures, considerably affect the final properties of the part. One way to achieve great functionality and optimized mechanical, physical and structural properties is to organize the printing procedure by taking into consideration the potential unfavourable events that may take place. This allows the engineer to optimize his design and bypass doubtful process constraints.[14]

The quality of a part fabricated with SLM is strongly influenced by the condition of each single layer.[30] Therefore, careful selection of the process parameters can minimize the clearance size, improve the anisotropic mechanical properties[32] and optimize the printing procedure.[33,34,64] Generally, there are more than 120 factors that influence the quality of the final mechanism.[18]

Energy density, layer thickness and laser power can be regarded as the most crucial factors, since they directly affect the performance of the process.[35] Layer thickness is essential, because connectivity among layers can only be achieved if the previous deposited layers are remolten too.[64] However, energy density is the most important factor depending on the rest of them. As the laser selectively irradiates the loose powder, this energy is transformed into heat. This energy is transmitted to the powder and the surrounding region, since the temperature of the laser is well above the melting point of the material.[35,36] That is why the energy density is directly dependent on the scanning speed and laser power.

Specifically, it is reduced when the velocity is raised, or the power is decreased.[35] A higher laser energy makes sure the laser beam can deeply penetrate into the material and hence this results in better melting of consecutive layers. However, when the laser power exceeds a certain threshold value, it may result in undesirable defects, like increased hardness.[34,65] On the other hand, low laser power has been proven insufficient to melt the metal powder and that may give rise to abominable events like balling (surface tension divides the melting vector into distinct droplets) due to the bad wettability.[34] The balling phenomenon constitutes a severe impediment on the inter-layer connection and

gives further rise to the parts surface roughness.[30,37,64]

The material's heat absorption strongly depends on its nature, because powder conducts heat at a lower rate compared to the bulk material.[34,36,38] This is because the powders absorptivity is influenced not only by its physicochemical properties but also by its granulomorphometry and density.[38] What can be retrieved from the above mentioned, is that more energy will be transferred to the powder rather than to the solid part, which directs the molten powder to stick to the melt pool due to the capillary and gravity forces.[34,36] That is what is happening around the corners of the parts, and is better known as dross formation, which especially affects the quality of the downward surfaces.[20,24,39] These surfaces are affected, because they are fabricated against gravity, and this drives them to decline from their original dimensional site.[17]

Something that does not affect the down-ward surfaces, but has a great influence on the upper ones, is warping. The main cause of warping is the heat applied at the upper region of the part. During rapid cooling the temperature gradient is steeper for the upper regions compared to the lower layers, leading to the tendency to deform upwards.[40,64]

SLM is, therefore, a procedure that is accompanied by apparent thermal gradients which induce thermal stresses in the fabricated part.[30,41] When these thermal stresses are well above the material's strength, plastic deformation of the upper part affects its functionality.[20,24] Steep thermal gradients also lead to curling or delamination of the part and possible disconnection of the part from the build plate. Afterwards, rapid cooling occurs, and the plastically deformed surfaces begin to shrink. Scanning strategies have a strong influence on the formation of stresses, that is why proper selection of a scanning strategy is of great importance.[25] Inter layer scanning strategies or scanning along the x direction have been proven beneficial for the reduction of thermal stresses. Furthermore, partitioning of the scanning zone into smaller zones can even further reduce the residual stresses.[26]

Taking the above into account, SLM is a very complicated procedure and the engineer should consider various factors for its successful implementation. A proper pre-selection of process parameters is therefore judged essential for the absence of unfavourable events.[42,64]

Clearance: An essential feature of Non-Assembly Mechanisms

Ideally, joints within the mechanisms do not have clearance between their coupling mates. However, mechanical joints include a small gap that distinguishes the structural members of the mechanism.[43,44] For instance, the clearance of a simple pin joint that includes one journal inside a bearing, can be illustrated in Figure 3 where Rj refers to the journal and Rb to the bearing.[23]

The clearance constitutes a significant obstacle during the fabrication of non-assembly mechanisms with AM processes. The main concerns associated with the clearance are its need to be supported and the tendency of trapped powder to remain stuck inside. The latter affects the surface quality of the clearance which in turn affects the mobility of the mechanism.[21,45] Consequently, the most essential feature that should be taken into account before, during and after the printing is the clearance, since it has a strong influence on the kinematic response of the mechanical joints.[43]

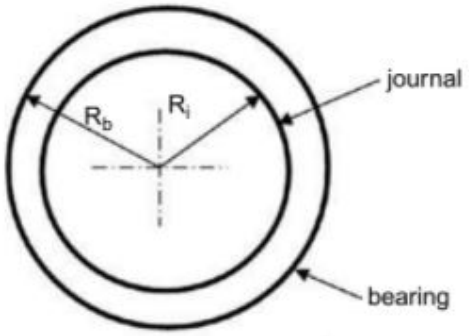

Figure 1.3: Illustration of the clearance inside a revolute joint.

Supports: A significant impediment during the printing of Metal Meta-Biomechanisms with SLM

Most mechanisms include overhang structures and their presence usually leads to undesirable effects. Overhanging regions (geometrical features in need of supports), are holes, internal channels, thin structures like clearance and round surfaces like fillets or chamfers.[46] **The well-known general rule regarding SLM is that downward surfaces at an angle less than 45 degrees, are in need of supports.[16,29,35]**

The negative thing about support structures is the increased fabrication time and the complexity of the part and the overall procedure.[29] Although many techniques exist to remove support structures and residual material (sand-blasting, machining, etching, electro-polishing and plasma spraying) the quality of the part is often harmed. Taking into consideration the joint's clearance, removing the supports can be a very challenging procedure.[20] Additionally, supports influence the mechanical and physical properties of the final part and in case of joints, they strongly influence their mobility. Moreover, the use of these post-processing techniques is time consuming and not always applicable.

The proper orientation of the mechanism inside the build chamber can also reduce time, minimize the number of supports and enhance the mechanism's strength.[20,47] The orientation of the part can be defined as the rotation of the part inside the build box around the axes of the machine's coordinate system.[14] For example, positioning the part's hole parallel to the fabrication direction has been shown to lead to a stronger outcome. It is favourable to position a part along the vertical direction, but in that way the height of the part may increase the fabrication time.[35] A tilted configuration may constitute an efficient way to reduce the amount of support structures in that case. However, this method gives rise to an undesirable phenomenon known as the staircase effect.[16,35] Based on the above, positioning properly the part seems to be more complicated that it sounds.

It is therefore important to find other ways to reduce the number of support structures.[48] Despite the fact that supports can be reduced with the right orientation or alteration of the process parameters, it is favourable, though challenging, to modify the design of the parts.[20] Design optimization is therefore used towards the supports' elimination of metal meta-biomechanisms manufactured with SLM.

1.2 Study Aim

Taking into account the above, the aim of this research is to **directly** print **meshes** of titanium joints with **SLM**, the so-called **meta-biomechanisms**, followed by a **certain (>1)** amount of **DOF** and no **supports** within the **clearance**.

According to the background information, **direct** fabrication of joints, especially using SLM, poses an additional obstacle. The gap separating them is usually in need of **supports**, which are not always accessible. Additionally, they strongly influence the functionality of the joints. Achieving **no supports** within the joint's clearance of the mechanism, is the first goal. Implementing a combination of both systematic and intuitive design methods, used as the approach, to minimize their supports and ease their fabrication. Particularly, new designs of joints were conceived and subsequently modified to eliminate the design and process constraints.

Additionally, since these structures intend to take the role of highly deformable implants (**meta-biomechanisms**), they should demonstrate a sufficient **range of motion**. In this regard, the design should also be modified to increase the DOF.

Generally, this study proposes new designs of **meta-biomechanisms**. To define the possibilities of these structures as **meta biomechanisms**, evaluation and classification of their motion and mechanical properties will follow.

1.3 Design Criteria

Based on the above, the proposed meta-biomechanisms were conceived according to certain design criteria. The role of the supports has already been analysed, as well as the importance of an increased range of motion (DOF). However, the kind of motion plays an important role, since movements of twisting and turning are preferable to sliding ones. This is why high deformability can be achieved by rotational DOF rather than translational. One major characteristic that determines the final outcome is the incorporation of an individual joint in a multi-joint configuration. This can be explained, by the fact that a joint with multiple rotational DOF could meet the requirement of motion, with no possibilities of being incorporated in a structure though. These criteria assisted the design procedure and determined to a certain level the final evaluation of the proposed Meta Biomechanisms. Below, they have been ordered according to their importance, along with the respective requirements and wishes.

1. Amount of Supports
Rationale: The amount of supports should be minimized, especially around the clearance site. Otherwise, the printed design will not have functionality, because the supports will prevent its mobility.
Quantification: The amount of the supports will be measured in terms of supported area (m^2). This will be held out in Solidworks.
Requirements:
1. The structure should not have supports inside the clearance, to ensure its functional mobility.
Wishes:
1. The structure should include only the supports that ensure its structural integrity.

2. DOF

Rationale: The design should present the ability of fitting to any irregular surface.
Quantification: This motion will be defined in terms of DOF.
Requirements:
1. The structure should perform at least one movement (e.g. sliding, rotational).
Wishes:
1. It would be preferable for the meta-biomechanism to present a wide range of motion. This is translated to more than two DOF.

4. Type of DOF

Rationale: The intended area of implantation will be irregular in terms of shape and size. Consequently, the design should preferably perform movements like twisting and turning.
Quantification: The degrees of freedom will be determined (e.g. translational or rotational). The DOF of a joint, are equal to the number of motions that are performed. A joint can move rotationally or translationally around three axes. That is equal to six DOF. For instance, a joint that allows a rotational movement around two axes, has two DOF.
Requirements:
1.The design should perform at least one translational or rotational motion.
Wishes:
1. Greater motion can be achieved, if the structure performs both rotational and translational motions.

1.4 Performance Criteria

Design criteria assisted the conception of new designs. The proposed designs will be subsequently evaluated according to these using a Harri's Profile. Instead of selecting which of these designs is the best, further evaluation of all of them will follow, according to certain performance criteria. Below, they have been ordered according to their importance, along with the respective requirements and wishes.

1. Fitting to an irregular bone surface.

Rationale: The proposed designs are intended to fill irregular bone defects. Thus, they should change their shape and volume according to the intended area.
Quantification: The models will be positioned on an acetabular surface and Surface Morphing Experiments will measure their fitting. This will be done, by measuring the mean absolute difference of their distinct points.
Requirements:
1. The structure should follow the mean shape of the concave bone model (Absolute Difference below one).
Wishes:
1. The structure should fit perfectly each point of the bone model (Absolute Difference equal to zero).

1. Break Strength

Rationale: The proposed designs intend to fill irregular bone defects. An acetabular defect is used as an example. Thus, they should be strong enough to sustain loads acting on the human hip joint during activities, like walking and standing.
Quantification: The models will be mechanically tested and their break force will be measured.

Requirements:
1. The force needed to break the structure should not be lower than the average peak contact force of a hip joint during standing (1.5kN) .[49]
Wishes:
1. The force needed to break the structure should not be lower than the maximum peak contact force of a hip joint during walking (3.9kN).[49]

1.5 Study Approach

The first step in fabricating meshes of joints in-situ, is to successfully fabricate a single joint. Unfortunately, reported literature around the in-situ fabrication of metal joints is significantly limited. Thus, new designs of joints are essential. Brain-storming is always preferable, to find innovative design solutions towards a problem. Systematic approaches though, help this path, by establishing steps to easily find new concept solutions. Generally, all the design approaches start with the design solutions and end with the selection of the best one. This research though, does not aim the finding of the best concept solution, but as many as possible new concepts that will be finally evaluated.

In this research we therefore started with some well-known design methods, while we later combined intuitive methods to achieve innovative solutions. One well-known, systematic design approach is the ACRREx method. The first step used in this method, is the categorization of existed knowledge to find research gaps. After the categorization of the design object database, the fundamental differences between its categories are pointed out. Then, these categorizations lead to new design solutions.[50]

The mechanical joint constitutes the design object database in the current research. For this reason, already existed mechanical joints were categorized to find out the research gaps. In this regard, mechanical joints that have been already studied, are excluded from the research (revolute joint). Afterwards, the remained mechanical joints were categorized and their fundamental differences in terms of DOF are pointed out. Table 1.1 depicts how the reported joints, including the Prismatic and the Ball-socket joint, are categorized based on their differences. Implementation of the ACCREx method, results in the following assumptions: Can a Prismatic joint with 3 rotational DOF be manufactured? This type of questions filled the gaps in the above categorization. Table 1.2 includes the answers to all the possible assumptions. The designs, which were successfully conceived, along with the reported ones, were modified according to the general design rule of 45°. Their design constraints in terms of printing were analytically addressed and modifications were held out through brainstorming.[51]

Table 1.1: Implementation of the ACCREx Method. Categorization of reported mechanical joints results in triggering ideas for new designs of joints.

Mechanical Joints			
	1 DOF	2 DOF	3 DOF
Translational Motion	Prismatic Joint	?	?
Rotational Motion	?	?	Ball-Socket Joint

New designs were indeed proposed and their incorporation in a multi-joint configuration followed. Their incorporation demanded further modification. This resulted in the design and fabrication of new

meta-biomechanisms, which were evaluated according to the exported criteria. The following diagram depicts schematically the steps followed in this study.

Table 1.2: Implementation of the ACCREx Method. The reported mechanical joints were categorized in terms of number and type of DOF. New concept ideas filled the gaps.
** The Prismatic Joint has 1 translational DOF and the Ball-Socket Joint 3 rotational DOF*

Mechanical Joints			
	1 DOF	2 DOF	3 DOF
Translational Motion	Prismatic Joint Ball-Socket with 1 translational DOF	Prismatic Joint with 2 translational DOF Ball-Socket with 2 translational DOF	Prismatic Joint with 3 translational DOF Ball-Socket Joint with 3 translational DOF
Rotational Motion	Prismatic Joint with 1 rotational DOF Ball-Socket Joint with 1 rotational DOF	Prismatic Joint with with 2 rotational DOF Ball-Socket 2 rotational DOF	Slider with 3 rotational DOF Ball-Socket Joint

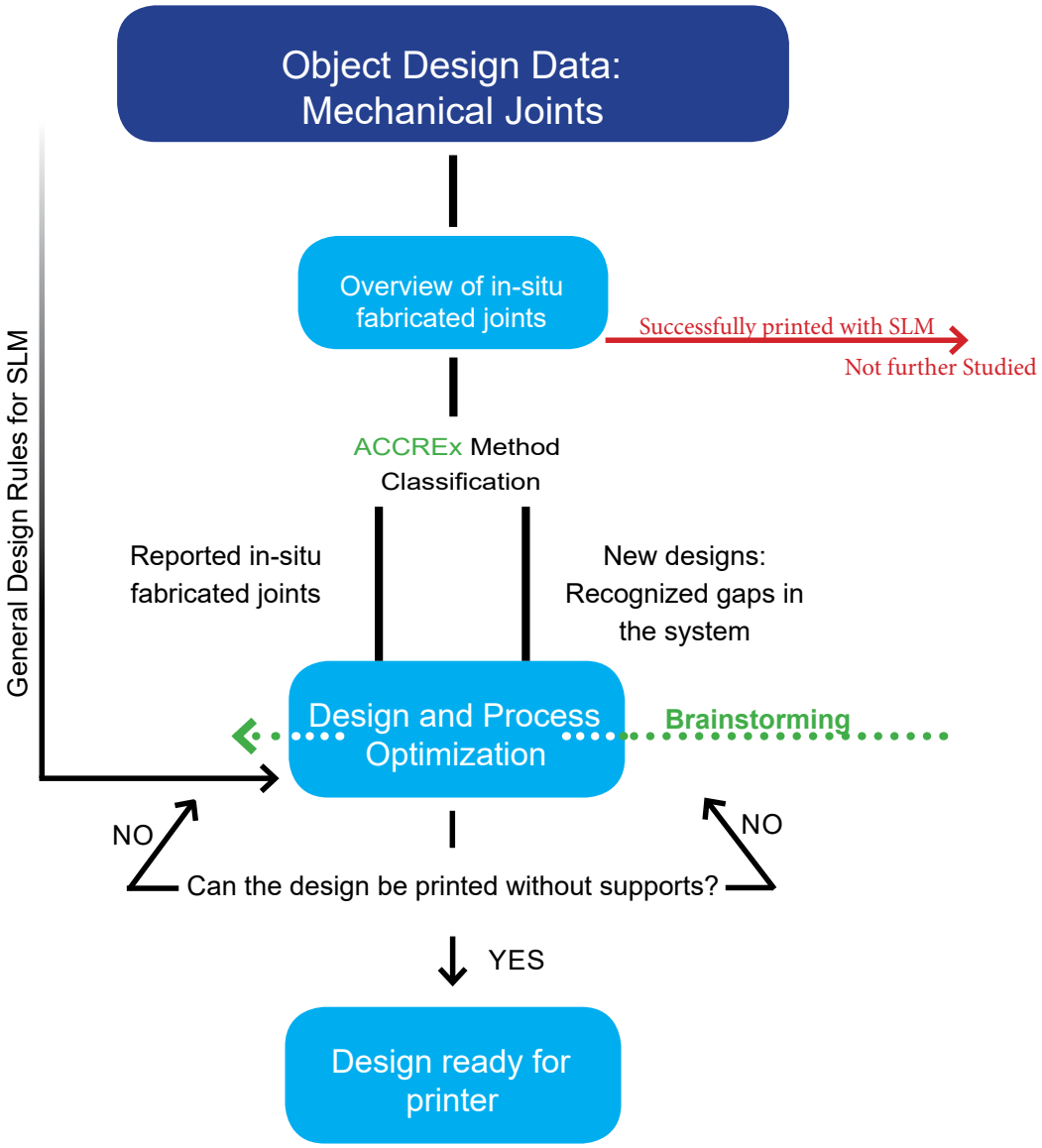

Figure 1.4: Schematic illustration of the design approach followed in this study.

Materials and Methods

2.1 Design

2.1.1 Design of Non-Assembly Joints

The first step in fabricating non-assembly mechanisms with AM processes, is to successfully fabricate individual joints. Thus, all the reported mechanical joints were registered and research around their in-situ fabrication with SLM was held out. There are three types of mechanical joints, including the revolute joint, the prismatic and the ball-socket joint. Based on the reported literature, revolute joints with one DOF have already been printed with SLM. This is why only a small printing example was held out, to examine the potential of printing it in situ. However, other joints like prismatic, have been printed only with other polymer-based techniques. Consequently, these types of joints were chosen as the research object. The chosen mechanical joints were categorized in terms of number and types of DOF. The implementation of the ACCREx method was subsequently implemented and new designs have been found. Table 2.1 includes how the reported mechanical joints (highlighted in red colour) categorized in terms of number and types of DOF and what are the concept solutions filling the research gaps. Among these, the ones highlighted with green colour were successfully conceived. Taking into account the aim of this research, which is to minimize the supports, the concept ideas of the selected joints were modified accordingly. This section studies the design constraints of each joint and proposes solutions for its direct printing using SLM. All the intermediate, design steps are registered, to assist the reader in understanding the reasoning behind the upcoming design modifications.

Table 2.1: Implementation of ACCREx Method. The reported mechanical joints were categorized in terms of number and type of DOF. New concept ideas filled the gaps.
** The Prismatic Joint has 1 translational DOF and the Ball-Socket Joint 3 rotational DOF*

Mechanical Joints	1 DOF	2 DOF	3 DOF
Translational Motion	Prismatic Joint	Prismatic Joint with 2 translational DOF	Prismatic Joint with 3 translational DOF
	Ball-Socket with 1 translational DOF	Ball-Socket with 2 translational DOF	Ball-Socket Joint with 3 translational DOF
Rotational Motion	Prismatic Joint with 1 rotational DOF	Prismatic Joint with with 2 rotational DOF	Prismatic Joint with 3 rotational DOF
	Ball-Socket Joint with 1 rotational DOF	Ball-Socket 2 rotational DOF	Ball-Socket Joint

Revolute Joints

Revolute joints constitute the most common type of joints and they only have one rotational DOF.[52] There are various known configurations, but the most representative has been shown in Figure 2.1a. This one includes two rings with a stem attached where a pin, which constitutes the axis of revolution, passes through the center of the rings.[53] The non-assembly fabrication of a revolute joint with SLM is feasible but under studied conditions. Yang *et al.*(2011), managed to print a non-assembly revolute joint using a vertical orientation. This orientation was preferred to reduce the number of support structures.[35] For a better comprehension of the above procedure, a preliminary effort took place to examine the potential of directly fabricating a Ti-6Al-4V revolute joint with SLM in this specific build orientation.The clearance chosen was 0.3mm and the detailed dimensions of both the designs can be found in Appendix B.

However, the bending phenomenon was demonstrated along the length of the bars. It is already mentioned, that SLM is characterized by apparent thermal stresses, which lead the upper region of the part to deform upwards. These thermal stresses acting upon the part, are proportional to the cross-section area and the length of the part.[54] One potential solution would, therefore, be to reduce the surface area and the length of the rings, by redesigning them in the form of diamonds (Figure 2.1b).

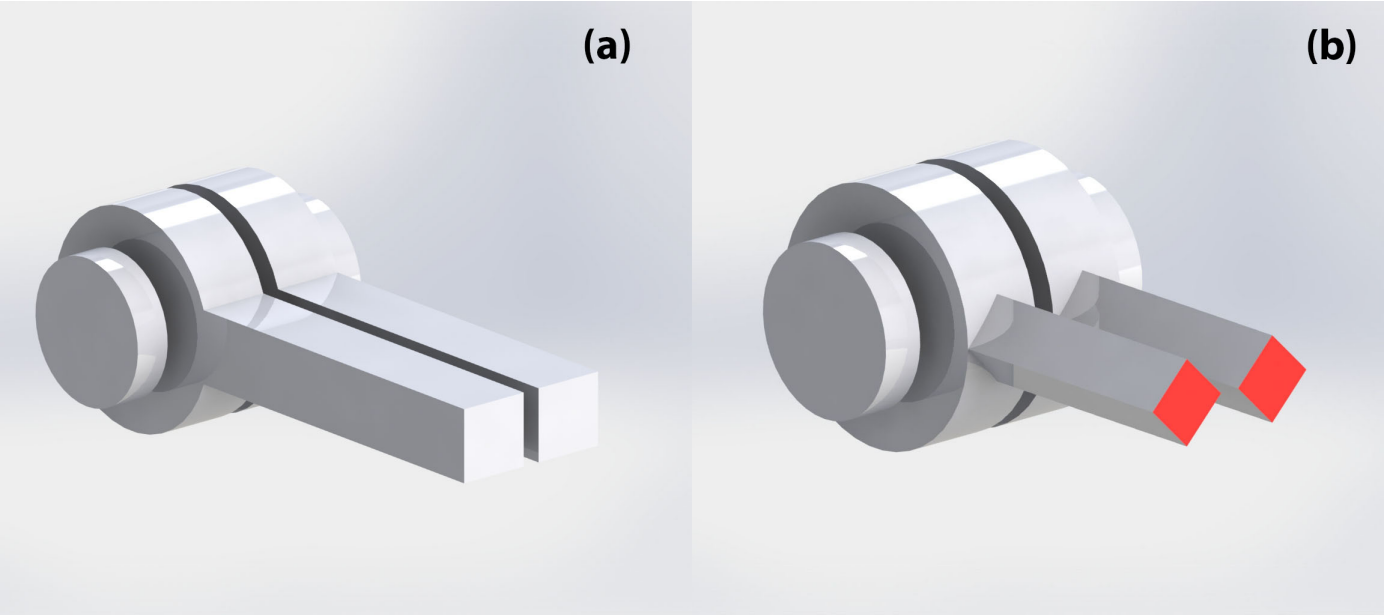

Figure 2.1: Illustration of a revolute joint with two rings and one pin (a) and a modified revolute joint with minimized surface area and ring length to prevent upwards bending (b).

Prismatic Joints

The prismatic joint, also known as a slider, provides a sliding movement between the mating surfaces of two different parts without allowing rotation. A prismatic joint may often be designed as a piston inside a cylinder, but that is not possible through a non-assembly fabrication.[55] Mavroidis et al.(2000) proposed a different design, which is depicted in Figure 2.2a. The new joint allows a sliding movement between the different parts and the rectangular shape of the parts avoids potential problems caused by the approximation of curved surfaces.[55] Due to the shape and the design of the prismatic joint, the possibility of fabricating it with SLM, seems feasible compared to other types of joints. However,

reducing the amount of supports and reaching sufficient clearance for powder removal, is still demanding. One potential modification would be the transformation of sharp vertical edges to inclined ones at an angle of 45^o(Figure 2.2b). The above designs were created according to the dimensions used in Mavroidis′ research.[55] These can be found in Appendix B.

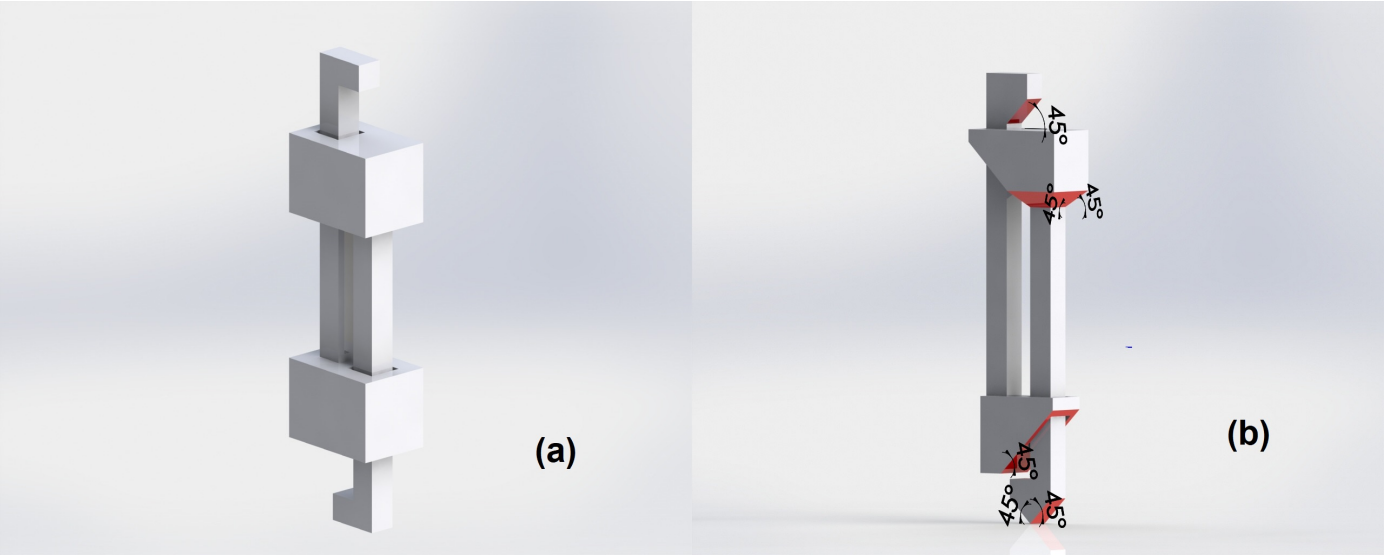

Figure 2.2: Illustration of a prismatic joint (a) and of a modified prismatic joint with inclined edges at an angle of 45^o (b).

Ball-Socket Joints

Another type of mechanical joint, the well-known ball-socket joint, has numerous advantages (Figure 2.3a). Its spherical appearance provides a wide range of motion with 3 DOF, which may even be adjusted by creating a socket opening which is modified acquisitively (red region in Figure 2.3b). Apart from openings in the socket, the ball may also be further cut to facilitate the removal of supports. These feasible modifications provide adequate design freedom to successfully build this joint in-situ, without compromising its wide range of motion.[56]

Mavroidis *et al.*(2000) managed to fabricate ball-socket joints with SLS by orienting them in a vertical configuration. In this case the neck is printed first, after which the socket part follows. This way, the neck takes over the role of support and the in-situ fabrication can be successful. The same configuration has also been used the other way around, with the ball-socket joint built first and the neck last. To support the joint, an opening at the bottom of the socket was created (red region in Figure 2.3c). These designs were also created according to the dimensions used in Mavroidis' research. Appendix B includes detailed dimensions of them.[53]

Cali *et al.*(2012) proposed a different design for the ball-socket joint in order to enhance removal of trapped material and add a lock configuration (Figure 2.3d).[56] The modified ball-socket joint offers space for the removal of excess powder. The printed position is proposed with the bands inside the cavities (Figure 2.4a) while during the joints motion, the bands slide across the socket surface (Figure 2.4b).[56]

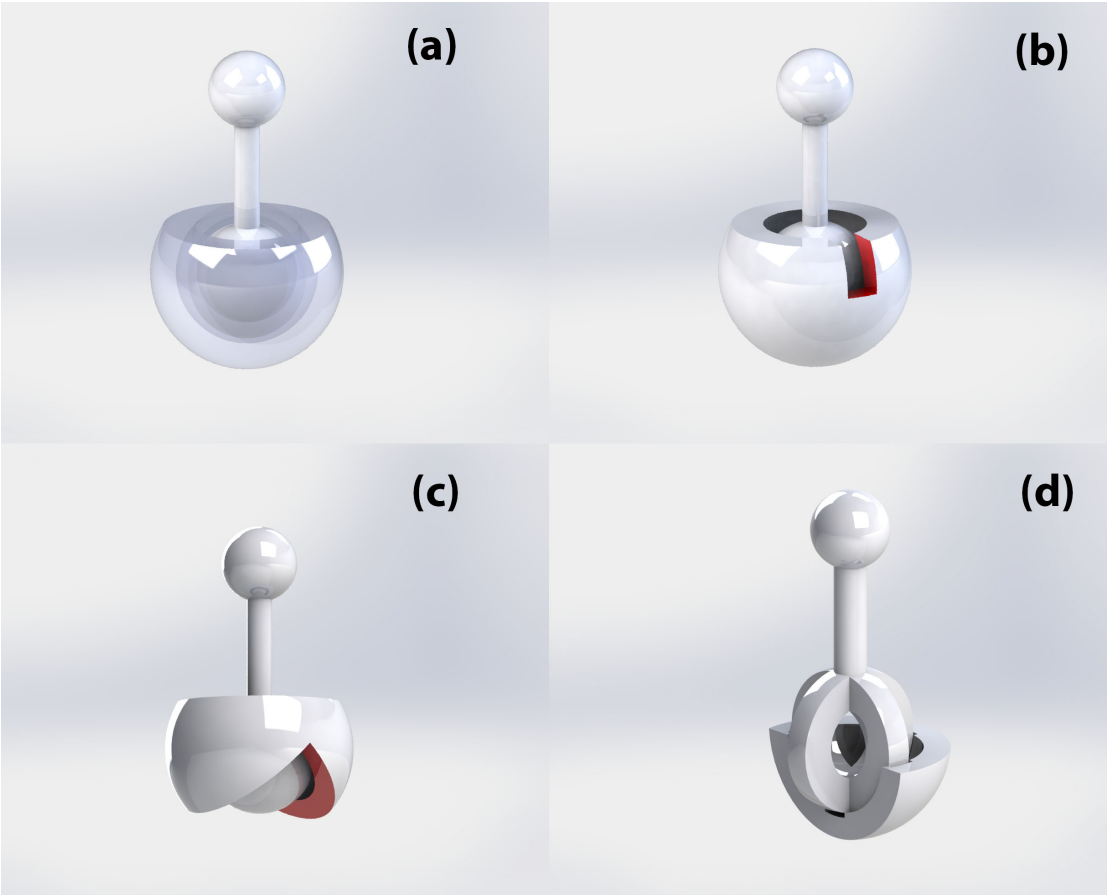

Figure 2.3: (a) Illustration of a regular ball-socket joint, (b) Illustration of a regular ball-socket joint with incorporated opening, to achieve increased range of revolute motion around 1 axis, (c) Illustration of a regular ball-socket joint, with incorporated bottom opening in socket, to support the joint,[53] (d) Illustration of modified ball-socket joint with cavities. The socket is cut in two different planes, for an easier illustration.[56]

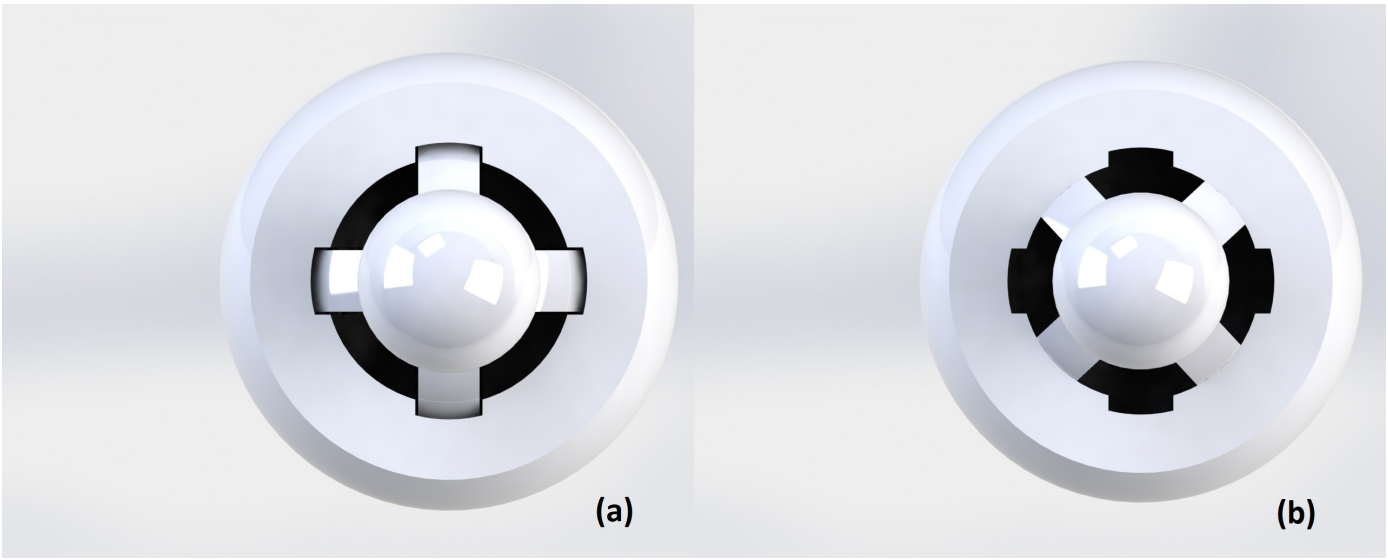

Figure 2.4: Printing position of the ball-socket joint with cavities. The bands are printed enclosed by the respective cavities. (a) After moving the joint. (b)[56]

Li *et al.*(2017) proposed another modified ball-socket joint for its successful in-situ fabrication. This modified ball-socket joint has, instead of bands, a lattice structure for efficient removal of trapped powder. The ridges are present to provide a lock configuration. Figure 2.5 illustrates the subsequent steps that a ball-socket joint should undergo to reach the proposed modified design.[57]

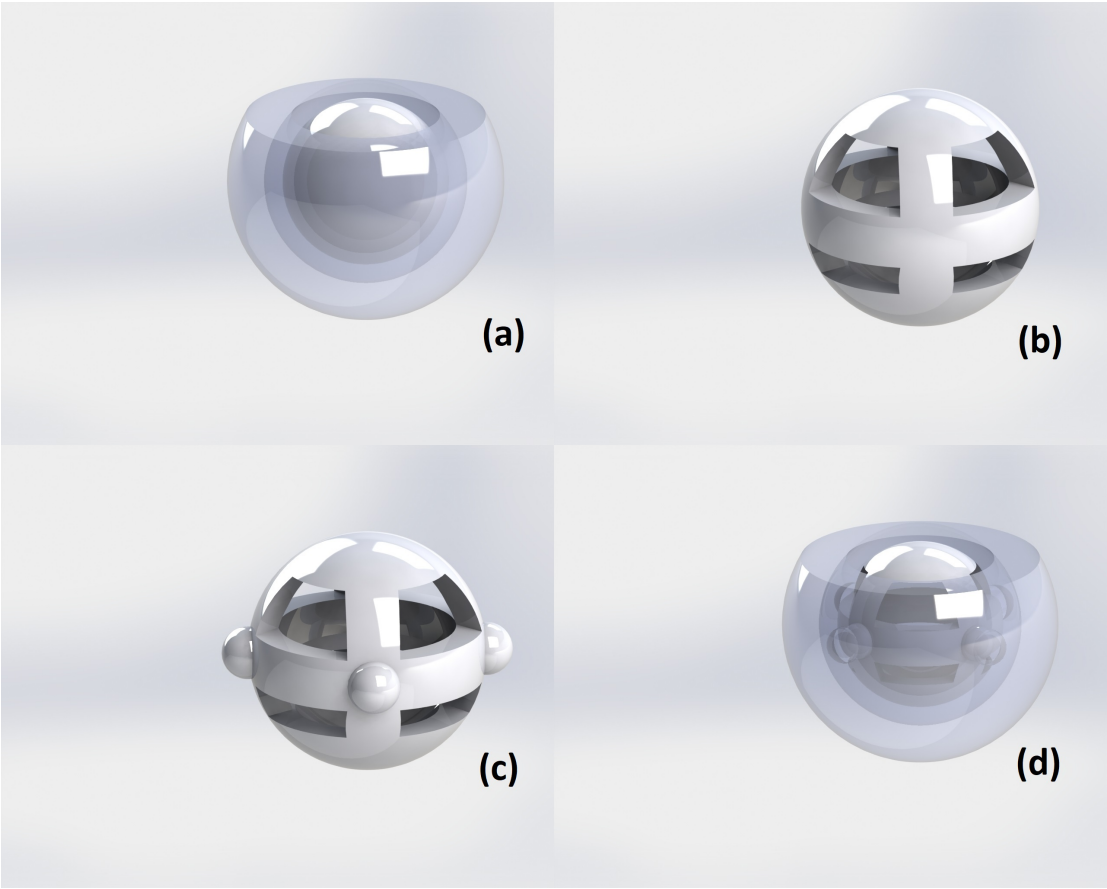

Figure 2.5: (a) Regular ball-socket joint, (b) Lattice structure incorporated in the ball, (c) Ridges added to the ball, (d) Final result.[57]

Despite the fact that these modified joints are optimal designs for a successful in-situ fabrication, they were manufactured with SLS or Objet machines and not with SLM. The great need for supports makes the fabrication of ball-socket joints using SLM troublesome. Many modifications will therefore be necessary to investigate the direct fabrication of ball-socket joints with SLM.

One concept idea of the design approach, was a ball-socket joint with 1 or 2 rotational DOF. The printing complexity of spherical joints with SLM is reduced by eliminating the DOF. The ball-socket joint proposed by Cali, has the possibility to be transformed to a revolute joint (1 DOF), if two planes vertical to the axis of rotation are formed (Figure 2.6a). In the case of a vertical configuration, the existence of these planes immediately eliminates the number of supports around this region. Furthermore, the range of rotation can be adjusted by creating slots in the socket(Figure 2.3b).[57]

However, printing the above configuration with SLM encounters two problems. The first one is the opened regions of the ball, since they constitute overhangs and will be in need of supports (pink regions in Figure 2.6a). The solution is to remove specific parts of the ball, but keep it solid. The removed parts are similar to the ones removed in the ball of Figure 2.3c and the design of such a

ball has been depicted in Figure 2.6b. The pink regions depict the removed parts, whereas the green regions depict the cutting planes vertical to the axes of rotation. Thus, the absence of opened areas directly eliminates the need for supports.

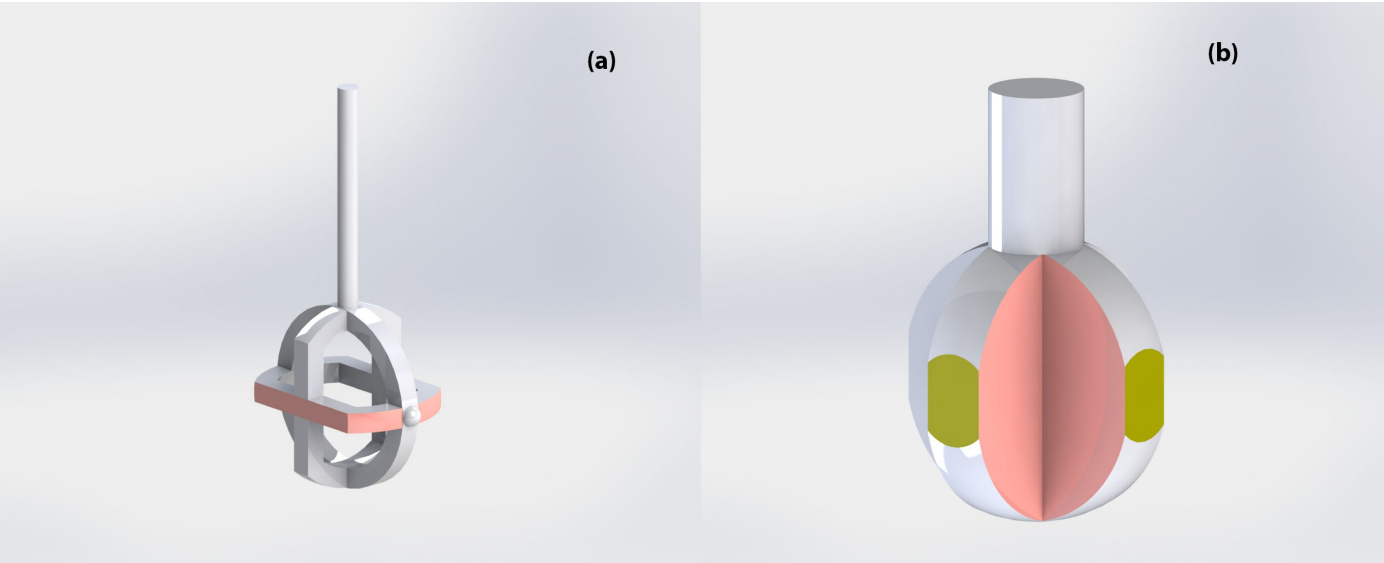

Figure 2.6: (a) Illustration of a modified ball-socket joint that inherits the role of a revolute joint,[57] (b) Illustration of the proposed ball for elimination of overhangs.

The second problem is the spherical shape of the socket. This creates the need for both external and internal supports. What Mavroidis *et al.* (2000) proposed regarding the opening at the bottom part of the socket, is regarded an interesting improvement towards the elimination of external supports. The bottom opening can be designed in a way of creating an angle of 45° with the built-plate. However, the bottom opening should not allow the ball to leave the socket. This is why, its height from the upper ball's plane is of great importance. The threshold of this height is 3.5mm, since this height lets the ball to be outside of the socket. Generally, it should be :

Height of Bottom Opening from the Upper cut plane= (Socket's External Diameter/2) - x

** x= Height of the upper opening=1.5*

To reassure a ball enclosed by a socket, the clearance reduced to 0.5mm (ball's diameter of 10mm) and the height was defined 4.55mm. The reason is, that this height along with a smaller clearance, creates a sufficient overlap of 22% (1.23mm) between the ball and the socket (Figure 2.7a). Figure 2.7b depicts detailed dimensions of the proposed socket's design. Furthermore, incorporating an upper opening in the socket's design, where the tangent of the ball's internal sphere creates an angle of 45° with the built plate, makes the socket internally self-supporting (dot lines in Figure 2.7b). The overall range of motion of the ball inside the socket is 120°. The range of the revolute motion can be further increased with incorporated slots to 180°.

The entire proposed assembly of both the ball and the socket has been depicted in Figure 2.7c in its printing position. Despite the fact that the ball and the socket are concentric, the ball is placed downwards to a point, where a greater surface area is exposed from the bottom opening. Thus, only the external socket and the exposed bottom part of the ball will be in need of supports, where they can be removed fairly easily (pink region of Figure 2.7c).

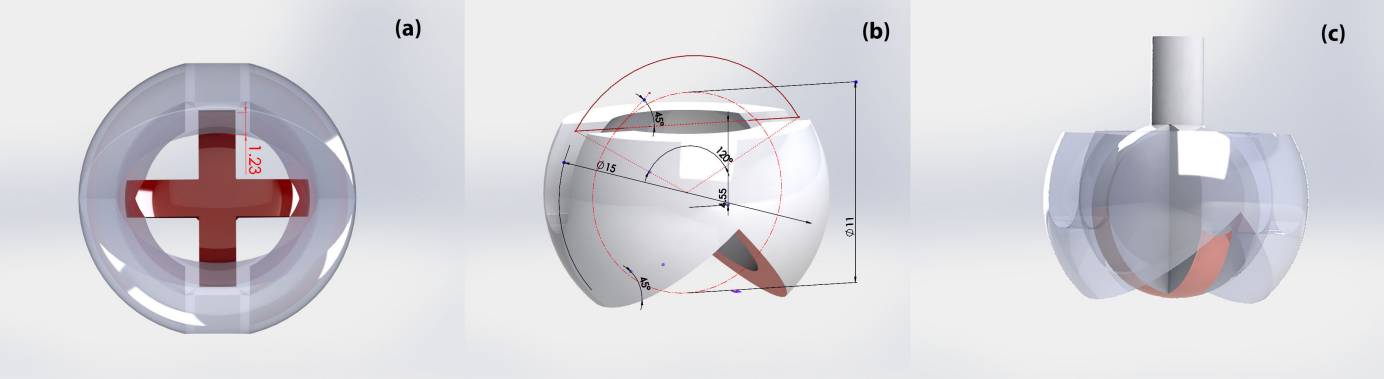

Figure 2.7: (a) Dimensional depiction of the overlap between the ball and the socket, (b) Descriptive depiction of socket's angular relationships, c) Illustration of the proposed ball-socket assembly.

Despite the fact that supports can be removed since they are exposed, the socket still needs to be supported externally due to its spherical shape. This problem can be resolved by modifying the external shape of the socket, while keeping the internal one spherical. Thus, the external shape of this socket can be modified, according to the aforementioned design rules, to also be externally self-supporting. A modification like this has been depicted in Figure 2.8a.

The above proposition for an externally non-spherical socket is suitable, for a self-supporting ball-socket joint manufactured using SLM. However, it is regarded favourable to keep the socket's shape as spherical as possible, for aesthetic reasons.[56] This seems impossible with a metal-based technique. The common ball-socket joint would be printed using SLM, with its bottom hemisphere only externally supported. This is why, the upper hemisphere is supported by the part, which has already been printed. Thus, the problem is how to transform the bottom hemisphere, to minimize the number of supports. One solution is to keep the bottom opening of 45° and transform the bottom hemisphere with inclined edges of 45° from every possible plane. This design and its angular relationships have been depicted in Figure 2.8b. The overall assembly has been depicted in Figure 2.8c.

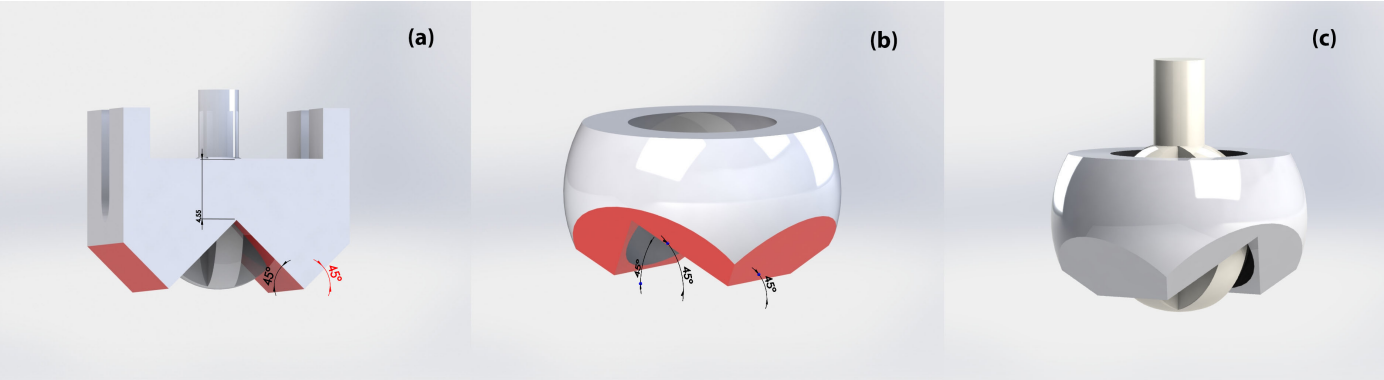

Figure 2.8: (a) Illustration of a socket with a non-spherical external shape, (b) Illustration of a spherical socket with its bottom hemisphere modified to be less supported, (c) Illustration of the proposed assembly.

The range of motion is again 120°, but induced slots can further expand the range of motion to 180° (Figure 2.9a). This modification creates an additional problem though. With slots from every direction, the ball can be out of the socket from the upper plane (Figure 2.9b). Something like this is

not favourable since the socket should enclose the ball. However, induced slots that are not perpendicular to each other can avoid this problem. Figure 2.9c illustrates the incorporated slots that restrict the ball inside the socket, since a sufficient overlap exists between them. The dimensions of all the proposed ball-socket joints can be found in Appendix B.

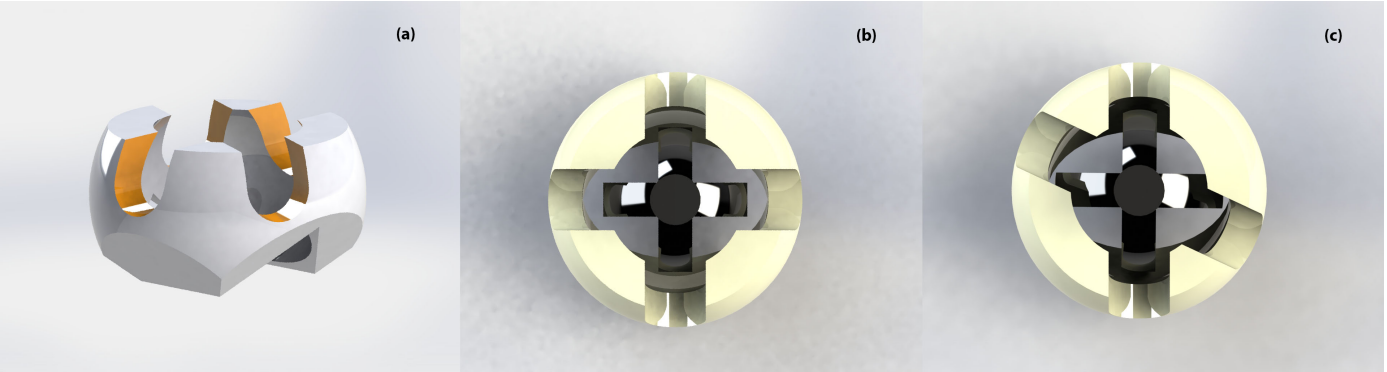

Figure 2.9: (a) Induced slots in the socket, (b) Slots towards directions that are perpendicular to each other, do not restrict the ball inside the socket during motion, (c) Slots towards directions that are not perpendicular to each other, restrict sufficiently the ball.

2.1.2 Design of Meta-Biomechanisms

Prismatic Joints

Since the individual prismatic joint was designed with no clearance supports, the challenge is to incorporate it in a multi-joint configuration. One potential arrangement is aligning them, one next to another, with inclined edges of 45°, to avoid intermediate supports. Figure 2.10a depicts the idea. The dimensional properties can be found in Appendix B. The last configuration can be expanded towards different dimensions to create a web of metal joints (Figure 2.10b).

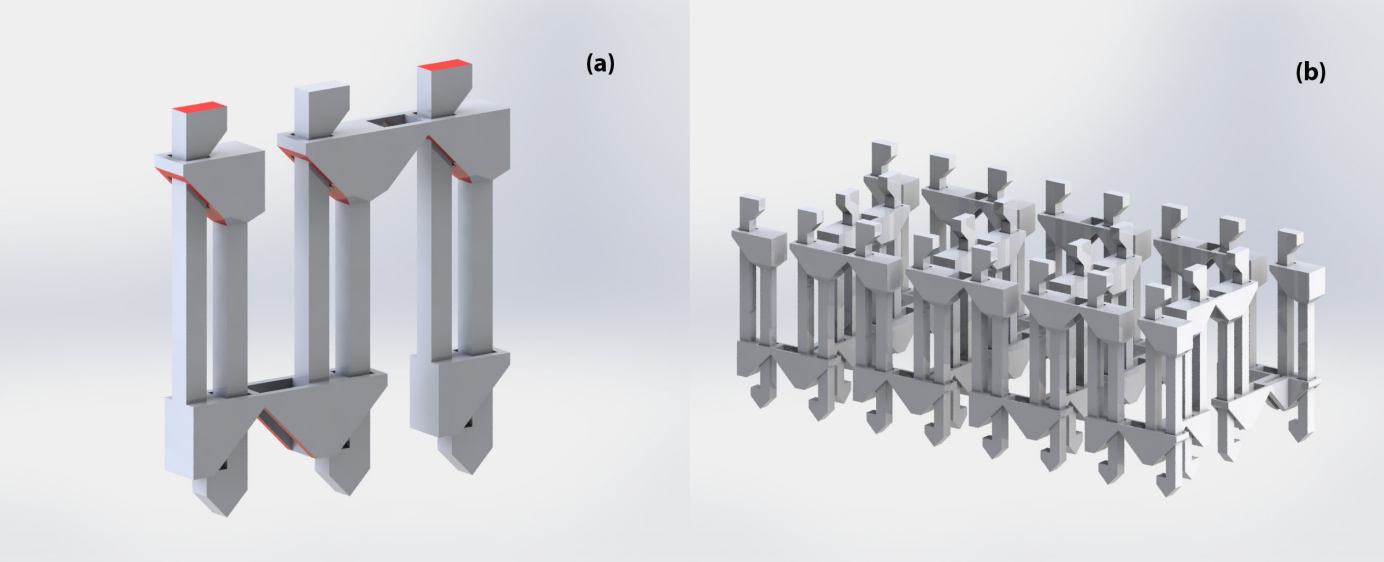

Figure 2.10: (a) Configuration of multiple vertical prismatic joints in series, interconnected with inclined edges of 45°, (b) Proposed configuration of multiple vertical prismatic joints in a multi-dimensional web of metal joints.

Slider: Prismatic Joint with 2 translational and 2 rotational DOF

The aforementioned configuration allows sliding motion only towards one direction, without allowing rotation. This is the definition of a prismatic joint. The next step is to increase the DOF as much as possible, since this was another concept idea of the design approach. In this regard, the upcoming designs are not prismatic, since they allow sliding motion towards two directions. Consequently, they are referred as "sliders" with increased DOF. Instead of building these multi-joint configurations vertically, an alternative scenario is to orient them horizontally. The clearance of the previous prismatic joint is vertical, so it is not regarded favourable to print it horizontally, considering the number of supports. Thus, a new design without vertical clearances is essential. One simple structure of horizontal sliders with increased DOF has been depicted in Figure 2.11a. Several rectangular bars interfering with each other (Figure 2.11a), allows sliding motion, whereas intermediate bars can optionally restrict the motion. However, this idea would be feasible with other techniques rather than SLM. In the case of SLM, the overhangs (pink regions) would be in need of supports and their removal from the entire configuration would be extremely tedious. Considering the certain rules of SLM, replacing these horizontal overhangs with inclined edges of 45° allows the printability of this structure without supports (Figure 2.11b). Although, intermediate bars restricts the translational motion along one axis, very limited motion is still achieved. Additionally, the unit cells can rotate around two axes with a

limited range of motion.

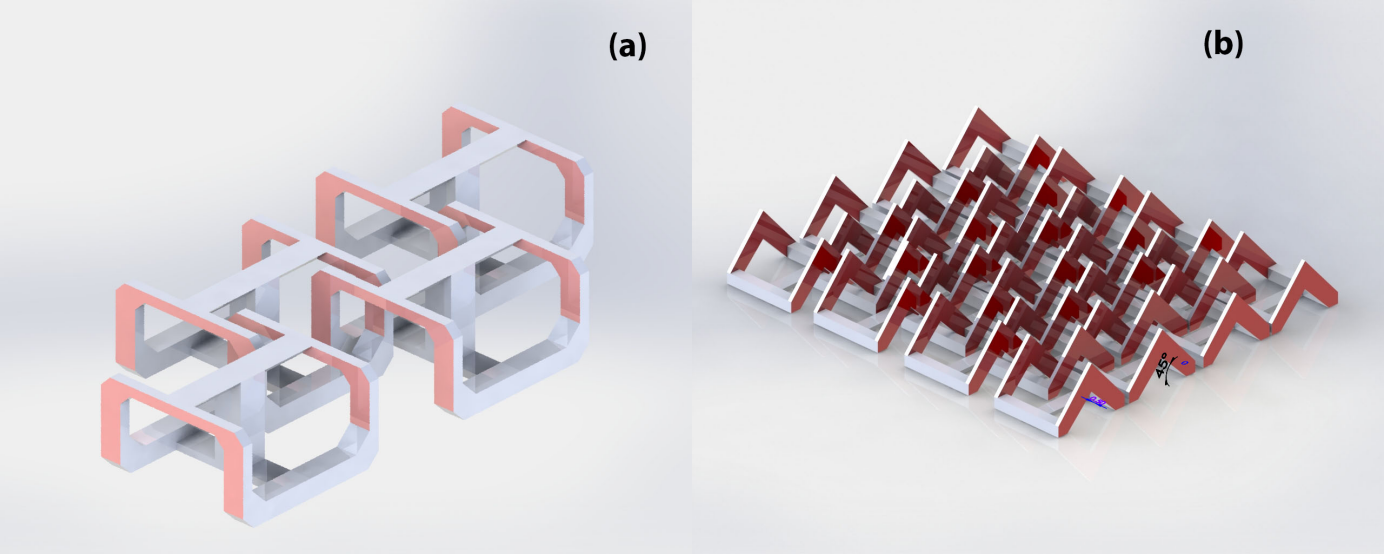

Figure 2.11: (a) Proposed horizontal configuration of 2-DOF "prismatic" joints, (b) Modified horizontal "prismatic" configuration to achieve no supports.

Rhombus Metallic Clay (Prismatic Joint with 3 rotational and 3 translational DOF)

The above configurations achieved increased DOF through design modification. Further increased range of motion with SLM remains a challenge though. New designs and ideas are essential to accomplish a metallic clay, able to twist and turn at a component level. In other words, a "prismatic" joint with both translational and rotational DOF. The previous ideas can be considered as multiple units interfering with each other. If these units can be designed with an angle of 45º towards each direction, the entire structure can be self-supporting with multiple DOF. The challenge is how to combine these unit cells, to achieve motion between them. One potential solution would be to orient the same unit cell differently. In this way, this unit cell takes the role of the connector. This idea has been depicted in Figure 2.12a. It can be easily understood that these units-connectors are in need of supports because they constitute horizontal overhangs (pink regions in Figure 2.12a). The supports are accessible to be removed, but it would be a great hassle to remove all of them from the entire configuration.

This obstacle can be bypassed, if different connectors are used. This idea has been depicted in Figure 2.12b. In this case, the well-known self-supporting face-centered cubic unit cell (FCCZ), found in lattice structures, takes the role of the connector. The whole structure has been depicted in Figure 2.13. Regarding the range of motion, this specific configuration offers 3 translational and 3 rotational DOF at a component level, of course with limited range of motion.

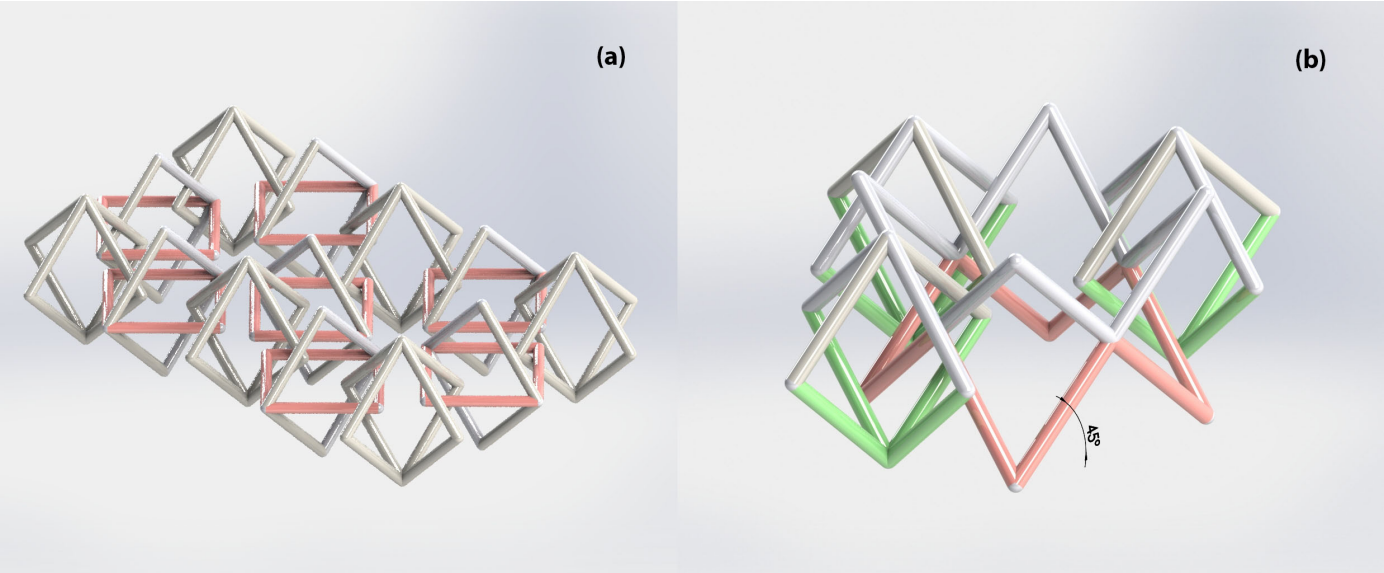

Figure 2.12: (a) Proposed structure with interfered unit cells to achieve increased DOF at a component level, (b) Illustration of the idea with self-supporting FCCZ unit cells as connectors.

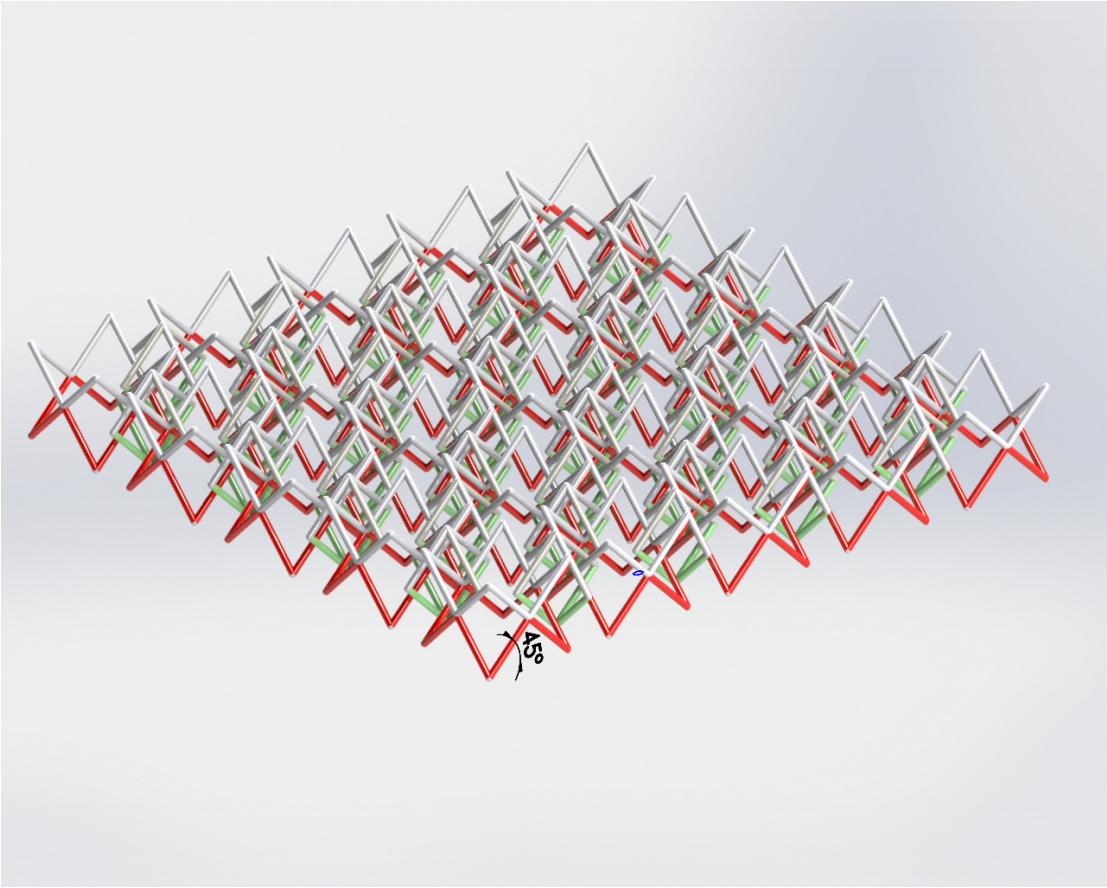

Figure 2.13: Illustration of the expanded structure with interfered self-supporting unit cells to achieve increased DOF.

"Caterpillar" Chain of interconnected Balls-Sockets (Ball-Socket Joint with 1 rotational DOF)

Positioning the ball-socket joints vertically is translated with the least amount of supports. However, the ideal aim of the current research is the direct fabrication of a mesh of joints with multiple DOF. Unfortunately, the vertical configuration does not give space for possible structures that satisfy the demanded criteria. The possibility of printing interconnected ball-socket joints horizontally, is considered an ideal option towards this aim.

The above notion encounters several obstacles though. Vertical orientation allows the neck or the socket to take the role of supports, whereas suitable openings and slots can improve the range of motion and eliminate the number of supports. In contrast, horizontal orientation does not permit this.

Eliminating the DOF is again the concept idea inherited to cope with the above problem. Thus, printing ball-socket joints with 1 rotational DOF horizontally, constitutes the starting point. Instead of printing the ball and the socket separately, one possible modification is to connect them with inclined edges of 45º (red region in Figure 2.14a). With the addition of an opening in the socket, a revolute motion of the next ball's neck is achieved. The cutting planes induced in the ball also eliminate the supports around this point (green region in Figure 2.14a). Consequently, by positioning these connected "joints" one by one, a chain of ball-socket joints is the result (Figure 2.14b).

However, as Figure 2.14b illustrates, both the ball and the socket will be in need of supports (pink regions). It is always regarded favourable to start with a horizontal plane without curves, when building horizontally. Thus, adding a cutting plane parallel to the transverse would ease this attempt. That eliminates the need for bottom supports and at the same time takes the role of support for the upper part (light green region in Figure 2.14c). Internally, the socket can be self-supporting the same way as the proposed designs in the previous sections. This can be done, through an upper cutting plane, parallel to the axis of rotation, at a point whose tangent creates 45º with the build plate. Externally, the number of supports can be minimized as well. Applying the modifications proposed in the previous sections led to this desired outcome (Figure 2.14d).

The ball should also be modified to achieve less supports. For this reason, the ball of Figure 2.6 was used. This successfully achieved less amount of supports, but not a self-supporting ball yet. Modifying the bottom hemisphere of the ball would solve this problem. However, due to the elimination of DOF, further ball's modification would lead to its insufficient motion inside the socket. Thus, inducing a part, that would not affect the motion, while it would take the role of support for the ball, constitutes the ideal solution. The modified ball's design has been depicted in Figure 2.14e.

The last proposed design can be further improved. The ball can be supported differently, using less material and easing the ball's revolute motion. Figure 2.14f depicts such a modification and Figure 2.14g its assembly. Taking the last modifications into account, the only part in need of supports, is one bottom quarter of the ball (pink region in Figure 2.14g).

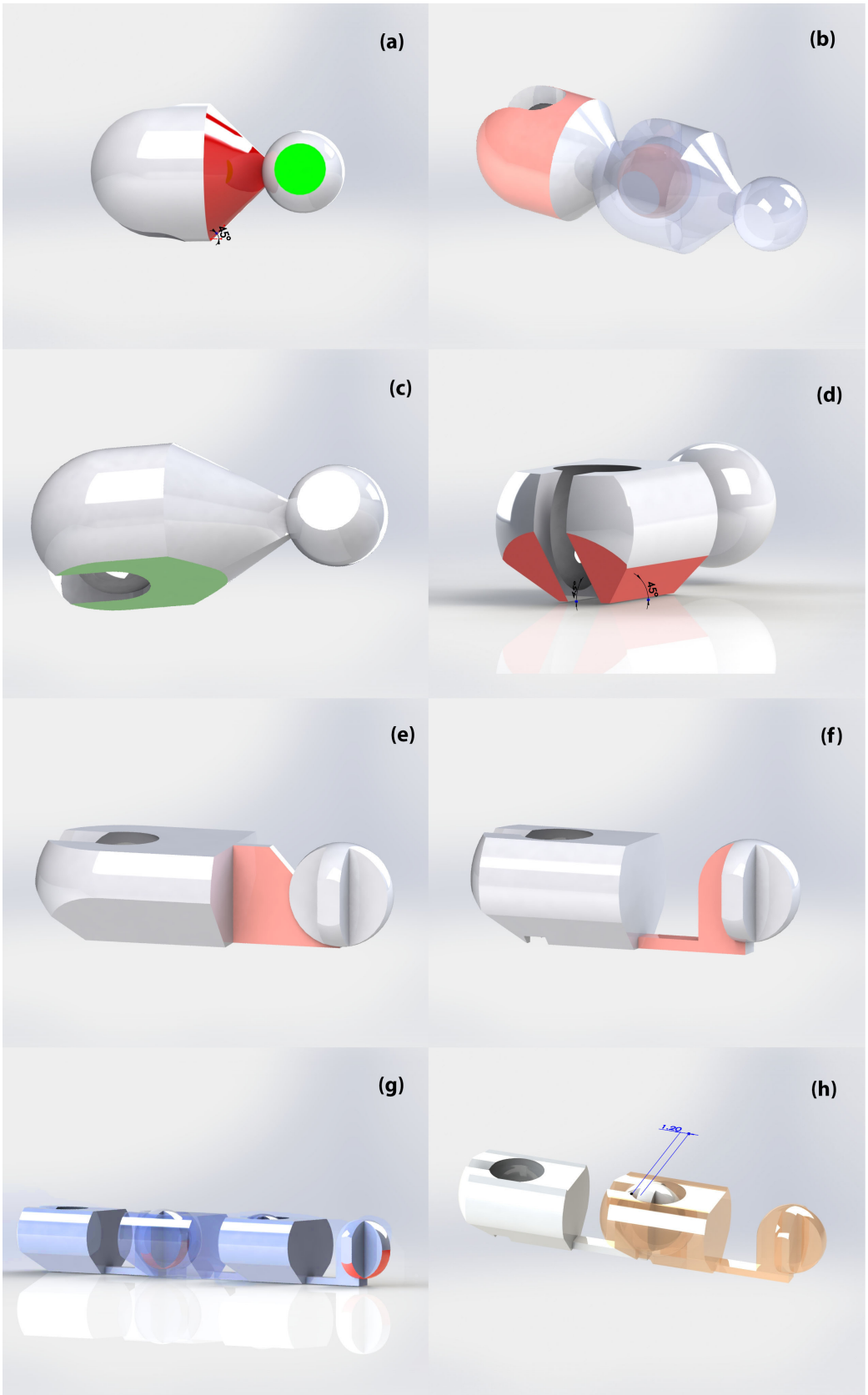

Figure 2.14: (a) Ball and socket interconnected , (b) "Caterpillar" Chain, (c) Cutting of socket, (d) Self-supporting socket, (e) Incorporation of a support-part for elimination of supports, (f) Improvement of the support-part to use less material, (g) Modified "Caterpillar" Chain, (h) A small distance separates the ball and the socket during printing.

Sadly, this design encounters problems. Taking into account the modified ball, only one couple of ball's bands are accessible in terms of supports (Figure 2.15a). Thus, it is regarded necessary to induce a bottom opening for reaching the supports of the other couple of bands (Figure 2.15b). This opening should restrict the ball inside the socket though. At the same time, there should be enough space to reach the supports of the ball. However, if the ball is not positioned concentrically with the socket during printing, but with a small horizontal distance between them (1.20mm), the supports of the other couple of bands are fully accessible and they can be removed easily (Figure 2.14d).

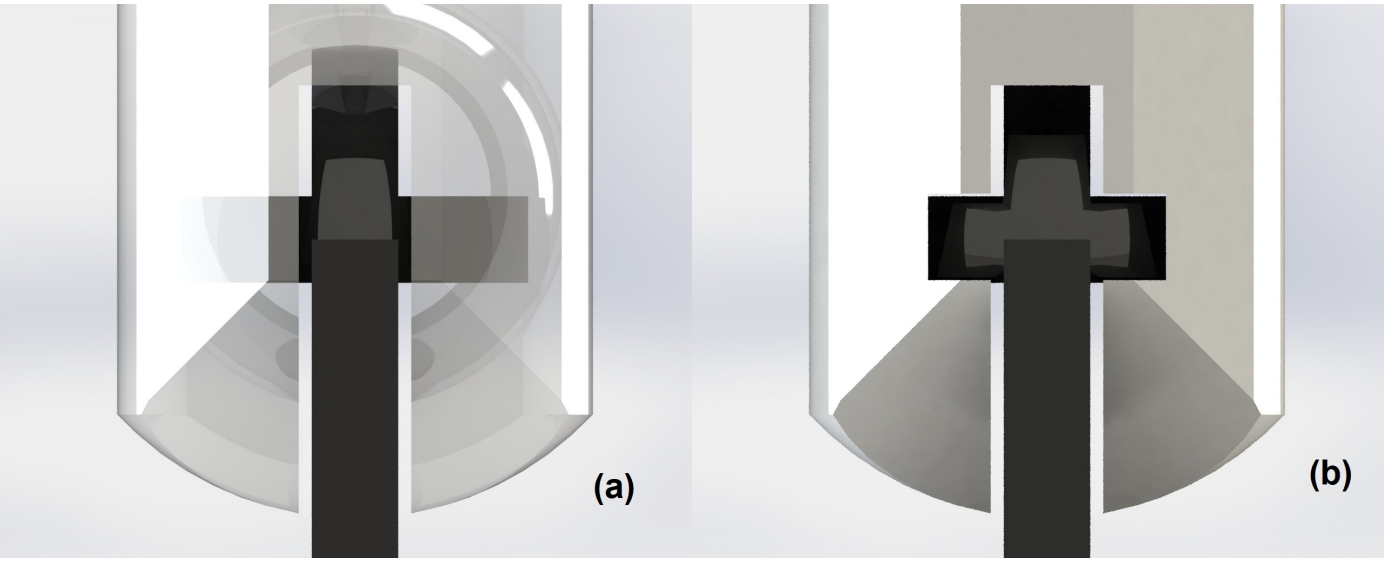

Figure 2.15: (a) Illustration of the problem in the above design. The supports of the horizontal bands cannot be reached. (b) Incorporation of a bottom opening that allows the supports' removal.

Star-Shape interconnected Ball-Socket Joints (Ball-Socket Joint with 2 rotational DOF)

The previous section revolved around the printing of a metal chain, including inter-connected ball-socket joints, that allows only revolute motion. Considering the desired aim of a metallic clay with increased DOF, these designs should be further modified to achieve increased DOF.

In order to cope with this problem, the designer should separate the proposed ball and the socket. Their assembly has been depicted in Figure 2.16. Again, the ball and the socket are not concentric, but a small distance of 1.20mm separates them. Furthermore, the ball has a vertical distance of 1mm from the build plate, exposing a greater amount of supports in this way. Thus, the only supported part is the pink region of Figure 2.16, where the previous proposed openings and distances give space for effortless supports' removal.

This configuration has the ability to form a metal clay with increased DOF. One potential combination of them has been depicted in Figure 2.17. The only difference is a star, that is incorporated behind the socket, in order to connect it with other parts in a potential network of joints.

Diagram 2.18 depicts the way the proposed Meta-Biomechanisms were developed and Figure 2.19 which design represents each concept solution.

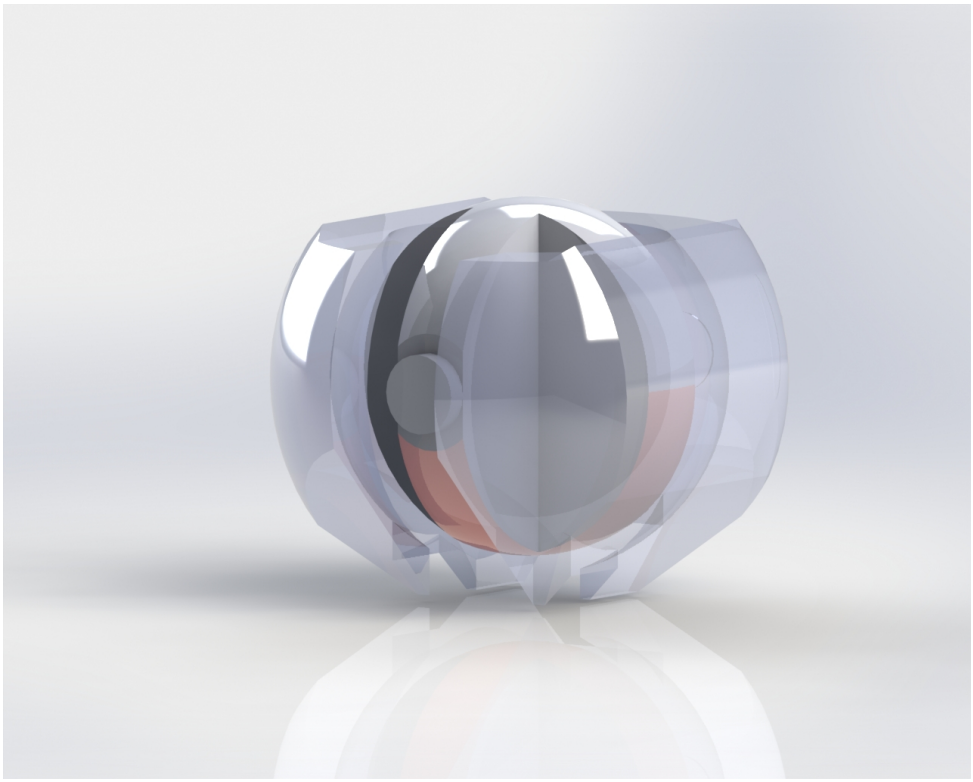

Figure 2.16: Illustration of the horizontal configuration of a ball-socket joint.

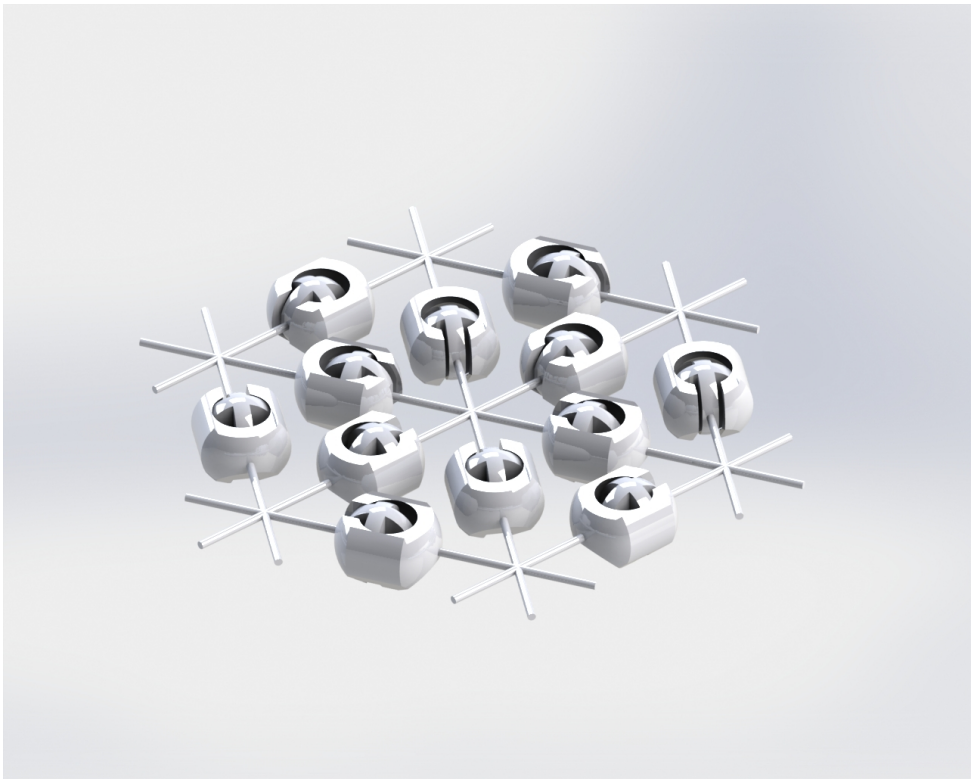

Figure 2.17: Star-shape configuration of multiple ball-socket joints.

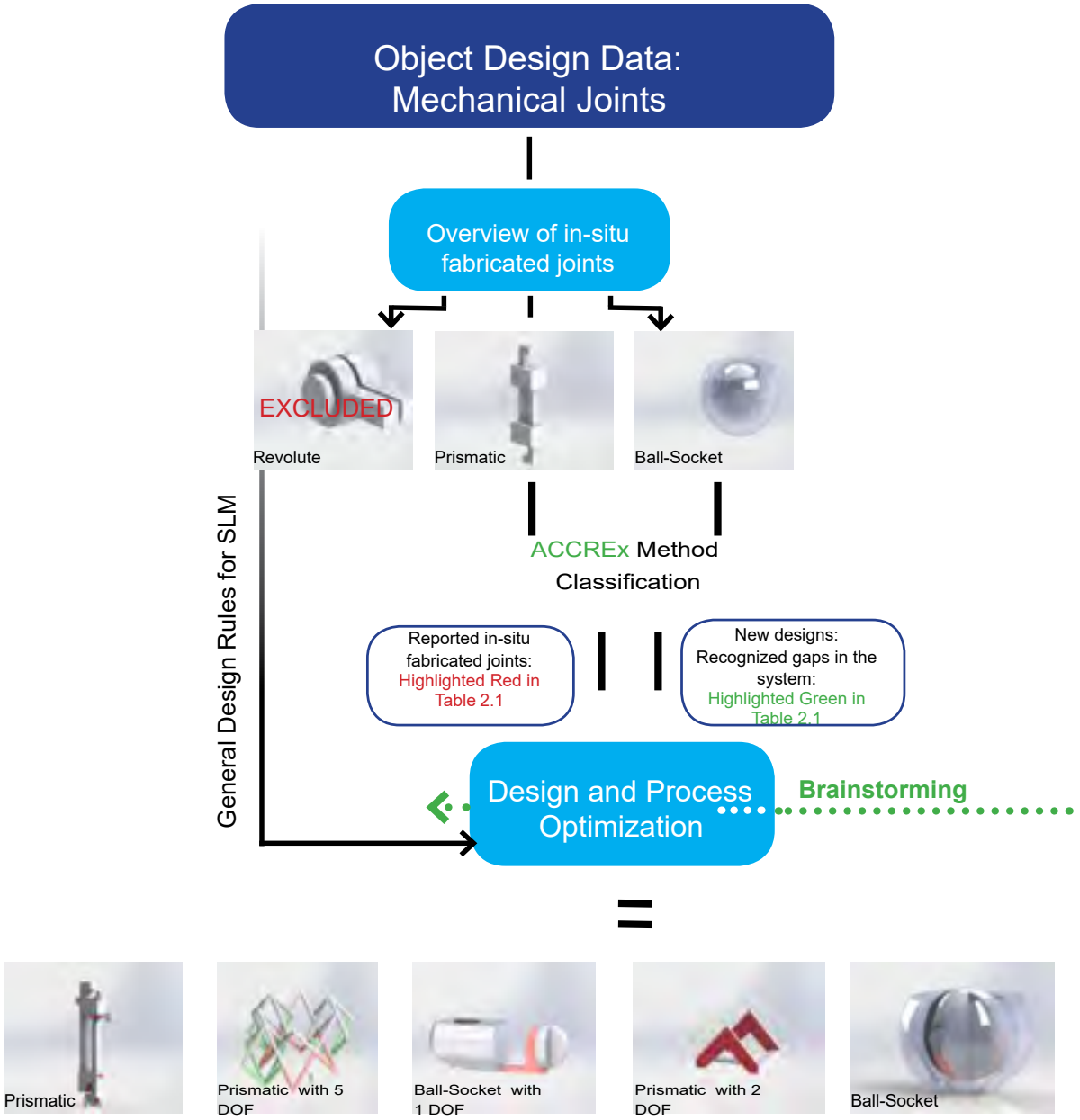

Figure 2.18: Schematic illustration of how initial reported joints were categorized and new joints were proposed using the ACCREx method.

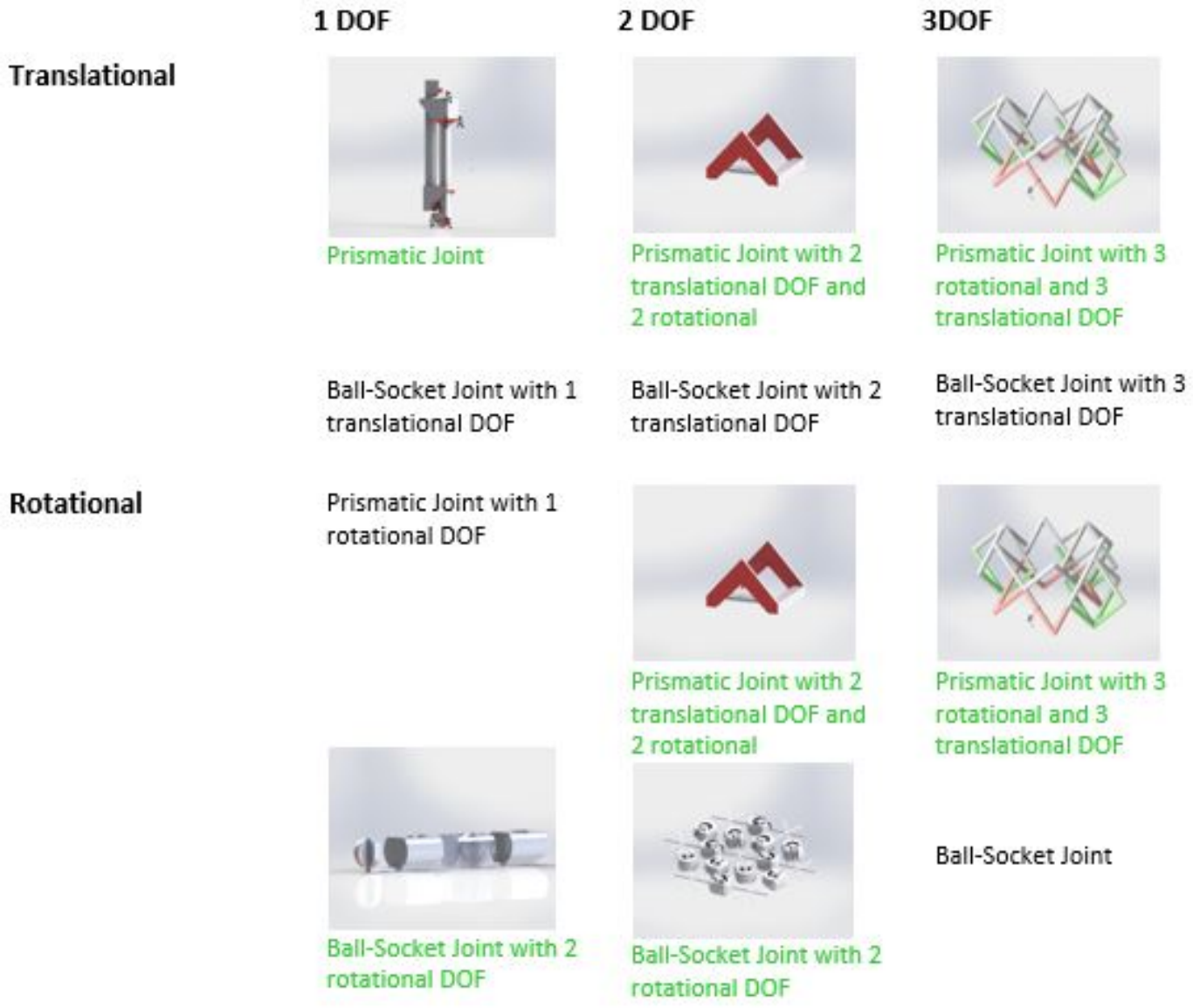

Figure 2.19: ACCREx implementation triggered new concepts. Figures depict schematically the ones successfully conceived.

2.1.3 Acetabular Shape Models

The aforementioned design configurations are indented to fill massive bone defects of irregular shape and location. Consequently, they should offer the possibility of transforming their shape and volume according to the target.

Evaluation of their kinematic performance is, therefore, necessary to define their ability to fit any space. This ability should be quantified to objectively decide how each design can be further improved in terms of application. For this reason, the proposed meta-biomechanisms will be classified, based on their fitting to a specific surface, consistent with the final application.

There are several classifications for cavitary bone defects, that constitute the final application of this research. According to the Bargar and Gross (1992), these can occur in the femur, tibia, patella as well as in the pelvis.[58] Additionally, bone ingrowth can occur, only if the implanted mechanism is in contact with the host bone for at least 40-60%.[59] This is why the evaluation of the under-research meta-biomechanisms, is very important.

Pelvic bone is the model used in the evaluation procedure. A real human pelvis model was downloaded from Sketchfab.[60] This model was scanned by students in Dr.Eric Bauer's human anatomy lab at the Elon University of North Carolina. However, a few modifications were necessary to achieve the desired outcome.

The tessellated file of the pelvic bone included a huge amount of facets, making its manipulation difficult. For this reason, a simplification procedure was taken place in MeshLab (ISTI - CNR, Pisa, Italy) reducing the faces to 20.000.[61] The reduced file then was imported to Rhinoceros (Robert McNeel Associates) for further processing.[62] Taking into account that Ilium remains intact through severe acetabular defects, only a specific region was selected.[59] Based on that, the only region that was selected includes the acetabulum along with a small area of Ilium for potential stabilization of the implant. Effortless comparison between the pelvic surface and the meta-biomechanisms would be taken place if both of them were of comparable sizes. For this reason, the trimmed pelvis surface was scaled down with a factor of 0.602. Figure 2.20 depicts all the subsequent steps that the original pelvic model underwent to reach the final result. However, the concave shape of the acetabulum does not help the visual observation of the designs' fitting. This is why, the final model was cut in two different planes. Figure 2.21 depicts the distinct views, used in the Surface Morphing Experiments.

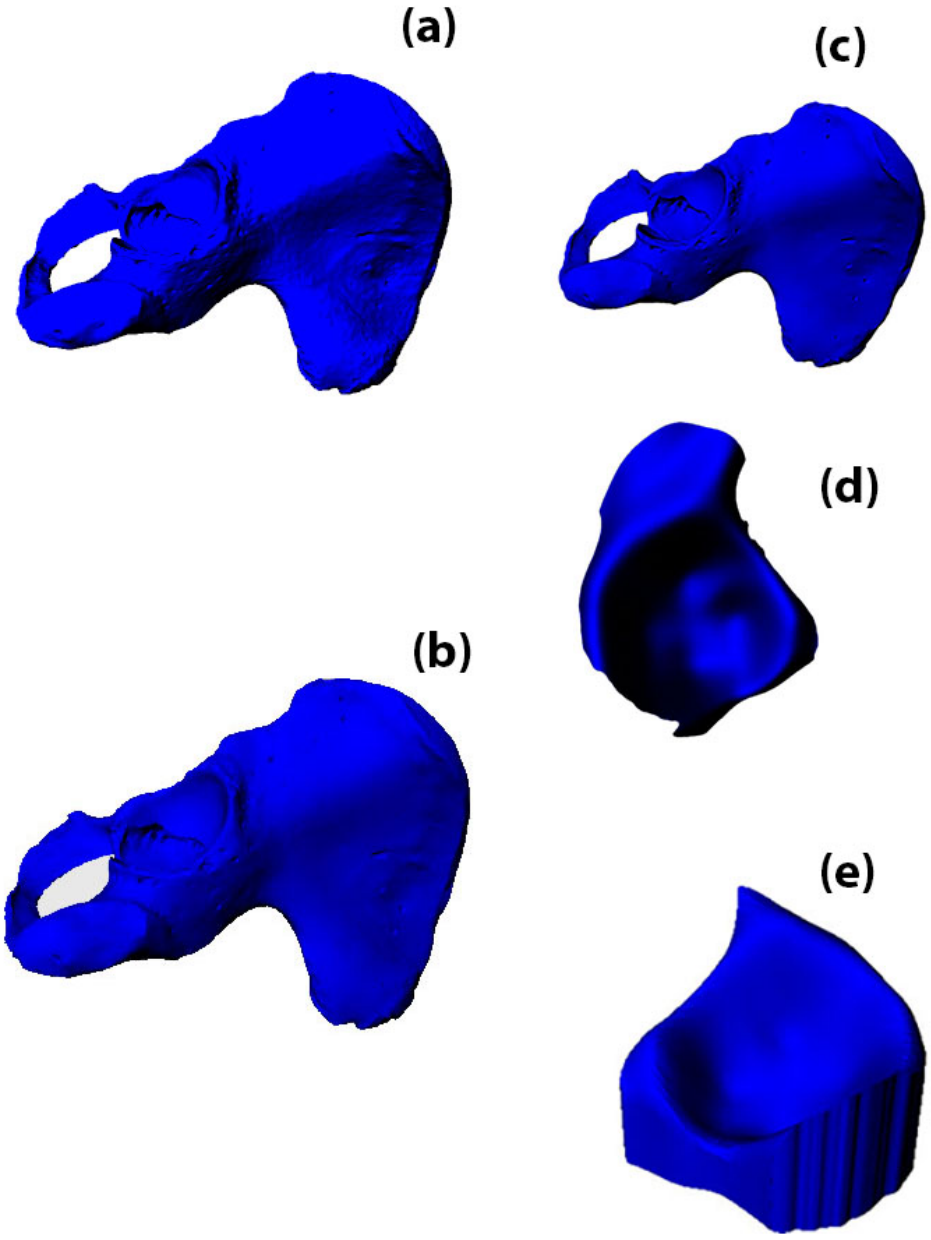

Figure 2.20: (a) Original pelvic bone downloaded from Sketch-Fab,[60] (b) Simplified pelvic bone in terms of tessellated facets, (c) Scaled pelvic bone, (d) Acetabular region used as reference surface (e) Final model used in Surface Morphing Experiments.

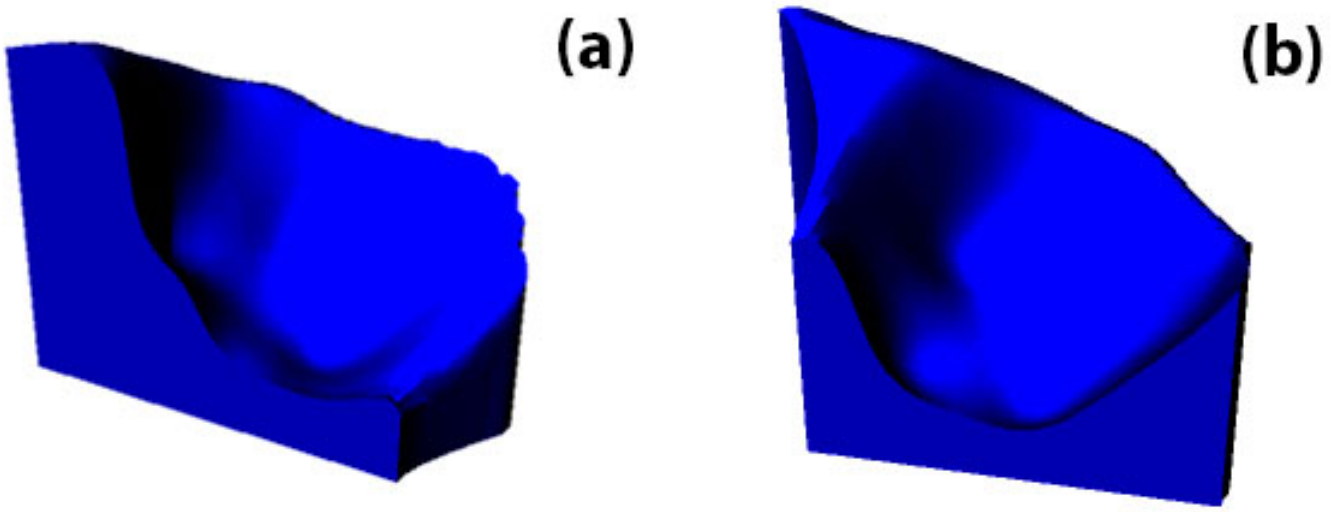

Figure 2.21: Cut views of the final acetabular model used in Surface Morphing Experiments for easier comparison.

2.2 Manufacturing

2.2.1 Additive Manufacturing of Non-Assembly Joints and Meta-Biomechanisms

Material

The material used was a Titanium Alloy, named Ti-6Al-4V, which is an alloy powder special for being processed on metal-based 3D-Printing techniques^{TM}. The density of the powder was 2.51 g/cm^3.

The whole procedure is carried out under a protective gas atmosphere. In case of titanium, which has a high reactivity with nitrogen and the tendency to form oxides and carbides,[63] it is preferable to use an argon atmosphere to keep the oxygen percentage low.[64,65]

Scanning Strategy

It is already mentioned in Chapter 2, that scanning strategy plays an important role in the formation of stresses during printing with SLM. This is why, the inter-layer scanning strategy was used. Particularly, each layer thickness was divided in smaller regions of 2x2mm (overlap:0.05mm), where the scanning path was alternated between horizontal and vertical direction from layer to layer.

Process Parameters

Table 2.2 depicts the process parameters used during the printing procedure with SLM.

Table 2.2: Process parameters used in SLM experiments.

Inner/Outer Boundary	
Exposure Time	20μs
Point Distance	10μm
Laser Current	1000μA
Hatch	
Exposure Time	5μs
Point Distance	10μm
Laser Current	1000μA
Laser Power	80W
Layer Thickness	50μm

2.2.2 Additive Manufacturing of Acetabular Models

The acetabular models used in the Surface Morphing Experiments, were printed with another additive manufacturing technique. This is a polymer-based technique, named Fused Deposition Model (FDM). FDM is the most commonly used additive manufacturing technique, where a material in the form of filament is molten and deposited through a nozzle on the built plate. Two rollers push the filament towards one direction and thermal elements liquify the material. The nozzle is controlled in a 3D way to build parts of specific thickness.[66] A schematic representation of the procedure has been depicted in Figure 2.22. The process parameters of the FDM procedure can be found in Table 2.3. The infill density used in manufacturing of acetabular models was 22%. However, another acetabular model of 100% infill was used during the mechanical testing, to sustain the compression load, and avoid any breaking prior to the testing of the structures.

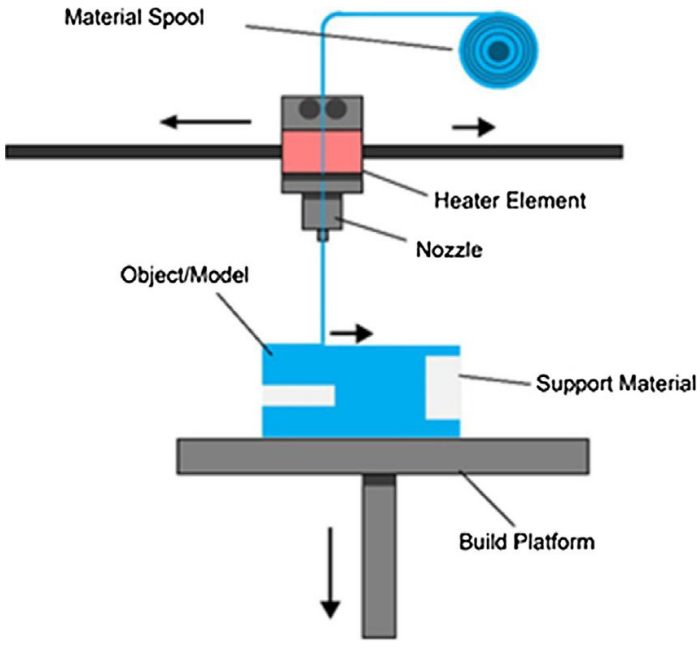

Figure 2.22: Schematic Representation of FDM procedure.[67]

Table 2.3: Process Parameters used in FDM experiments

Material	PLA
Nozzle Diameter	0.4mm
Layer Height	0.06mm
Infill Density	22%
Infill Pattern	Grid

2.3 Experimental Testing

2.3.1 Surface Morphing Experiments-1st Approach

The proposed designs will be positioned on an acetabular surface after which, classification of their fitting will follow. For this reason, all the proposed design configurations were fitted to the final acetabular cut views, and detailed photos of them were taken (Figure 2.24).

Rough conclusions can easily be exported from photos, like Figure 2.23. However, for scientific reasons a new method to assess the kinematic behavior of the design configurations was developed. The photos taken were imported into the design software Rhinoceros (Robert McNeel Associates),[62] using the command "PictureFrame". The frame used for each meta-biomechanism was of identical dimensions (40mm x 26mm). Based on the imported photos, new poly-line curves following the cut views were created, as well as the fitting of each design with as many points as possible (e.g Rhombus Clay design, Figure 2.24)). Then, quantitative comparison between the two curves was taken place for each design. The designs were positioned as similar as possible into the acetabulum. Photos that illustrated best this position were selected and then imported into Rhinocerros. After that, the curves of both the fitting and the acetabular edge were created in the same PictureFrame. The fitting was held out only at the areas that designs touch the acetabulum. The comparison of the curves was subsequently held out in a plug-in of Rhinoceros, named Grasshopper. Grasshopper is an algorithmically modelling tool, tightly connected with Rhino design environment, that allows mathematical manipulation of design models.

The script used for the comparisons of the two curves has been depicted in Figure 2.25. The same script was used for every meta-biomechanism assigning the respective curves. The script includes two groups of algorithmic comparison between the two curves. The first one takes the control points of the two curves and with the command "Similarity" returns the absolute difference of their distinct points. However, the same command can return the mean absolute difference between two regions, e.g surfaces, and not between multiple points. This is why, the two curves are extruded and the "Similarity" command was used to return their absolute difference (Figure 2.25a). Figure 2.25b depicts the regions generated in Rhinoceros design environment, based on the curves of both the reference model and the meta-biomechanism.

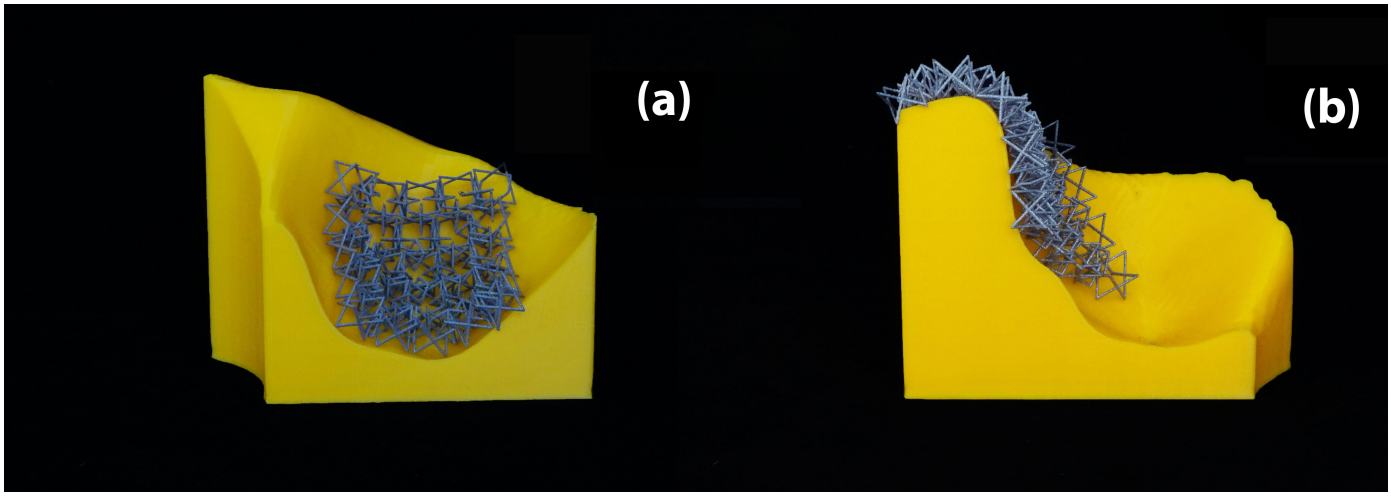

Figure 2.23: Fitting of the proposed meta-biomechanism on the reference surface (a) 1st Cut View, (b) 2nd Cut View.

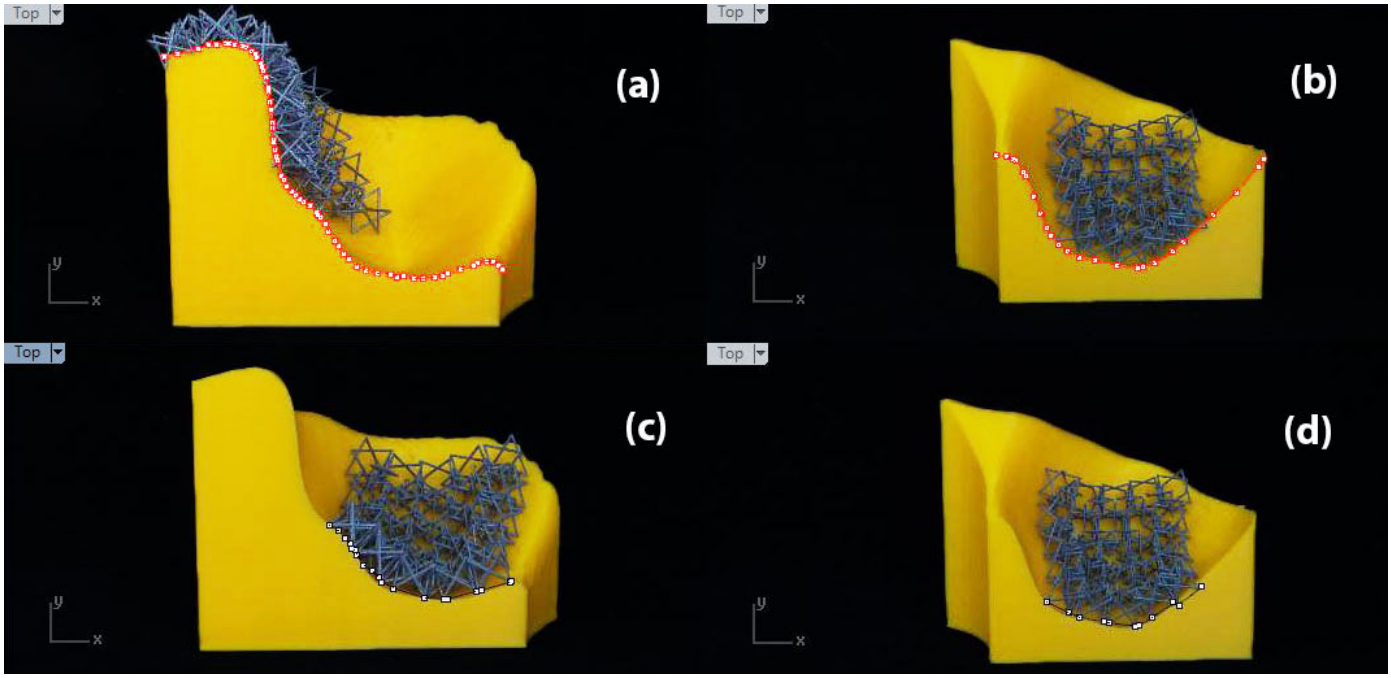

Figure 2.24: (a) Curve follows the 1st Cut View of the reference model with its points on, (b) Curve follows the 2nd Cut View of the reference model, (c) Curve follows the fitting of Rhombus Clay on the reference surface, (1st Cut View), (d) Curve follows the fitting of Rhombus Clay on the reference surface (2nd Cut View).

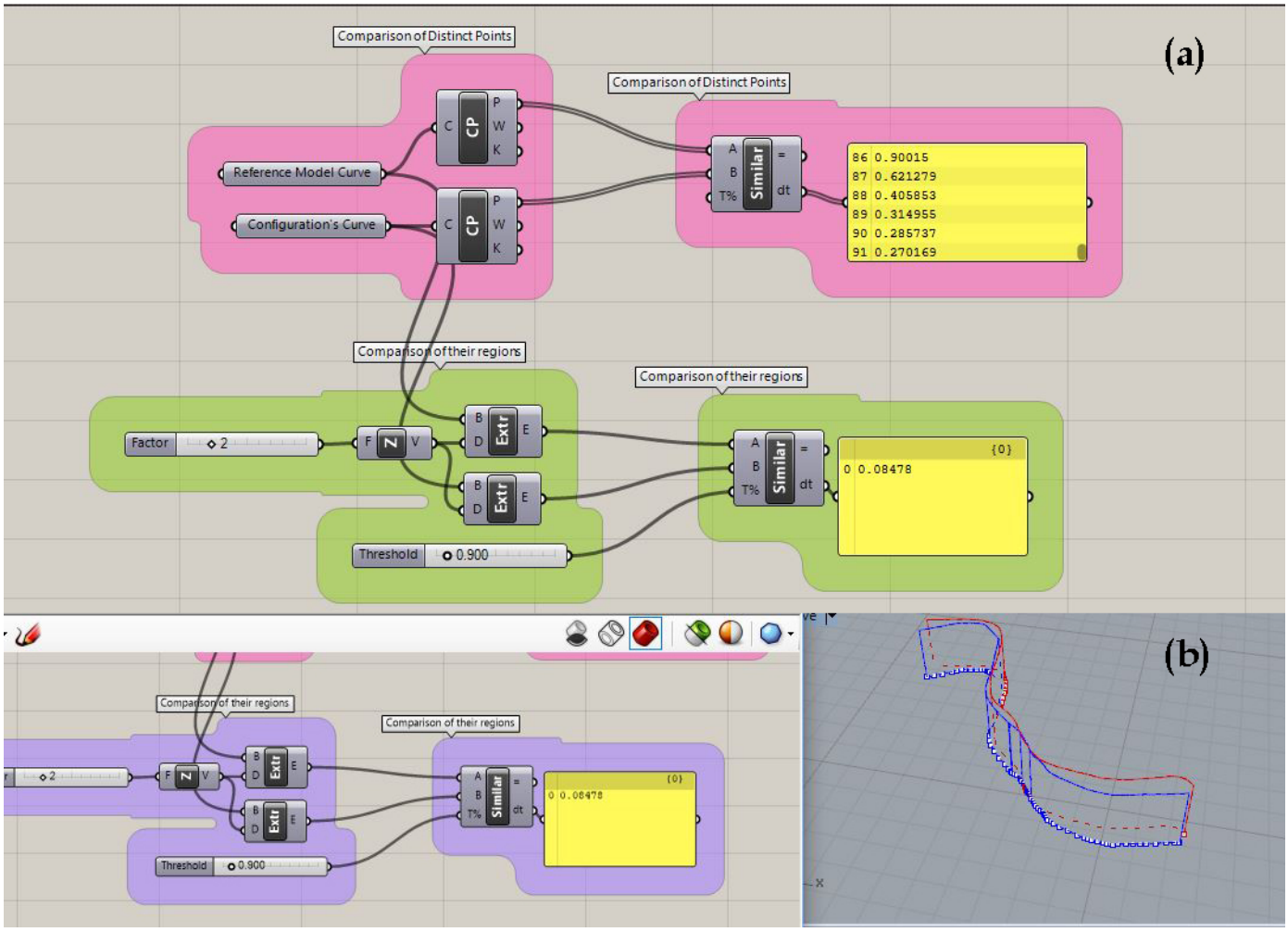

Figure 2.25: a)Grasshopper script used to compare the distinct points of two curves, b) Grasshopper script to compare the extruded surfaces of the two curves, along with the respective regions of the curves in Rhino environment.

2.3.2 3D-Scanning Evaluation-2nd Approach

The above method is considered an approach to take quantitative results about the fitting of the proposed meta-biomechanisms on a concave shape. However, it does not give any detailed information regarding the fitting of the meta-biomechanisms in a three-dimensional space.

The proposed meta-biomechanisms were therefore scanned inside the acetabulum using a 3D scanner. The scanner, named Scan in a Box-FX, followed by the respective software IDEA (Open Technologies Srl, Italy).[68] The 3D Scanner scans the model in different angles and the software acquires the scans and manipulates the obtained data, until the 3D model is produced. The software demands at least 8 angles of the same model, which aligned in order to generate the different point clouds that represent the 3D model (Figure 2.26). The 8 point clouds are subsequently imported in another software, named CloudCompare (ENST-Telecom, Paris, TSI Laboratory) (Figure 2.27).[69] This software offers the possibility of merging the distinct point clouds into one, which in its turn is transformed in an STL file (Figure 2.28a). In this way, this method gives detailed information of the model in a 3 dimensional space. The above advantage, though, is translated with great computational demand. The STL file includes more than 1 million facets and cannot be further processed in Rhinocerros. This

is why, MeshLab (ISTI - CNR, Pisa, Italy) is again essential to reduce the number of facets, in order to be computationally manipulated (Figure 2.28b).[61] Although the final STL file includes a rough representation of the model (65.000 facets), it still constitutes an approach to take quantitative results about the fitting of meta-biomechanisms inside an acetabulum.

Figure 2.26: Setting of he subsequent elements during the 3D Scanning.

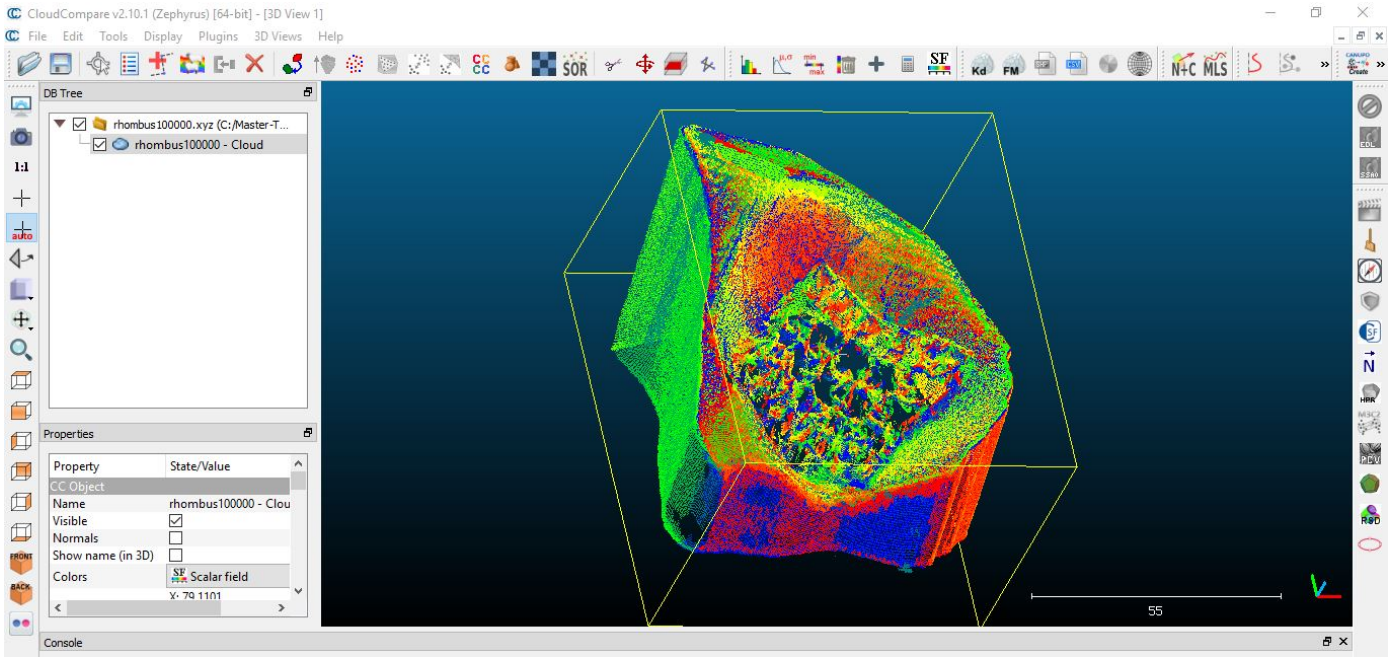

Figure 2.27: The Point Cloud, representing the scanned model with the structure in CloudCompare software (ENST-Telecom, Paris, TSI Laboratory).[69]

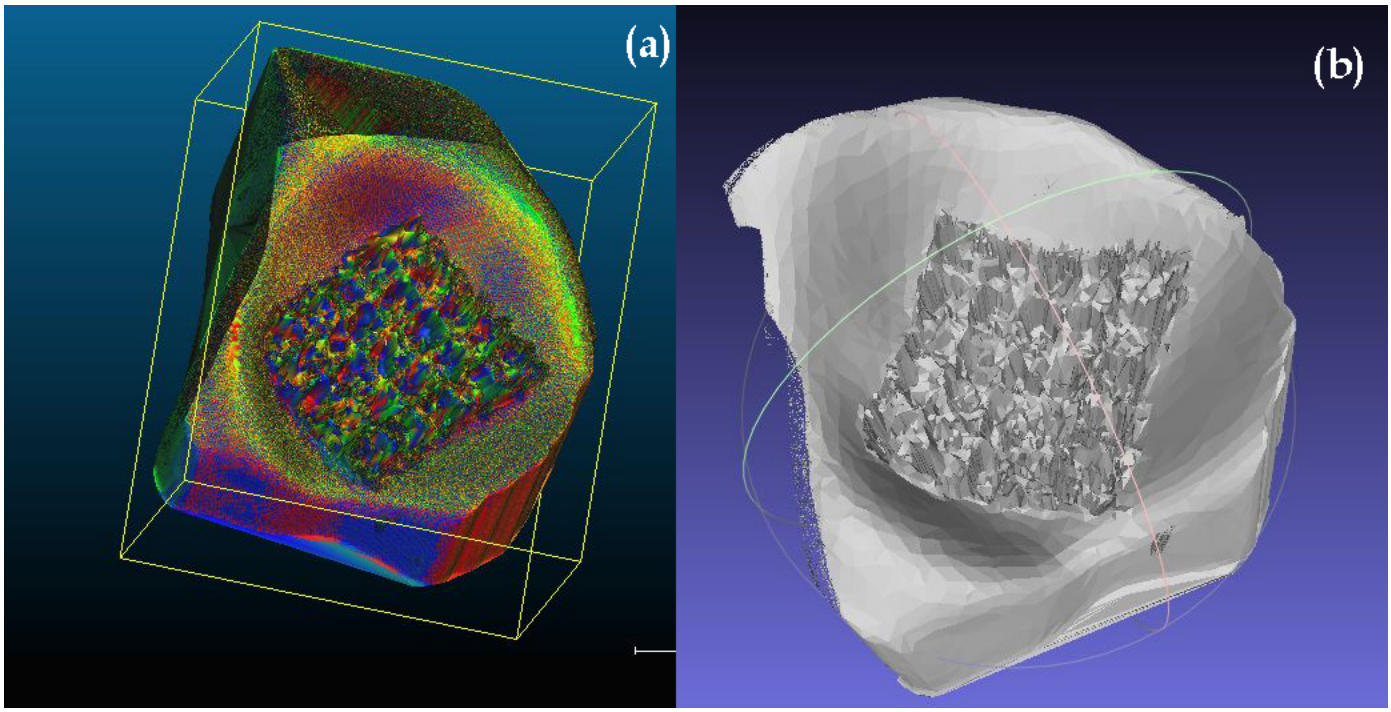

Figure 2.28: a) The STL file generated from the Point Cloud in CloudCompare software (ENST-Telecom, Paris, TSI Laboratory),[69] b) Simplification of the STL file in MeshLab software (ISTI - CNR, Pisa, Italy).[61]

This can be achieved in Rhinocerros with the well-known Boolean operations. This software offers the possibility to get the Boolean difference of two STL files. By importing both the acetabulum alone and the acetabulum with the structure above (Figure 2.29a), the structure itself is the result of the Boolean operation (Figure 2.29b) . The only requirement is to position them one above the other to get the difference. However, the STL files contain a lot of noise and further manipulation is necessary. The "noisy" facets can be selectively deleted with the command "DeleteMeshFacets". This unfortunately is not an objective procedure and it strongly depends on the user's perspective. After that, the "cleaned" STL file (Figure 2.30a) can be patched (command "Patch"). The result is a surface that mimics the STL file as much as possible (Figure 2.30b). Although this surface is irregular in terms of space, it can be easily trimmed to its limits by the User (Figure 2.30c). This also goes under the user's perspective. This surface can finally be compared with the acetabulum's surface with the same script used in the previous section. The two surfaces should be aligned (command "align", "concentric alignment"), in order to compare only their common surface area. Additionally, the surface of the acetabulum is bigger, so it should be trimmed to the limits of the structure (Figure 2.30d). This can be done by implementing the command "Dupborder", and then using this border to trim the acetabulum's surface (Figure 2.30e).

Since two steps in the above procedure go under the user's perspective, the user's variability was taken into account. Evaluating the observer's variability is a significant task when a new method is applied. There are two types of variability; the intra-user's variability and the inter-user's variability. The first one shows the difference in distinct measurements of the same user, whereas the second the differences in measurements of distinct users. The minimum necessary to obtain variability is to have two observers who repeat the measurement more than one time.[70] In this research, three users implemented the same procedure. Specifically, each user performed three times the same procedure for the same structure. To obtain the interobserver variability, the first value of the 1st user is paired to the first effort of each of the other users.

Calculating the user's variability using SEM is always preferable.[70] However, an additional method was implemented to calculate the intra- and interobserver's variability. This method calculates standard deviation of individual pairs of measurements for the same user. This is how intra-observer variability is calculated. Similarly, the interobserver's variability is calculated by finding the individual standard deviation of pairs of users for the same measurement. Then, the mean value and the standard deviation of all these individual standard deviations, are calculated. The SEM is then calculated by the following equation:[70]

$$Var_{\text{intra(inter)}}obs = Mean_{\text{individual}}SD^2 + SD_{\text{individual}}SD^2 \tag{2.1}$$

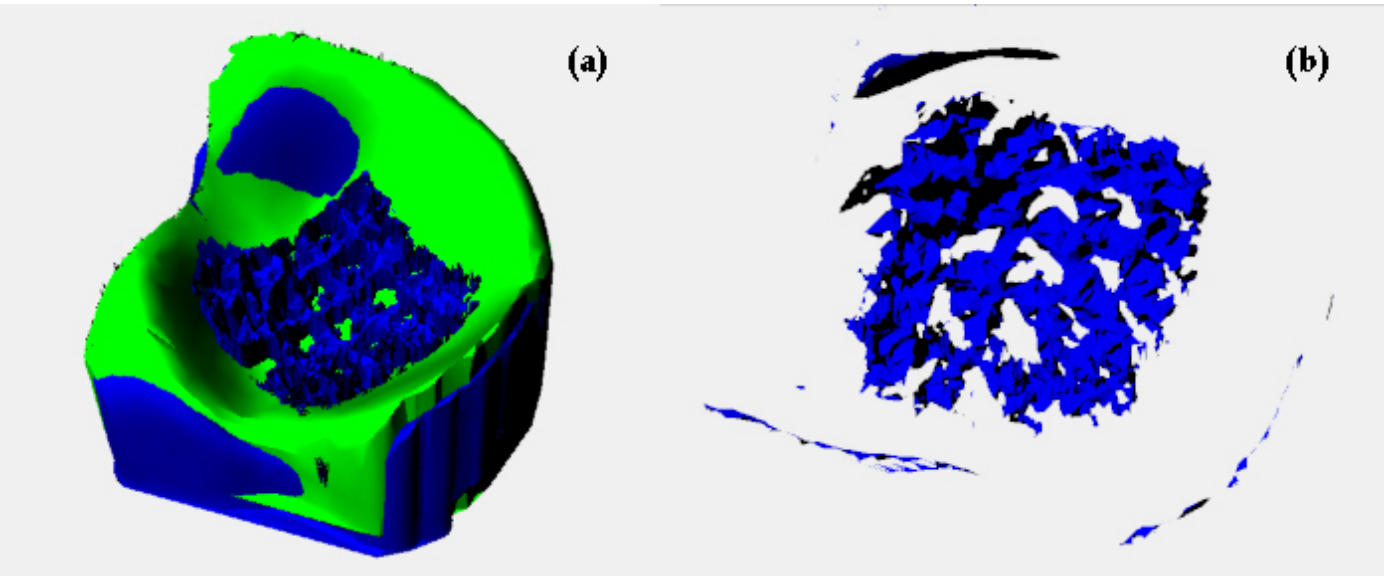

Figure 2.29: a) STL model of both the acetabulum and the acetabulum with structured aligned in Rhinocerros (Robert McNeel Associates),[62] b) Implementing the command "MeshBooleanDifference" gives us the structure alone.

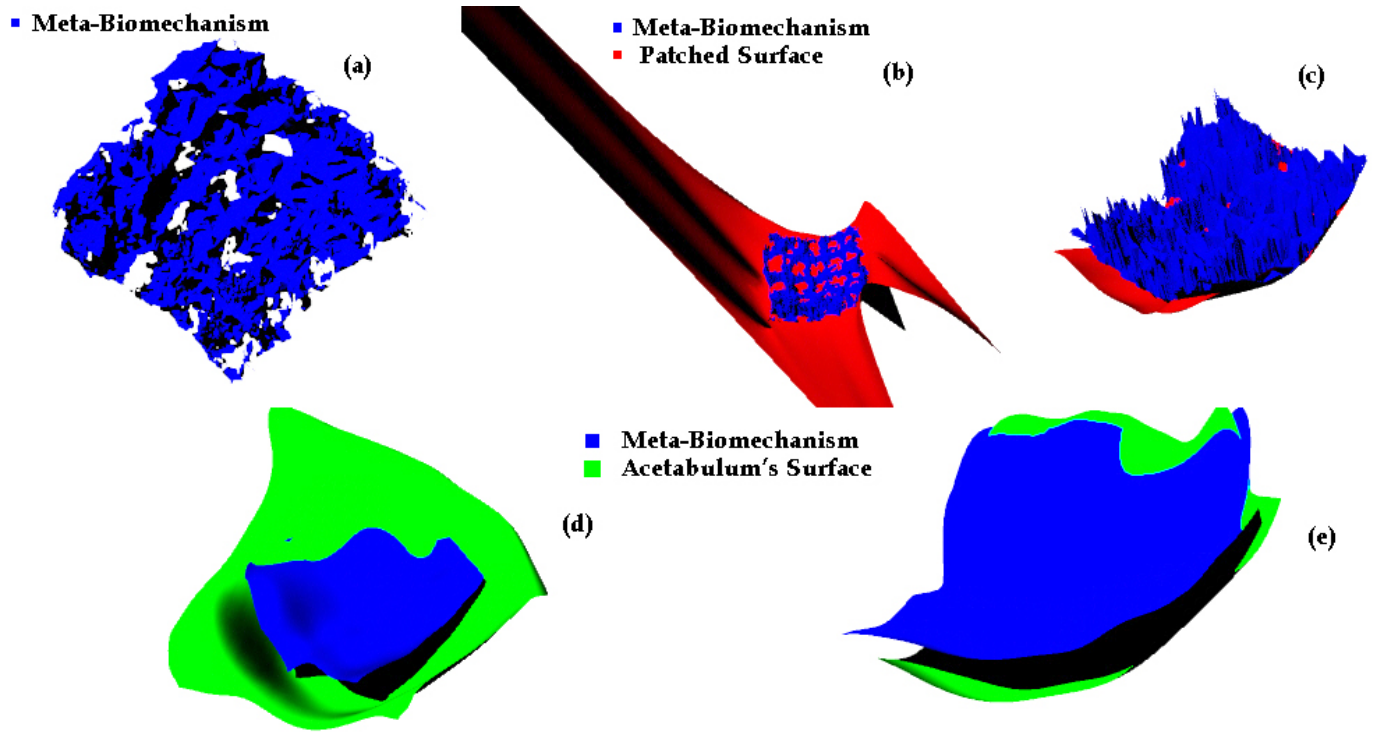

Figure 2.30: a) "Cleaned" model of structure in terms of noise facets, b) "Patched" Surface imitating the structure's fitting, c) this surface is irregular, so it is trimmed to the limits of the structure by the user, d) Importing the acetabulum's surface along with the trimmed "Patched" surface, e) Trimming of the acetabulum′s surface.

2.3.3 Uni-axial Compression Testing

Despite the fact, that this research is only at a preliminary stage towards the final aim, it is quite interesting to derive some indicative mechanical properties. One common way to mechanically evaluate structures is the uni-axial compression testing.

The proposed structures are not comparable in terms of shape, size and cross-sectional area. This is why, this mechanical testing does not aim the comparison of them, neither the derivation of the stress-strain curves. For the same reason, well-known ISO standards could not be implemented. Taking these into account, the Prismatic Joint was excluded from the testing, because its dimensions have a great difference from the other structures.

Their evaluation in terms of motion was held out in their potential configuration on an acetabulum. Similarly, the structures were positioned between the same acetabulum and a respective ball. The reason was to mechanically evaluate the structures in their potential application. The acetabulum′s model was printed with 100% infill density, to ensure its structural integrity under compression loading. Due to the concave shape of the acetabulum and the dissimilar shapes of the structures, the ball of a specific size could not touch every structure sufficiently. This is translated to a gap between the ball and the structure that affects the measured displacement. For this reason, balls of three different sizes were used. The sizes were calculated with the following equation:

$$Ball'sDiameter = Acetabulum'sDiameter - (2xStructure'sHeight) \tag{2.2}$$

Table (2.4) includes the different balls' sizes and the respective standards that were selected. Figure (2.31) illustrates how the subsequent elements were positioned on the compression machine. Concerning the test's settings, a load of 5kN was positioned on the machine and the structures were compressed with a speed of 0.085mm/s (strain rate= 0.01 s^{-1}) up to a maximum deflection of 8.50mm. The latter is the mean height of all the structures.

Table 2.4: Ball's Diameter per each structure

	Ball's Diameter (mm)	ISO Standards (mm)
Slider with increased DOF	44	42.862
Rhombus Clay	46	45
"Caterpillar" Chain	39.8	39.687
Star-Shape ball-socket	39.8	39.687

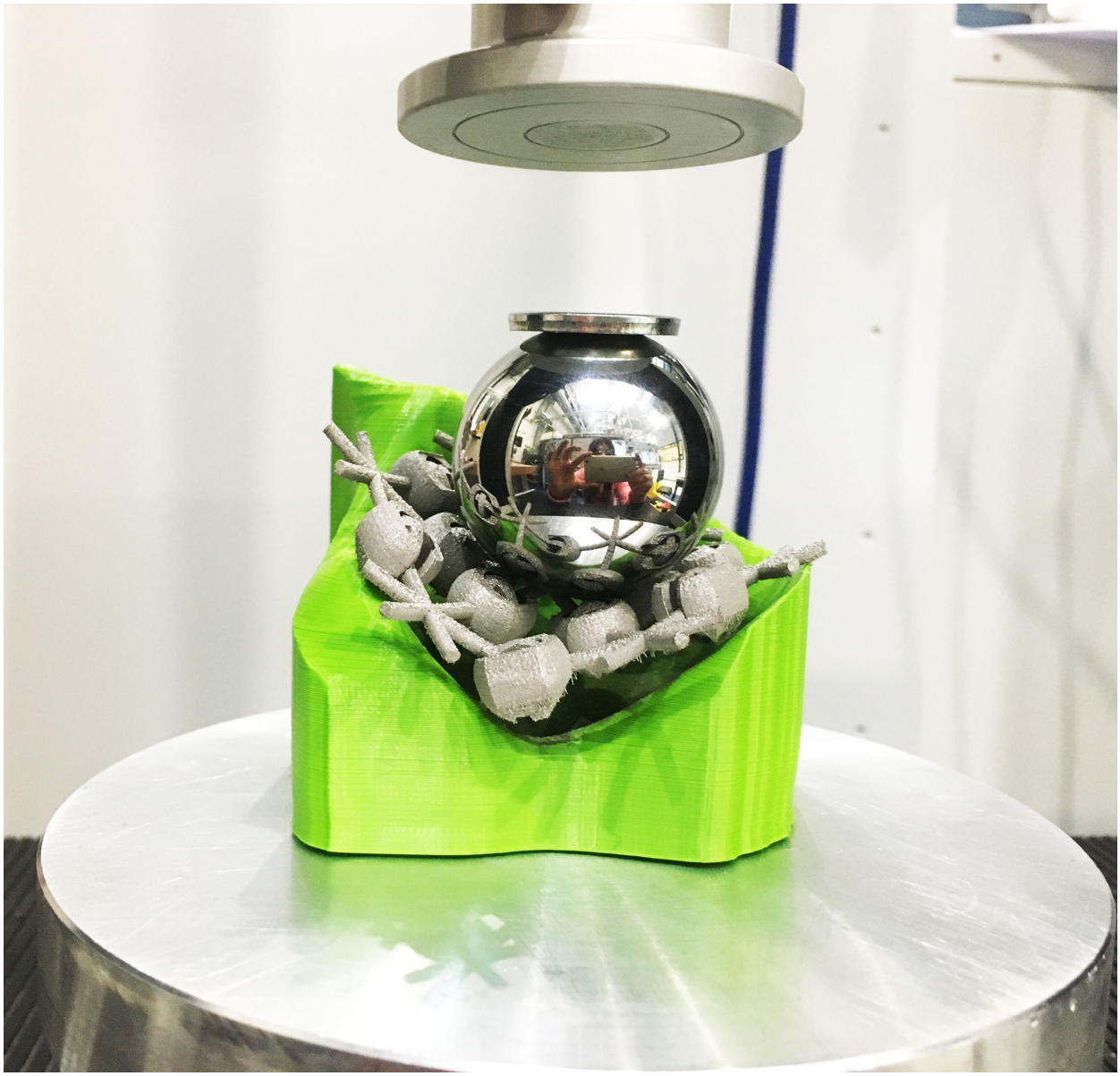

Figure 2.31: Setting of subsequent elements during the uni-axial compression testing.

Results

3.1 Post-Printing Evaluation

Revolute Joints

The revolute joints were the only joints printed in-situ with SLM in previous researches. It is already mentioned in Chapter 2, that a preliminary effort took place for verification of the literature. However, due to the troublesome outcome (demonstration of the bending phenomenon) of the preliminary effort, two other build orientations were examined, including the horizontal one and the 45^o tilted with a certain distance between the rings. The three printed samples have been depicted in Figure 3.1. The only configuration that had not supports inside the clearances was the horizontal one. This is why, the rest of the supports were removed easily. The other two included supports inside the clearance, but the supports could be removed after putting some effort. The negative thing about every sample was that the surface deterioration inside the clearances and around the part itself was present.

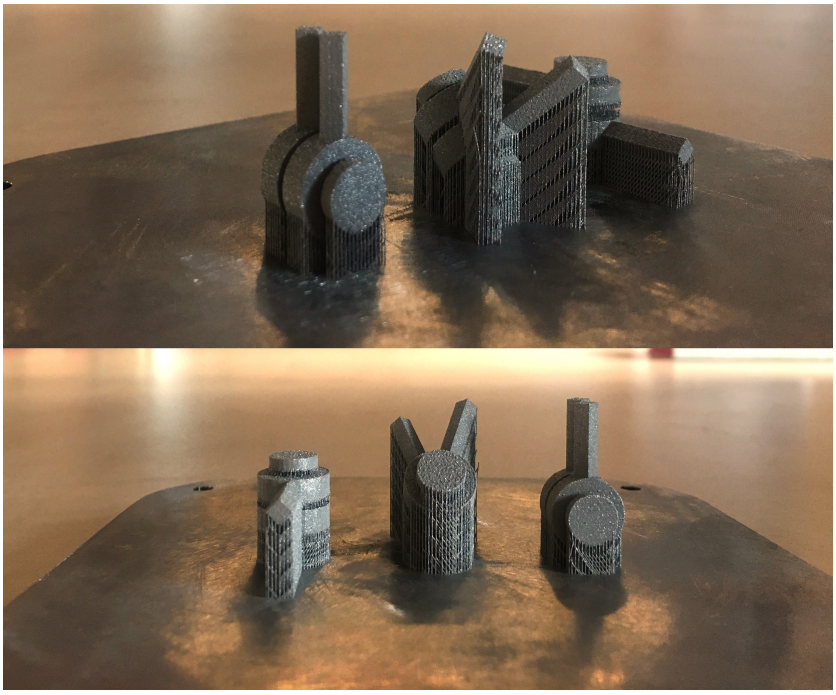

Figure 3.1: Illustration of the printed samples at the build plate. Three configurations are used including vertical, horizontal and tilted of 45^o.

Prismatic Joints

An attempt took place to examine the potential of printing the proposed design of the prismatic joint. A vertical configuration used and the successful printing was held out. The chosen clearance was 0.3mm. The detailed dimensions of this joint can be found in Appendix B. The printed sample also presented the adequate motion, since no supports were inside the clearances (Figure 3.2). Apart from the single prismatic joint, the mesh of prismatic joints as well as its expanded configuration were also printed (Figures 3.3a and 3.4). Again, no supports existed inside the clearances allowing adequate motion between the parts (Figures 3.3b and 3.4). Surface deterioration was noticed only around the supported areas.

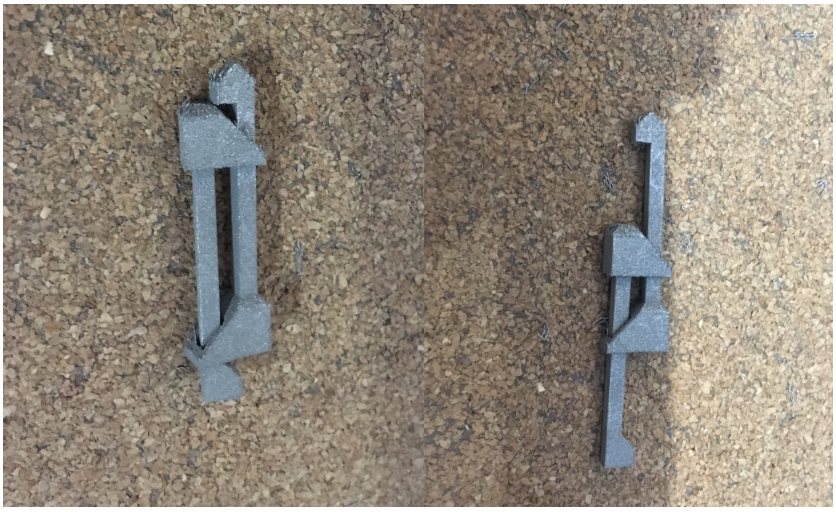

Figure 3.2: The successfully printed prismatic joint with adequate motion.

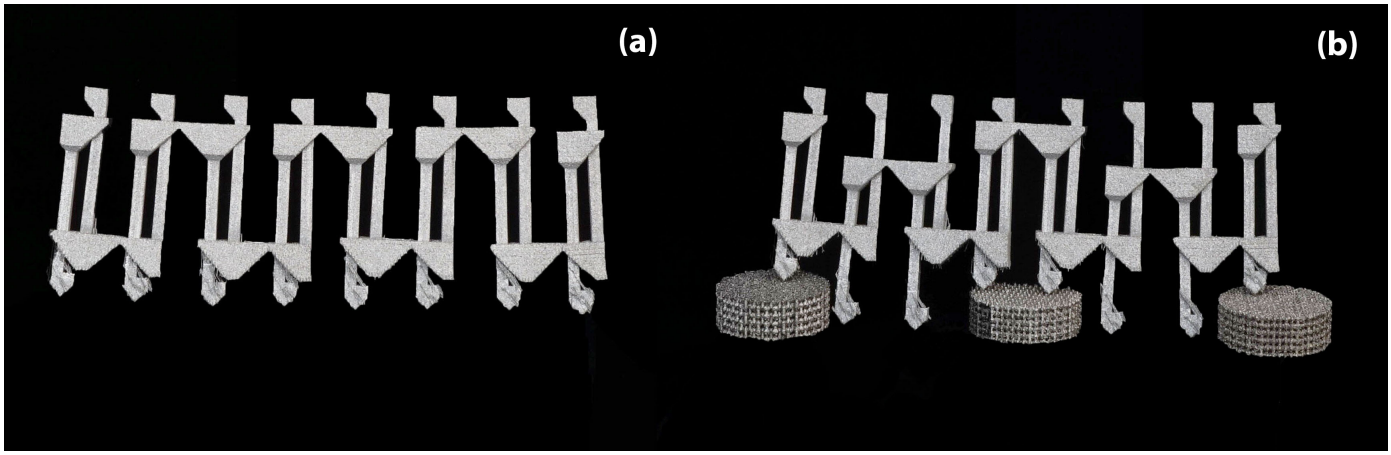

Figure 3.3: Printed configuration of multiple vertical prismatic joints in series in its printing position (a) and in motion(b).

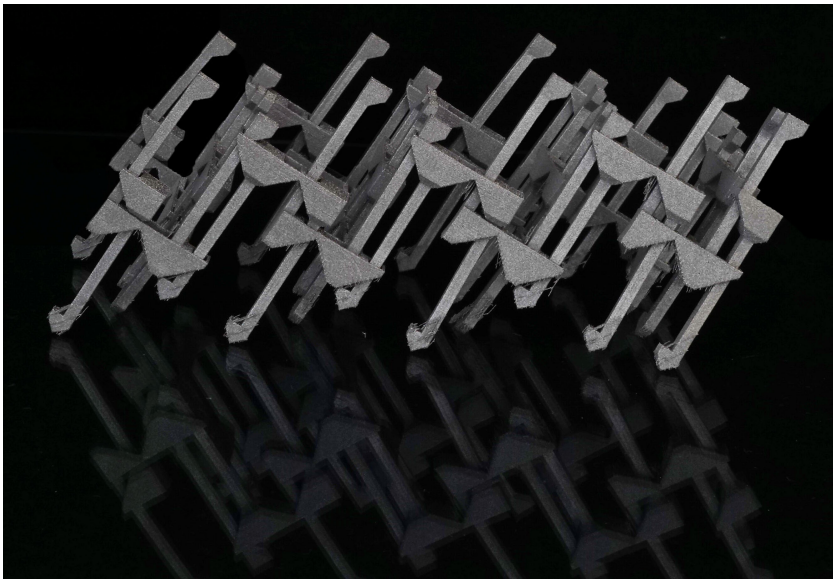

Figure 3.4: Printed configuration of multiple vertical prismatic joints in a multi-dimensional web of metal joints.

"Sliders" with Increased DOF

Replacing the horizontal overhangs of Figure 2.11a with inclined edges has been proven successful. The whole configuration of Figure 2.11b has been printed without supports (3.5a). Moreover, the entire configuration has the ability to twist and turn, like a metal clay that can take the form of irregular shapes (Figure 3.5b).

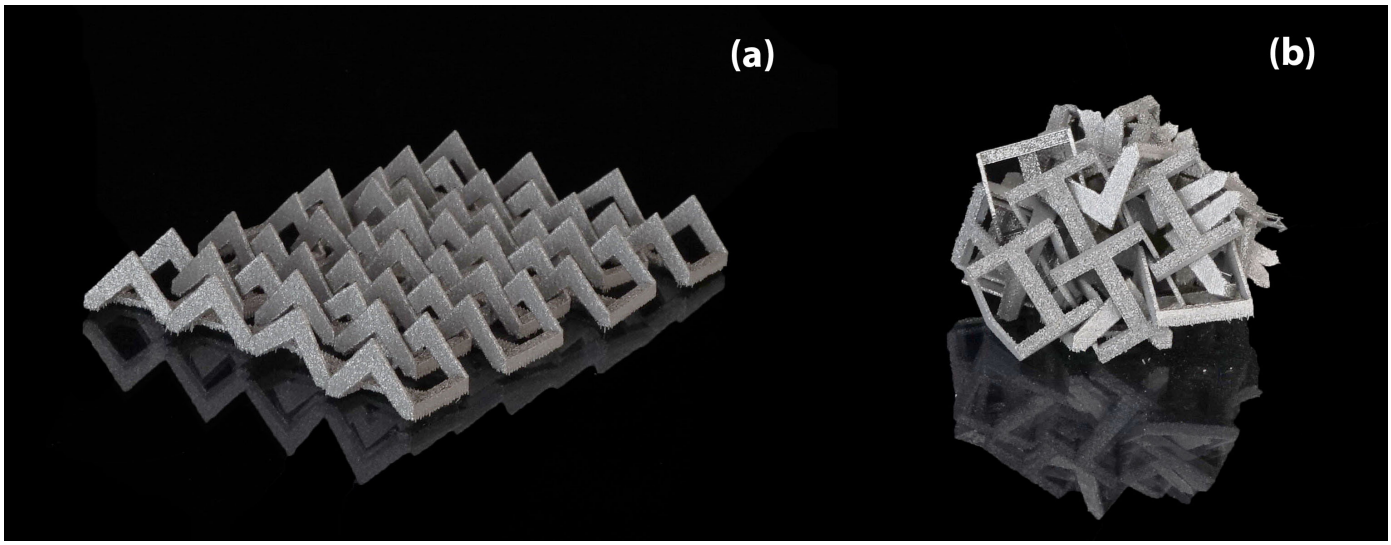

Figure 3.5: (a)Printed horizontal "prismatic" configuration without supports, (b) The proposed horizontal configuration has the ability to deform in any shape.

Rhombus Clay

The design configuration of Figure 2.13 has been printed with success (Figure 3.6a). Based on theory, this structure should not have been in supports, since it includes only inclined edges of 45°. However, to ensure its structural ability during printing, the bottom hemisphere of the meta-biomechanism has been printed with supports, as Figure 3.6 indicates. These could be removed fairly easily with hands. This design offers the possibility of both sliding and rotational motion at a component level. In this way, the structure can form any irregular shape, like Figure 3.6b depicts.

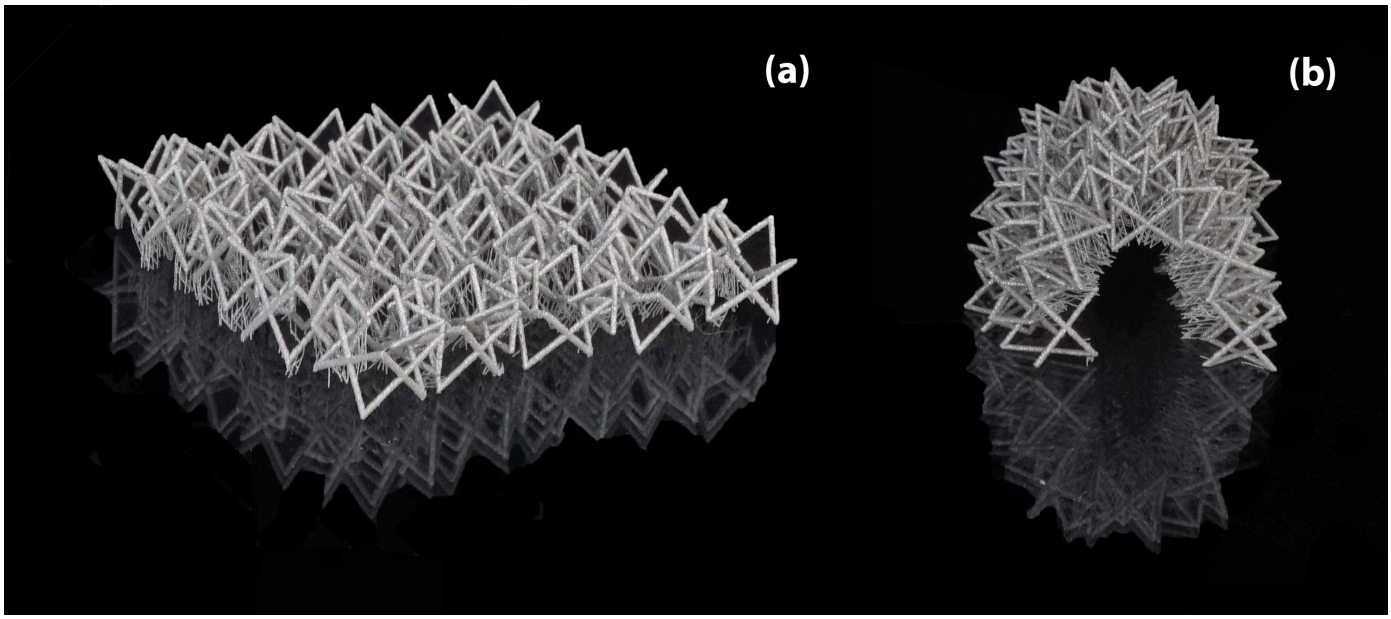

Figure 3.6: (a) Successful printing of the structure with interfered self-supporting unit cells to achieve increased DOF, (b) The proposed structure of interfered unit-cells offers the possibility of deforming in any irregular shape.

"Caterpillar" chain of interconnected Ball-Socket joints

The "Caterpillar" chain of interconnected ball-socket joints (Figure 2.14g) has been printed successfully (Figure 3.7a). The supports were accessible and could be removed fairly easily, since a clearance of 0.5mm was chosen. This clearance was smaller than the ones reported in research for a ball-socket joint. As Figure 3.7b depicts, this configuration allows a revolute motion between the balls and the sockets. However, the revolute motion was restricted due to the printed dimensional difference. Despite the fact that there was sufficient clearance between the connecting bars and the socket slots in terms of design, the printed result has proven the opposite.

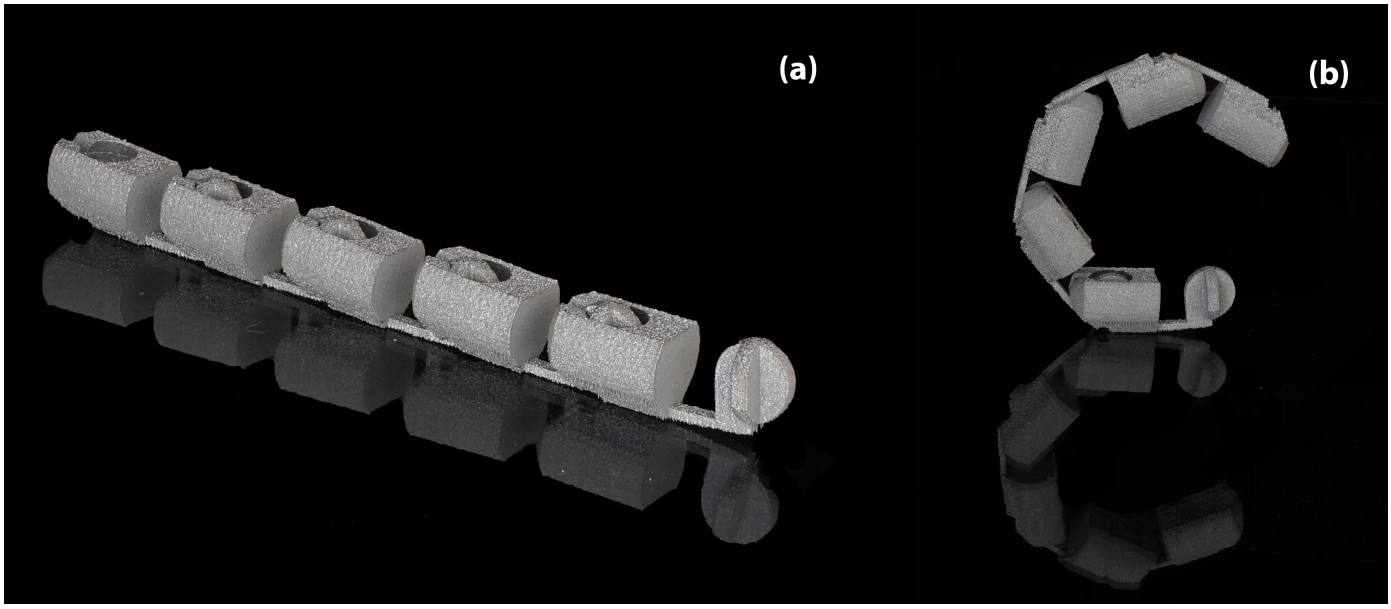

Figure 3.7: (a) Printed "caterpillar" chain of inter-connected ball-socket joints, (b) "Caterpillar" chain of inter-connected ball-joints in motion.

Star-shape interconnected Ball-Socket joints

The star-shape configuration of ball-socket joints has been printed successfully followed by adequate motion, as Figures depict. The supports could be removed easily, allowing the structure to move in multiple directions (Figure 3.8). This wide range motion is restricted though. The specific configuration of interconnected ball-socket joints with star connectors restrict its wide range of motion. Surface deterioration was once again noticed around the supported parts.

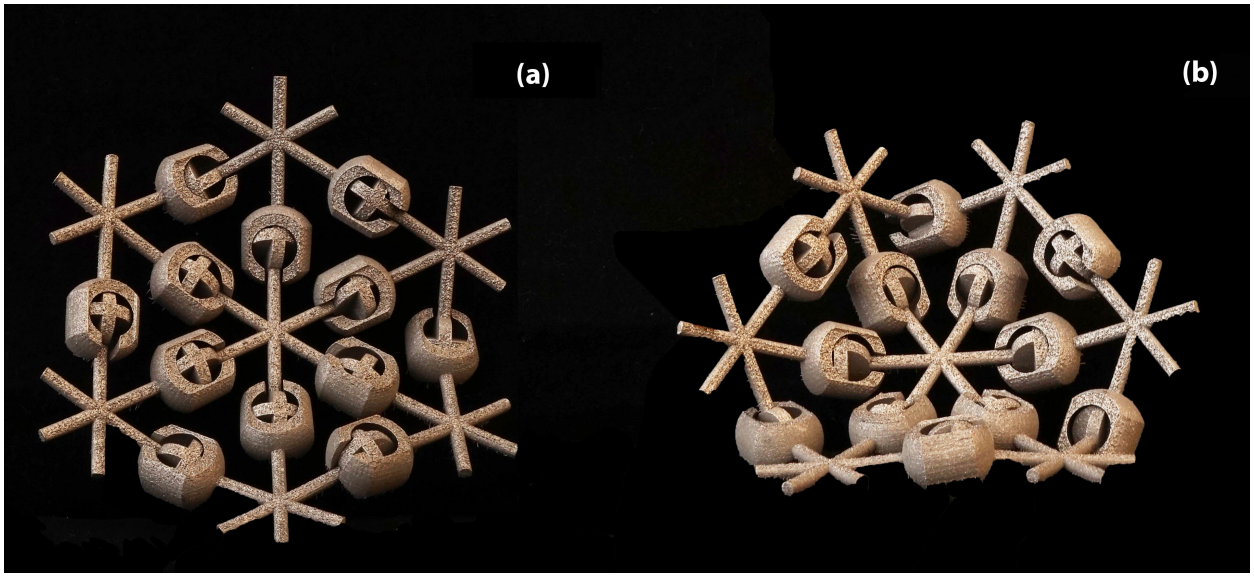

Figure 3.8: (a) Printed Star-Shape configuration of inter-connected ball-socket joints, (b) Star-Shape configuration of inter-connected ball-socket joints in motion.

3.2 Surface Morphing Experiments

3.2.1 First Approach

The results exported from the Surface Morphing Experiments have been depicted in Figures 3.9, 3.10, 3.11 and 3.12. The results are distinguished based on the Cut View for easier comparison. The absolute difference per meta-biomechanism, for each Cut View, can be found in Table 3.1.

Table 3.1: Shape Morphing Experiments-Results from the 1st Approach per cut view

Surface Morphing Experiments	Absolute Difference	
	1st Cut View (Mean +- STD)	2nd Cut View (Mean +- STD)
Prismatic	3.66 +- 2.558	6.606 +- 0.762
"Slider" with increased DOF	0.187 +- 0.055	0.358+-0.195
Rhombus Clay	0.157+-0.037	0.371+-0.314
"Caterpillar" Chain	0.513 +- 0.497	0.920+-0.729
Star-Shape Ball-Socket Joints	0.209+-0.172	0.643+-1.058

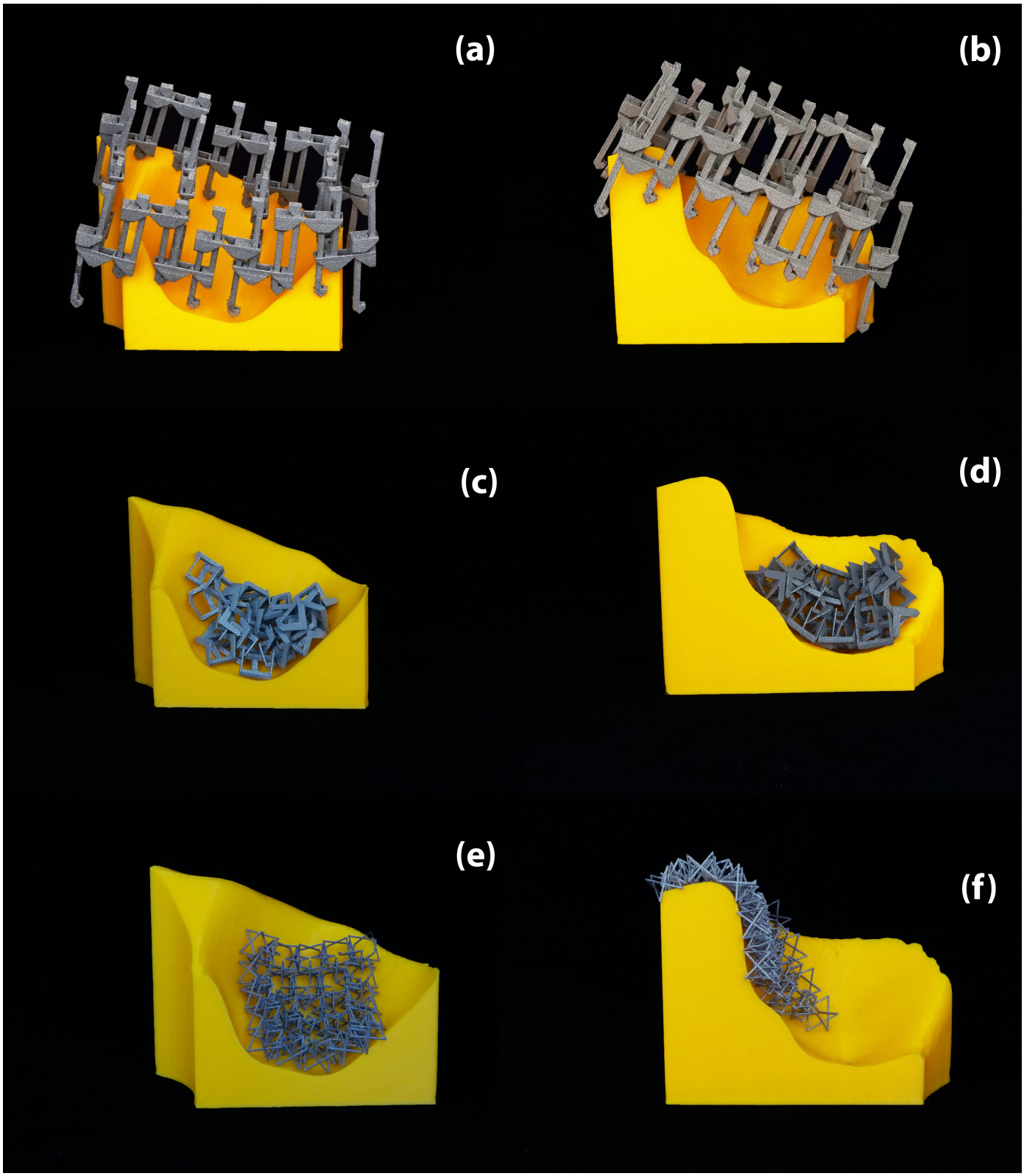

Figure 3.9: Fitting of the proposed meta-biomechanism on the reference surface (a) Prismatic: 1st Cut View, (b) Prismatic: 2nd Cut View, (c)"Slider" with increased DOF: 1st Cut View, (d) (e)"Slider" with increased DOF: 2nd Cut View, (f) Rhombus Clay: 1st Cut View, (g) Rhombus Clay: 2nd Cut View.

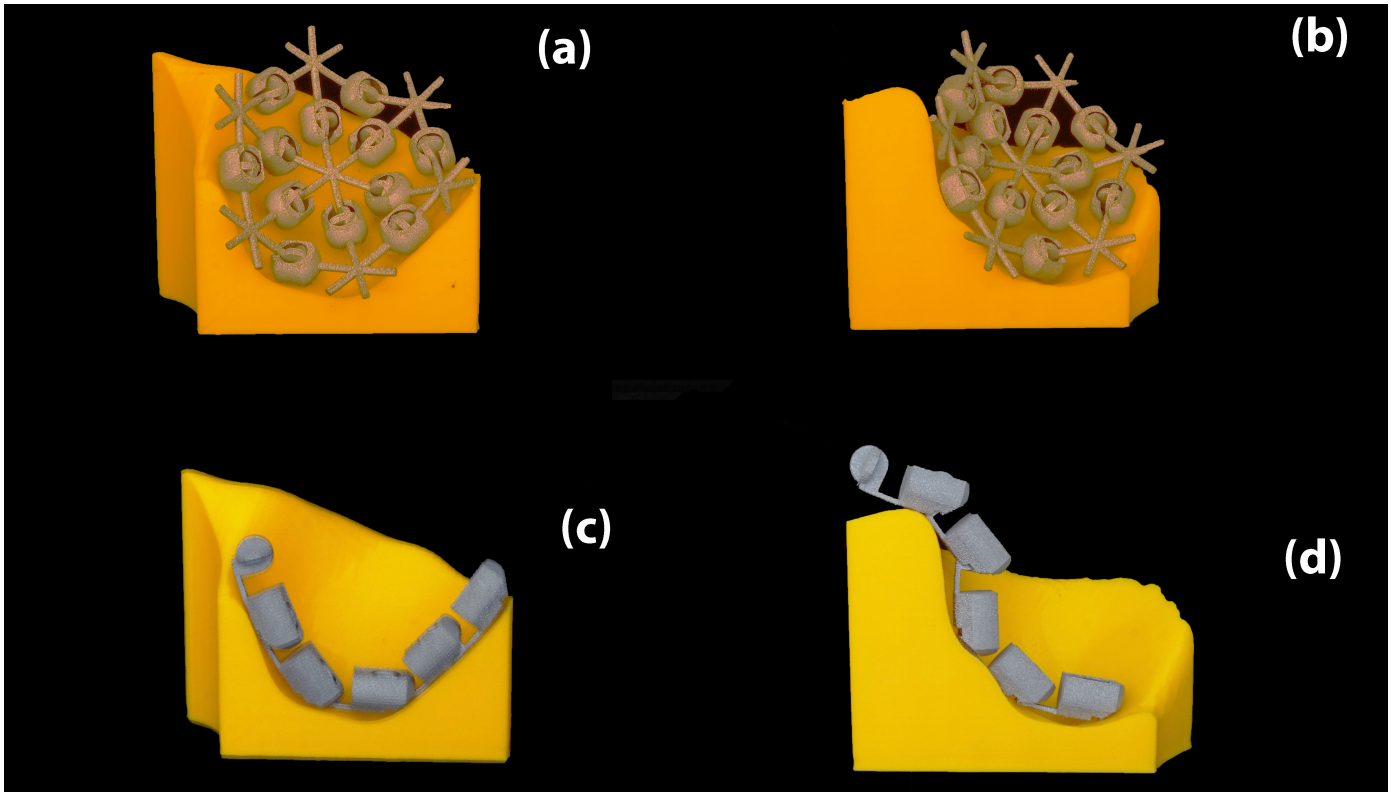

Figure 3.10: Fitting of the proposed meta-biomechanism on the reference surface (a) Star-Shape Ball-Socket: 1st Cut View, (b) Star-Shape Ball-Socket: 2nd Cut View, (c)"Caterpillar Chain: 1st Cut View, (d)"Caterpillar Chain": 2nd Cut View.

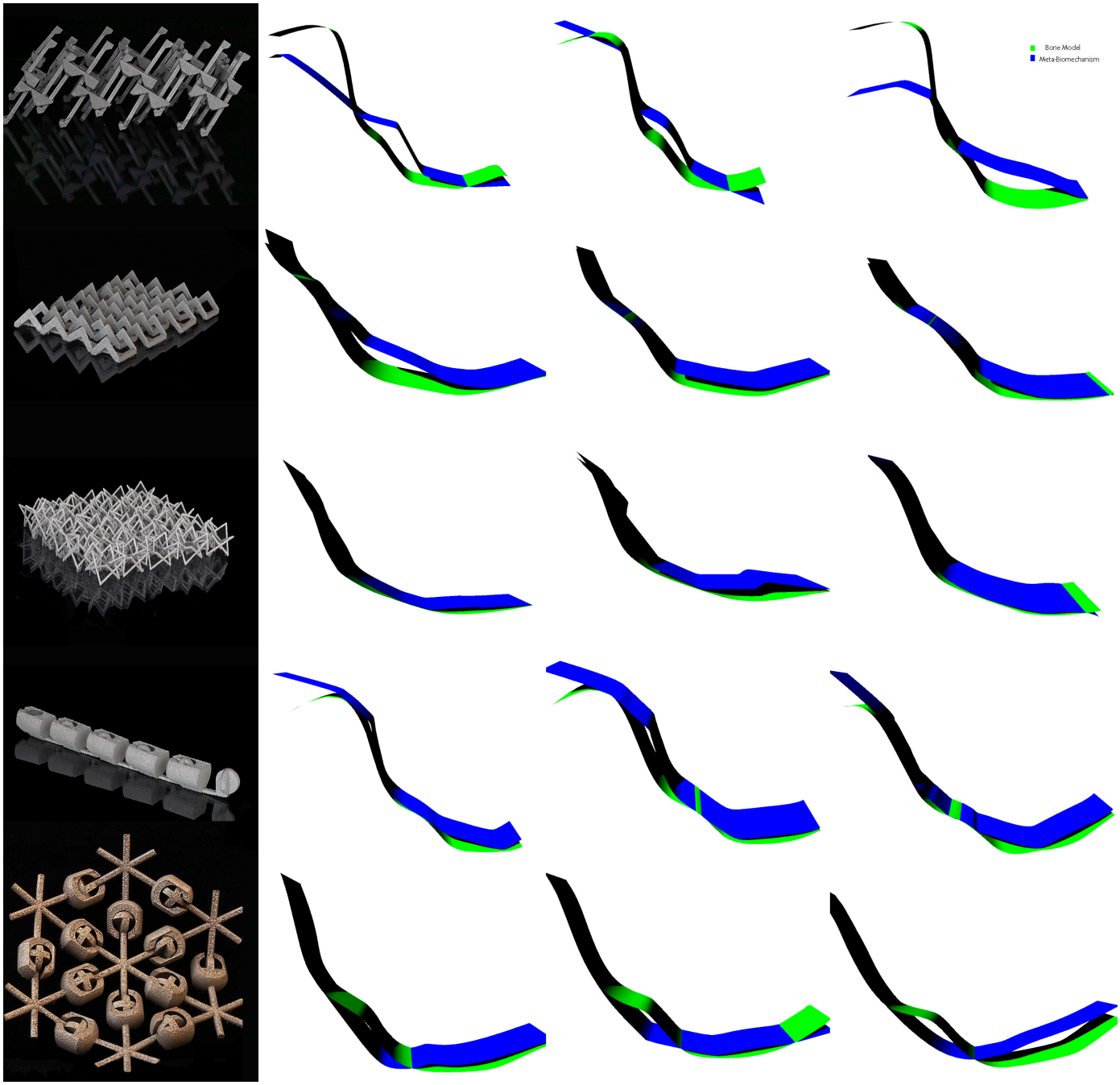

Figure 3.11: Surface Morphing Results-1st Approach:1st Cut view

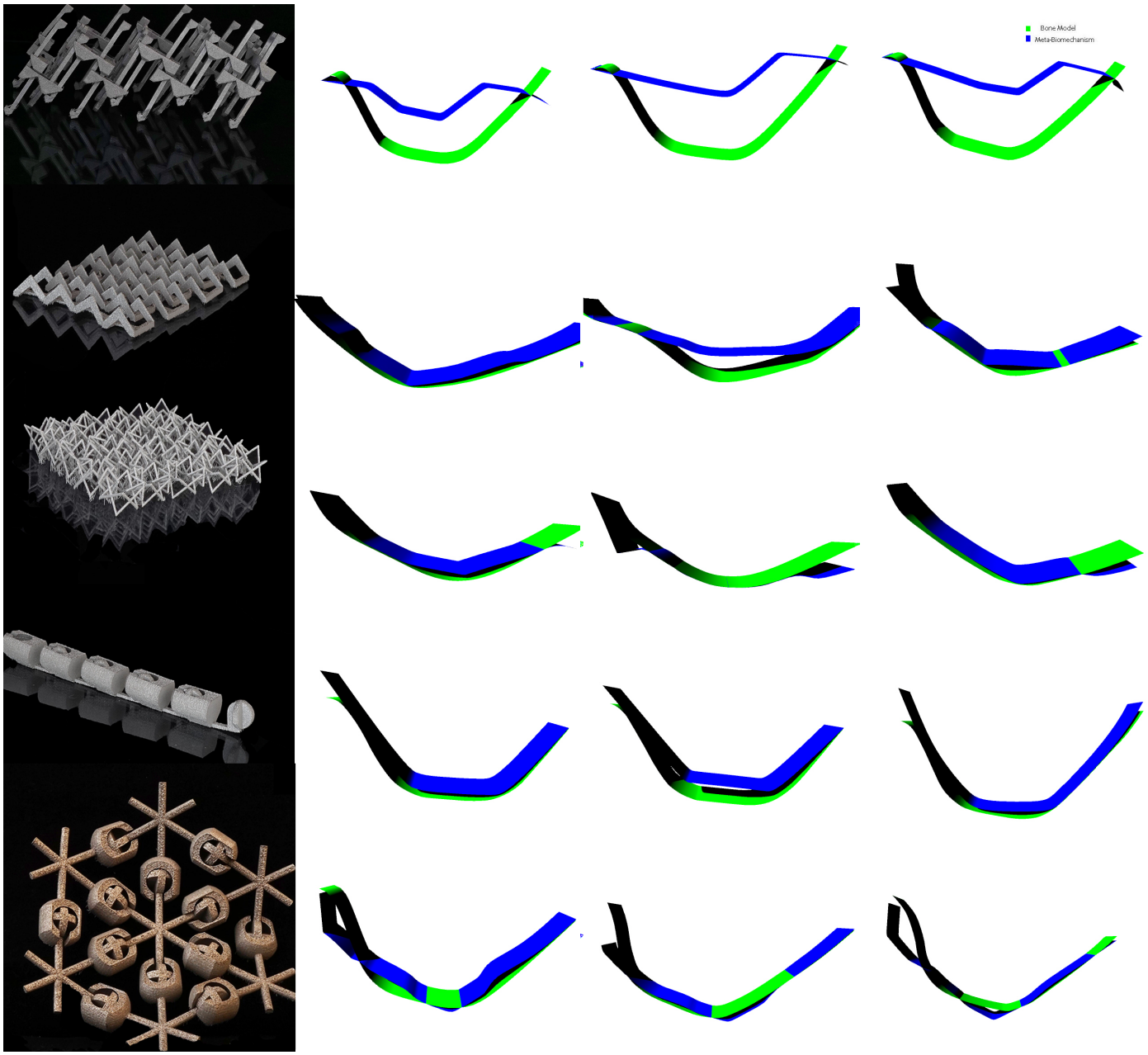

Figure 3.12: Surface Morphing Results-1st Approach:2nd Cut view

3.2.2 Second Approach

Table 3.2 includes the absolute difference (mean value +- STD) between the bone model and the structure, in a three-dimensional space. The graphical results have been included in Figure 3.13. It should be noticed, that results concerning the prismatic joint were not exported. This structure was scanned, but its big height did not result in sufficient cloud data, to assess its fitting.

Table 3.2: 3D Scanning Evaluation: Results

Surface Morphing Experiments- 2nd Approach	Absolute Difference (Mean +- STD)
"Slider" with increased DOF	34.086+-3.28
Rhombus Clay	24.31+-5.25
"Caterpillar" Chain	39.45+-3.324
Star-Shape Ball-Socket Joints	41.563+-1.32

Table 3.3 depicts all the values exported by three users, concerning the four structures. Two-way ANOVA analysis was then implemented on these data, and the respective SEM (Standard Error of the Mean) were calculated. The inter- and interobserver's variability were calculated according to the steps included in relevant literature.[70] However, transformation of the Table 3.3, was necessary to implement this method (Transformed Table is table 3.4). Table 3.5 represents the ANOVA table. The next step is calculating the appropriate variances (Table 3.6), using the components of ANOVA table. Finally, these values are used to calculate the final standard error of measurements (SEM) (Table 3.7). Additionally, one more method was implemented to measure the intra- and interobserver′s variability. This method calculates the SEM by using the individual Standard Deviations of multiple paired measurements and users. The SEM calculated with this method can be found in Table 3.8.

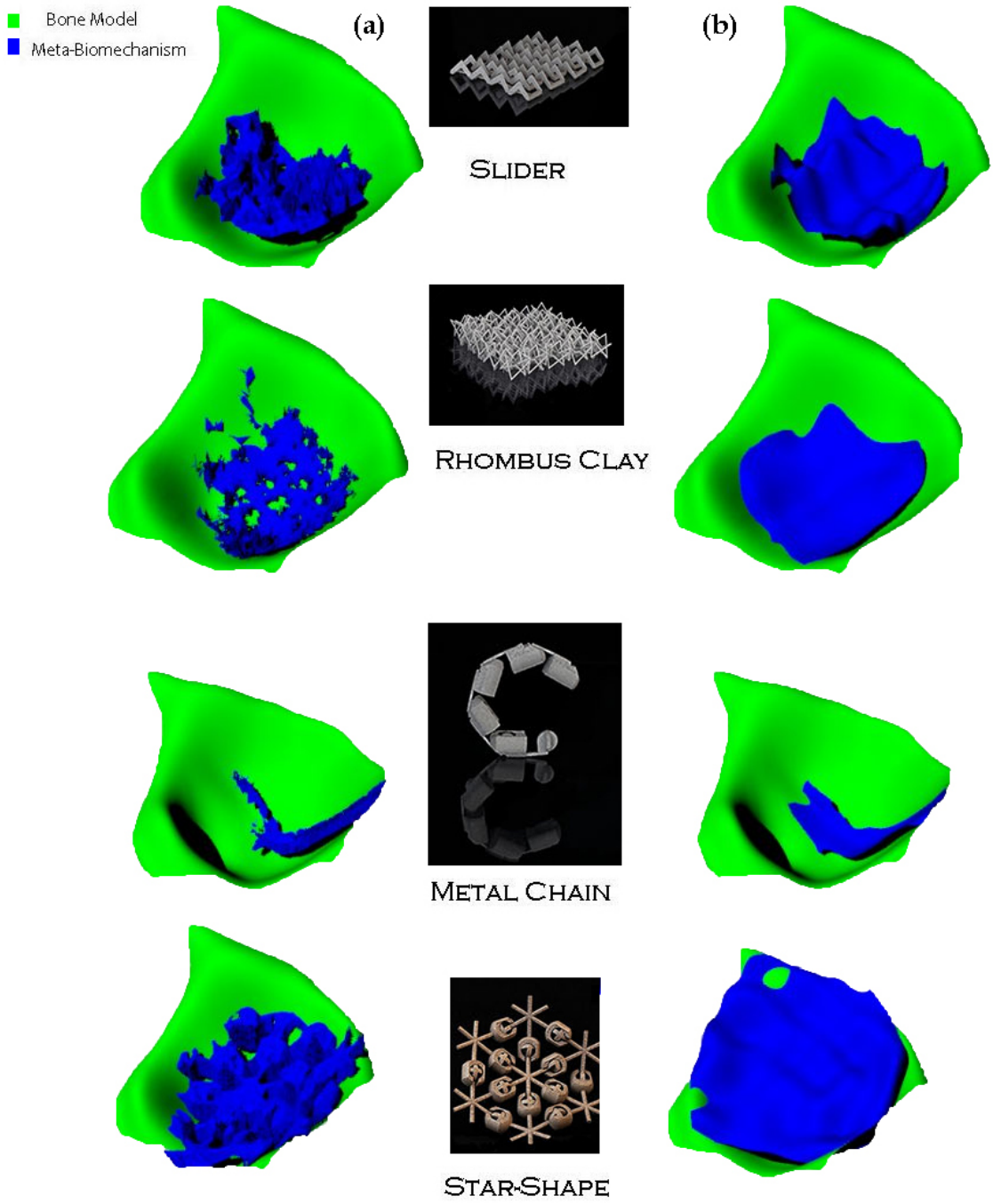

Figure 3.13: Surface Morphing Results-2nd Approach: a) Fitting of the structure on acetabular surface, b) Patched Surface of structure on the acetabular surface.

Table 3.3: Measurements reported by three users, three times, for each proposed structure.
* M=Measurement

Rhombus	User 1			User 2			User 3		
	M1 21.036	M2 18.112	M3 18.51	M1 20.893	M2 24.129	M3 28.88	M1 30.078	M2 30.635	M3 30.69
"Slider"									
	M1 37.859	M2 17.98	M3 25.851	M1 37.75	M2 35.82	M3 18.714	M1 35.38	M2 27.286	M3 70.681
Caterpillar									
	M1 30.288	M2 38.992	M3 12.65	M1 33.74	M2 35.085	M3 23.97	M1 32.453	M2 17.362	M3 12.125
Star-Shape									
	M1 43.91	M2 41.8	M3 42.75	M1 42.4	M2 50.747	M3 28.34	M1 42.96	M2 62.37	M3 57.925

Table 3.4: Transformation of Table 3.3 to implement a two-way ANOVA analysis

Designs		Rhombus	"Prismatic"	"Caterpillar"	Star-Shape
Observer 1	Measurement 1	21.036	37.859	30.288	3.91
	Measurement 2	18.112	17.98	38.992	41.8
	Measurement 3	18.51	25.851	12.65	42.75
Observer 2	Measurement 1	20.893	37.75	33.74	42.4
	Measurement 2	24.129	35.82	35.085	50.747
	Measurement 3	28.88	17.714	23.97	28.34
Observer 3	Measurement 1	30.078	35.38	32.453	42.96
	Measurement 2	30.635	27.286	17.362	62.37
	Measurement 3	30.69	70.681	12.125	57.925

Table 3.5: Implementing a two-way ANOVA analysis, by using data from Table 3.4.

Source	SS	dF	MS	F	Prob> F
Columns	2521.33	3	840.444	7.56	0.001
Rows	441.45	2	220.727	1.98	0.1594
Interaction	748.79	6	124.799	1.12	0.3793
Error	2669.42	24	111.22		
Total	6381	35			

Table 3.6: Calculations of appropriate variances using the components of Table 3.5

Repeatability and Reproducibility terms	Variance Nomenclature	Equation	σ^2
Repeatability (Intraobserver variability)	$\sigma^2 error$	MSE	111.226
Reproducibility (Observer variability)	$\sigma^2 observer$	(MSobserver MSO S)/(nxm)	7.994
Interaction	$\sigma^2 SxO$	(MSO S-MSE)/m	1.131
Total R and R (Interobserver variability)	$\sigma^2 R\&R$	Sum of the cells above	120.351

Table 3.7: Final Standard Error of Measurements(SEM)

Equation	Equals	
SEM intra	$\sqrt{\sigma^2 error}$	10.546
SEM intra	$\sqrt{\sigma^2 error + \sigma^2 SxO}$	10.6
SEM inter, fixed effects	$\sqrt{\sigma^2 error + \sigma^2 Observer + \sigma^2 SxO}$	10.97

Table 3.8: Intra and Inter SEM calculated, using the individual Standard Deviations of multiple paired measurements and users.

Inter-Observer Variability	Individual SD	Intra-Observer Variability (User 1)	Individual SD
Rhombus			
Users 1-2	0.101	Measure 1-2	2.067
Users 2-3	6.495	Measure 2-3	0.281
Users 1-3	6.394	Measure 1-3	1.786
"Slider" with 4 DOF			
Users 1-2	0.077	Measure 1-2	14.056
Users 2-3	1.676	Measure 2-3	5.567
Users 1-3	1.753	Measure 1-3	8.49
Caterpillar			
Users 1-2	1.068	Measure 1-2	6.154
Users 2-3	0.396	Measure 2-3	18.627
Users 1-3	0.672	Measure 1-3	12.472
Star-Shape			
Users 1-2	2.441	Measure 1-2	1.492
Users 2-3	0.91	Measure 2-3	0.82
Users 1-3	1.531	Measure 1-3	0.672
Mean +- STD	1.96+-2.21	Mean +- STD	4.96 +- 5.877
SEM using eq. 2.1	8.7257	SEM using eq. 2.1:	59.13

3.3 Uni-Axial Compression Testing

The force-displacement curves, exported from the compression testing have been depicted in Figure 3.14. Table 3.9 includes the Force needed to break each structure, in this specific configuration. To determine the failure point, the definition of the break type is necessary. A sharp break was selected, as indication. This is defined at the point, when the load drops by 5%, from its peak load.[72] Taking into account, that the tested structures include several joints, the amount of peak loads will be more than one. Thus, the force needed to achieve a sharp break, was calculated based on a drop of 5%, from the first load peak.

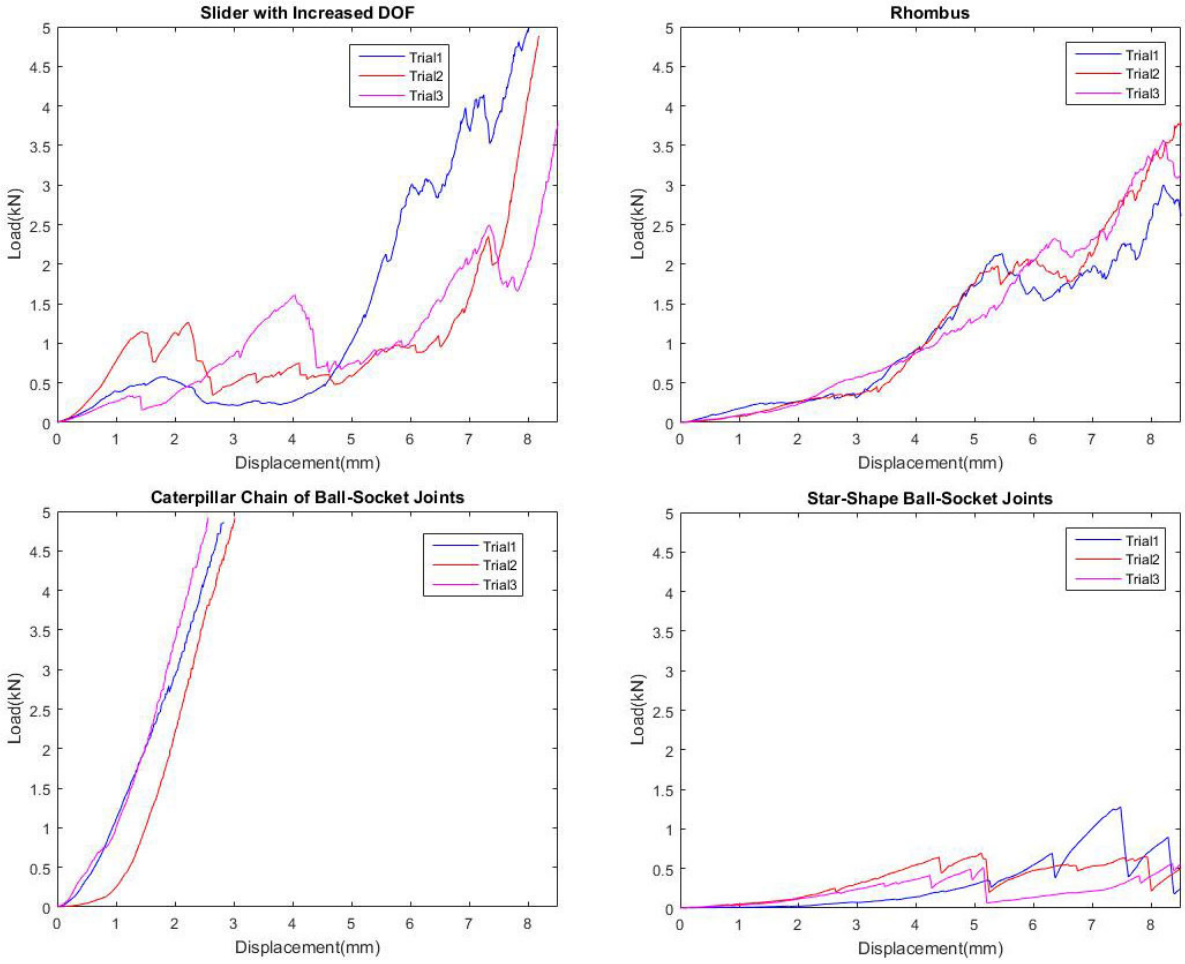

Figure 3.14: Force (kN)-Displacement(mm) diagrams of Meta-Biomechanisms.

Table 3.9: Force needed to achieve a sharp break- Load drop of 5%

Meta-Biomechanisms	Force (kN) at first Force drop of 5%
Slider with increased DOF	1.19 +- 0.898
Rhombus	0.710 +- 0.523
"Caterpillar" Chain	$\geq 5kN$
Star-Shape Ball-Socket Joint	0.4703 +- 0.153

Discussion

4.1 Analysis

4.1.1 *Design Analysis and Post-Printing Evaluation*

Generally, the selection of the design approach has been proven successful. Reported mechanical joints were unsuitable for their in-situ fabrication with SLM, let alone for their incorporation into multi-joint structures. Starting with a systematic design method, was proven sufficient, to find out of the box solutions. However, some suggesting gaps were empty, since no solutions existed for them. This is something strongly dependent on the author's creativity. Systematic design approaches can only assist, by showing where to search for creative solutions. New types of "joints" were indeed conceived and their design modification was effortless. Study of their design constraints and subsequent implementation of the general design rule assisted this step. Furthermore, brainstorming was an essential piece of this procedure, proving the superiority of this method.

Transforming them not to have vulnerable geometries, was a simple and efficient way. Generally, the scale used in the designs was similar to the one found in the majority of reported literature. Regarding the new concept solutions, there was no particular reasoning behind the scale, the size and the thickness. The mechanical properties of the designs, did not play a role in their design optimization. The most important factor determined this step, was the printability of each design. Incorporating mechanical properties, as a design criterion, can be implemented in future research. Finally, the proposed designs were printed with success using SLM.

Generally, the printed samples were a good representation of the STL models, besides some dimensional differences. Surface deterioration was present in every design, especially around the supported areas. However, each printed sample had distinct characteristics, explaining the following, detailed post-printing evaluation.

Revolute Joint

The revolute joint was the only joint printed in the reported literature, in its vertical orientation. For theoretical verification, a small printing example was held out. The vertical print of the revolute joint proved the existing literature wrong, since its supports could not be removed fairly easily. For this reason, the same joint was built with two different orientations (horizontal, tilted), to research its possibility of being printed in-situ. Again, the result was inefficient, since the printing procedure was interrupted by undesirable phenomena and further modification of design appeared to be necessary. Subsequently, the modified designs were successfully printed with adequate mobility.

It was proven that the vertical configuration led to less supports indeed, but the support structures within the clearances could not be removed easily. However, the adequate mobility was achieved, despite the apparent surface deterioration within the clearances. Regarding the tilted configuration, the sample had the adequate mobility and the supports inside the clearances could be removed fairly easily. As far as the horizontal orientation is concerned, sufficient mobility was achieved, since the supports within the clearances could be removed fairly easily. This was logical since the crucial part of the design was built perpendicular to the build plate.

Prismatic Joint

The prismatic joint was the easiest, in terms of design modification. The initial design could have been printed without clearances' supports. However, with the modifications implemented, the supports were significantly reduced. A vertical orientation was selected, positioning the clearance site perpendicular to the build plate. Thus, there were no supports within the clearance, resulting in a sufficient and smooth motion. The same observations count for the expanded version of the prismatic joint. However, the connections of the distinct joints in this configuration, are weak and can be broken under force.

"Sliders" with increased DOF

This structure is self-supporting, and the only supports existed, to reassure its connection to the build plate. Despite the fact that, it was designed to have two translational DOF, it demonstrated the ability to take irregular shapes (e.g. ball). The negative thing about this structure though, is its incapability to return to its original form afterwards.

Rhombus Clay

Rhombus Clay, is also a self-supporting structure, since everything is at an angle of 45°. However, supports were incorporated during printing, to ensure its structural integrity. The nice thing about this structure, is that multiple DOF, characterize each unit cell. Thus, it can take the form of every possible irregular shape. The most significant thing is, that it never loses its form. It was mentioned above, that the mechanical strength did not play any role in design optimization. Consequently, the strut thickness and the unit cell's size were abstractly selected. By modifying these characteristics, the motion and mechanical capabilities of this structure can be further improved.

"Caterpillar Chain of Ball-Sockets"

Ball-Socket joints are the most difficult, to be printed in-situ with SLM. Their spherical shape, eliminates the possibilities of being printed with SLM. Reducing the DOF of a ball-socket joint though was proven successful since the number of supports was significantly lower. The supports were accessible and could be removed fairly easily. Besides that, the clearance reduced to 0.5mm, without affecting the motion of the structure, neither its printability. This is very important if one considers the smallest clearance of an in-situ, polymer ball-socket joint (1mm). Nevertheless, it was the only structure with noticed dimensional differences from the CAD model. The bar connecting the socket and the ball, could not sufficiently be moved inside the socket's slot. In the CAD model, there was a distance of 0.3mm, separating the connecting bar and the socket's slot. However, this distance was

proven insufficient, taking into account the printing capabilities of SLM.

Star-Shape configuration of Ball-Socket Joints

The printing of this structure was successful. The supports were accessible and removed fairly easily. An adequate motion noticed although the specific configuration restricted the motion abilities of a ball-socket joint. In other words, the stars connecting the ball-socket joints, restrict the structure's motion. Thus, this structure can only fit small depths, despite the fact that was designed to take concave shapes of any depth. The solution towards this problem would be to incorporate revolute joints in the star's rings. The combination of two different types of joints would increase the range of motion.

Evaluation of Meta-Biomechanisms according to the initial design criteria

Figure 4.1 includes how each meta-biomechanism scores according to the initial design criteria, using a Harri's Profile. Both the Rhombus Clay and the Slider, score sufficiently in motion and the amount of the supports. However, the Rhombus Clay is characterized by two more DOF and less amount of supports compared to the Slider. The Prismatic Joint is second, with a total score of three, although it is characterized by the least amount of supports. The Prismatic is followed by the Star-Shape, which scores an overall score of one. The one DOF and the large amount of supports can explain that. Finally, the "Caterpillar" structure demonstrates an overall score of zero. This is why, it is characterized by one DOF and the greatest amount of supports. Generally, the best design is the Rhombus clay with six DOF and a small amount of supports. In terms of supports though, the Prismatic joint comes first. In contrast, "Caterpillar" is the last one with one DOF and the largest amount of supports.

	DOF	Amount of Supports (m2)	Type of DOF	Overall Score
Revolute	NOT EXAMINED			0
Prismatic	1	24.92	translational	3
Slider	4	47.5	translational, rotational	6
Rhombus	6	30.28	translational, rotational	6
Caterpillar Ball-Socket	1	184.01	rotational	0
Star-Shape Ball-Socket	2	138.03	rotational	1

-1	Does not meet the requirement
0	Just meets the requirement
1	Meets above the requirement and below the wish
2	Meets the wish

Figure 4.1: Evaluation of proposed meta-biomechanisms according to the initial design criteria, using a Harri's profile.

4.1.2 *Surface Morphing Experiments*

1st Approach

Generally, all the Meta-Biomechanisms score sufficiently in mobility, besides the Prismatic one. The one translational DOF of this joint led to this result. Four of the five proposed designs are characterized by an absolute difference below one, with the Rhombus Clay showing the smallest difference of 0.157. The high number of DOFs probably results in this great surface morphing property. However, the "Slider" with two translational DOF is just close to it. The small difference between the two cut-views of these designs, prove their ability to fit well on a three-dimensional irregular surface. In contrast, the bigger difference in the cut views, of the other two Ball-Socket joints, prove their inferiority. Only in case of an irregular curve, both the "Caterpillar" and the Star-Shape score pretty well. This is logical since the Star-Shape has two rotational DOF and the "Caterpillar" one.

This approach constitutes an effort, to take quantitative results of how a structure fits on a surface. The disadvantage is its two-dimensional nature, although the existence of the two cut-views, assist to a more realistic representation. This method, takes as a requirement, a constant continuity of the tested curve in space. This is not true, considering the irregular nature of the acetabular surface. On the other hand, this method is independent of the user's perspective, reassuring the repeatability of the exported results.

2nd Approach

The second method used in Surface Morphing Experiments, proves again that the Rhombus Clay is superior in terms of motion. The Slider with increased DOF comes second, with a moderate percentage difference of 28.68%. The "Caterpillar" Chain demonstrated quite comparable absolute difference with the Slider, by being 13.6% inferior to the latter. Finally, the Star-Shape, in its turn, is quite similar to the "Caterpillar", since their percentage difference is only 5%.

Generally, this method is a step forward towards a more realistic representation of the structure's fitting. However, the STL file generated from scanning contains a lot of noise. Consequently, the STL file characterizing the structure's fitting is again not a good representation of the reality. Moreover, this method is dependent on the user's perspective, since noisy facets should be deleted and the patched surface should be trimmed.

Generally, the results of both methods are consistent in terms of an order. Metal Clay is the most superior structure in mobility. The only difference is that in the first method the most inferior is the "Caterpillar", wherein the second the Star-Shape. Additionally, both methods, include two groups of comparable structures. The first group includes the Rhombus Clay and the Slider with increased DOF, whereas the second includes the "Caterpillar" and the Star-Shape. This is logical since each group contains similar types of joints. The differences between the two methods, in terms of numbers, were expected. The first method calculates the mean absolute difference of two curves, while the second the difference of two surfaces.

Unfortunately, the second method is user dependent and calculation of user's variability proves a big SEM of 10.97 between the three users and an error of 10.546 between the same user. Specifically, calculation of the user's variability using another method, proves that intraoberver's variability is significantly larger, compared to the interobserver's variability. Further improvement of this method is

judged necessary to obtain repeatable, reliable and representative results of how a meta-biomechanism fits an acetabular surface.

4.1.3 *Mechanical Testing*

The Force-Displacement curves of the structures are not comparable. This is logical since the structures are of irregular shapes and sizes. Moreover, conclusions concerning the influence of the type of joint or the amount of DOF in mechanical behaviour cannot be derived. However, this test intends to derive only the representative properties of the structures. Additionally, since this is the first time structures like these are mechanically evaluated, validation with prior results is not possible.

The Rhombus Clay and the Slider demonstrated similar behaviour. The only area affected by the applied force was the one beneath the femoral head. The rest of both the structures remained intact. In the Slider with increased DOF, the only point affected was the triangles which were enveloped inwards, while the rest of the structure remained intact. Respectively, the compressed areas of the Rhombus Clay broke into small pieces. The force needed to induce a sharp break in the Rhombus was 0.710kN, while in the Slider 1.19kN. Both the loads are lower than the average contact force found in hip joints during walking. Only the break force of the Slider is comparable with the mean force, found in hip-joint during sitting down. However, by changing the strut and cell size of these structures a greater strength could be achieved.

The "Caterpillar" chain and the Star-shape include the same type of joints. Particularly, the joints′ dimensions are identical. However, their mechanical behavior under compression loading is not comparable. The load of 5kN was proven insufficient to induce a sharp break in the "Caterpillar". Consequently, the break force of the "Caterpillar" is larger than the peak contact force, found in hip-joint during walking. On the contrast, the Star-Shape configuration was proven inferior to the "Caterpillar", with a break force of 0.4703kN. This is logical, since "Caterpillar" fits better in the acetabular model, compared to the Star-Shape. The latter has a significant gap, that separates it from the acetabulum′s surface. Consequently, the structure is not well stabilized inside the acetabulum, leading to its easy breaking. The way the structure fits, is therefore, proven very significant in the way it mechanically behaves under compression.

4.2 Limitations

3D Printing

The basic limitation of this research was the printer's availability. That posed an important obstacle in the research's progress. The amount of possible printed samples was limited, where the time needed for each was remarkable. A significantly bigger amount of concept designs would be tested, in the same time frame, if the printer was exclusively available to this. Furthermore, more printing efforts are necessary, to reassure the repeatability of each design's printability.

Surface Morphing Experiments

The methods used to assess the structures, encounters several limitations. The first approach is characterized by a 2D nature, whereas the 3D scanning incorporates a lot of noise. Besides that, it is characterized, by a dependency on the user's perspective. For this reason, the user's variability was

taken into account. Unfortunately, the big SEM of this procedure, makes its repeatability and reliability doubtful. Reduction of noise is therefore necessary, for a more realistic representation of the structure's fitting. The solution towards this problem, would be to directly compare the initial STL files. However, this procedure would demand extremely high computational capacity.

Mechanical Testing

The mechanical testing of this research aimed the force-displacement curves of the structures. This was the first time, for structures like these to be manufactured. Moreover, they were different to each other in terms of size, shape and weight. Consequently, the nature of these structures and the absence of a well-defined protocol, made the procedure extremely difficult. A new method is necessary to mechanically evaluate structures like these. However, effort was placed to perform a similar compression testing. Despite the fact that different balls were chosen, to reduce the distance between the structure and the femoral head, these did not attach to the structures perfectly. The existence of customized balls, ideally enclosed by the structure, is necessary to achieve an identical starting point for each structure. Moreover, the mechanical testing would have greater scientific importance, if different unit cells' sizes and strut thicknesses of the same structure were compared. The comparison of the structures would be possible, only if the cross-sectional area and the diameter to height ratio was the same. In that case, the stress-strain curves would be derived, and the elastic modulus would be calculated. That would be significantly important, in defining the proper size and shape of them, to be mechanically compatible with the human bone.

4.3 Future Research

This research offers several possibilities of how the study around Meta Bio-mechanism can be expanded. New designs can always be found by implementing this design method or others. The interesting thing would be, to expand the proposed structures towards different directions and planes, to achieve a greater range of motion.

The idea of combining self-supported unit cells could be further explored. Literature provides a big variety of self-supported lattice structures, including both strut-based and bio-mimetic.[74] Deformable implants incorporated with gyroid or diamond interconnected unit cells, would be the ideal candidates for bone substitutes.

Considering their long-term application, scalability should definitely constitute the next step, followed by modification of their biological properties at a nano-scale. In this way, they can be implanted while they promote tissue regeneration. The mechanical evaluation of multiple sizes of each design would be therefore necessary to define the most appropriate scale for implantation.

Depending on the scalability of the joints' dimensions, the applications can be further expanded. Ideas for future research would include the fabrication of multiple-joint mechanisms and the exploration of different materials, such as biodegradable magnesium. Since surface deterioration is prominent in SLM parts, the optimization of process parameters can be further studied and optimized. Various printing experiments will be necessary to define the optimal process parameters and strategies as well as the general rules to design non-assembly mechanisms.

Conclusion

The idea of fabricating non-assembly metal Meta-Biomechanisms using AM techniques sounds more than interesting. These structures can form foldable, metal meshes of joints, to fill irregular cavities of lost bone. Titanium seems a perfect material, considering its biocompatibility. Among several metal-based AM techniques, SLM seems the most suitable printing procedure. However, the available literature on the printing of metal non-assembly joints with SLM is limited. The troublesome removal of support structures, especially within the joint's clearance, poses an additional burden in this effort.

New designs of joints are therefore necessary, to ease the direct fabrication of metal joints with SLM. This research, proposes new designs, by implementing a combination of both systematic and intuitive design approaches. This indeed led to new designs, that were subsequently modified, considering their design constraints. Each design was separately studied, and its potential printability assessed. In this regard, new proposed designs replaced the original ones, which were printed with success. After that, multi-joint mechanisms were printed with success. All of them presented no supports within the clearance and sufficient motion. The interesting part is, that even the ball-socket joints, which seemed impossible to be printed with SLM, were manufactured with the least amount of supports. Additionally, the clearance used in these joints was the smallest ever reported. This is important if one considers that relevant studies, using polymer-based techniques, printed them with bigger clearance.

The successful printing of metal mechanisms, has proven that design plays the most crucial role in their direct fabrication. Despite the fact that supports can be reduced with the right orientation or alteration of the process parameters, it is favourable, though challenging, to modify the design of the parts according to the general rule to avoid excess support structures.

Furthermore, motion evaluation took place to assess the proposed designs. To do that, the new structures were positioned on an acetabular surface and surface morphing experiments evaluated their fitting. For this reason, two novel methods were developed, to obtain quantitative results. It was proven, that most of the proposed Meta-Biomechanisms fit well within the acetabular surface, with an absolute difference below one.

Since these structures intend to behave like highly deformable implants, their indicative mechanical properties were derived. Thus, uni-axial compression testing, evaluated how they mechanically behave under compression load. For this reason, they were positioned on an acetabulum, where a ball, inherited the role of the femoral head, was compressing them. Unfortunately, due to the shape and size differences, these structures cannot be compared. However, the force needed to break them, in a specific configuration, could be derived. This may constitute an indication, of how they can be modified, to achieve appropriate mechanical properties. By adjusting the strut thickness or the joint's size, their mechanical properties can be tuned properly. Additionally, the only area affected, was beneath

the femoral head, leaving the rest of the structure intact. Only one structure was entirely broken, since its restricted mobility, induced a gap between the structure and the acetabulum′s surface.. That proves the important role of the mechanism's fitting in mechanical behaviour.

This research project demonstrated that direct fabrication of non-assembly meta-biomechanisms is feasible, but after a logical planning. In this regard, the design plays the most crucial role. Creativity seems to be the difficult part of that. However, implementation of systematic steps come to assist this path, since innovative concept designs were the outcome. The fitting ability of them seems to be the most important factor, influencing both their tissue regeneration and the mechanical response. This study though, constitutes the starting point towards the fabrication of highly deformable implants, with appropriate biological nano-properties. Although proposed meta-biomechanisms were printed, followed by the ability to fit irregular spaces, there are several steps to be followed. The undoubtable potential of Meta-Biomechanisms as a solution to cavitary bone defects, needs to be further explored in the future.

Bibliography

[1] Kucera, T., Urban, K., Ragkou, S. (2011). Healing of cavitary bone defects. European Journal of Orthopaedic Surgery Traumatology, 22(2), 123-128. doi:10.1007/s00590-011-0831-9

[2] Cooper, G. M., Mooney, M. P., Gosain, A. K., Campbell, P. G., Losee, J. E., Huard, J. (2010). Testing the Critical Size in Calvarial Bone Defects: Revisiting the Concept of a Critical-Size Defect. Plastic and Reconstructive Surgery, 125(6), 1685-1692. doi:10.1097/prs.0b013e3181cb63a3

[3] Allison, D. C., Mcintyre, J. A., Ferro, A., Brien, E., Menendez, L. R. (2013). Bone grafting alternatives for cavitary defects in children. Current Orthopaedic Practice, 24(3), 267-279. doi:10.1097/bco.0b013e3182910f94

[4] Kheirallah, M., Almeshaly, H. (2016). Present Strategies for Critical Bone Defects Regeneration. Oral Health Case Reports, 02(03). doi:10.4172/2471-8726.1000127

[5] Song, B., Dong, S., Zhang, B., Liao, H., Coddet, C. (2012). Effects of processing parameters on microstructure and mechanical property of selective laser melted Ti6Al4V. Materials Design, 35, 120-125. doi:10.1016/j.matdes.2011.09.051

[6] Bandyopadhyay, A., Espana, F., Balla, V. K., Bose, S., Ohgami, Y., Davies, N. M. (2010). Influence of porosity on mechanical properties and in vivo response of Ti6Al4V implants. Acta Biomaterialia, 6(4), 1640-1648. doi:10.1016/j.actbio.2009.11.011

[7] Vandenbroucke, B., Kruth, J. (2007). Selective laser melting of biocompatible metals for rapid manufacturing of medical parts. Rapid Prototyping Journal, 13(4), 196-203. doi:10.1108/13552540710776142

[8] Dilip, J. J., Zhang, S., Teng, C., Zeng, K., Robinson, C., Pal, D., Stucker, B. (2017). Influence of processing parameters on the evolution of melt pool, porosity, and microstructures in Ti-6Al-4V alloy parts fabricated by selective laser melting. Progress in Additive Manufacturing, 2(3), 157-167. doi:10.1007/s40964-017-0030-2

[9] Kolken, H. A., Zadpoor, A. A. (2017). Auxetic mechanical metamaterials. RSC Advances, 7(9), 5111-5129. doi:10.1039/c6ra27333e

[10] Kolken, H. M., Janbaz, S., Leeflang, S. M., Lietaert, K., Weinans, H. H., Zadpoor, A. A. (2018). Rationally designed meta-implants: a combination of auxetic and conventional meta-biomaterials. Materials Horizons, 5(1), 28-35. doi:10.1039/c7mh00699c

[11] Rajagopalan, S., Cutkosky, M. (2003). Error Analysis for the In-Situ Fabrication of Mechanisms. Journal of Mechanical Design, 125(4), 809. doi:10.1115/1.1631577

[12] Chua, C. K., and Fai, L. K., 1997, Rapid Prototyping: Principles and Applications in Manufacturing, Wiley, New York, NY

[13] Murr, L., Quinones, S., Gaytan, S., Lopez, M., Rodela, A., Martinez, E., . . . Wicker, R. (2009). Microstructure and mechanical behavior of Tia6Ala4V produced by rapid-layer manufacturing, for biomedical applications. Journal of the Mechanical Behavior of Biomedical Materials, 2(1), 20-32. doi:10.1016/j.jmbbm.2008.05.004

[14] Leutenecker-Twelsiek, B., Klahn, C., Meboldt, M. (2016). Considering Part Orientation in Design for Additive Manufacturing. Procedia CIRP, 50, 408-413. doi:10.1016/j.procir.2016.05.016

[15] Ashley,S.,(1991) .Rapid Prototyping Systems. Mechanical Engineering, pp. 36-43.

[16] Su, X., Yang, Y., Xiao, D., Chen, Y. (2012). Processability investigatation of non-assembly mechanisms for powder bed fusion process. The International Journal of Advanced Manufacturing Technology, 64(5-8), 1193-1200. doi:10.1007/s00170-012-4079-2

[17] Luthria, K. (2016) Clearance analysis of 3D printed assemblies using fused filament extrusion (Unpublished doctoral dissertation).

[18] Di, W., Yongqiang, Y., Xubin, S., Yonghua, C. (2011). Study on energy input and its influences on single-track,multi-track, and multi layer in SLM. The International Journal of Advanced Manufacturing Technology, 58(9-12), 1189-1199. doi:10.1007/s00170-011-3443-y

[19] Won, J., DeLaurentis, K., and Mavroidis, C., aaRapid Prototyping of Robotic Systems,aa Proceedings of the 2000 IEEE International Conference on Robotics and Automation, April 24a28 2000, San Francisco, CA, pp. 3077a3082.

[20] Calignano, F., Manfredi, D., Ambrosio, E., Biamino, S., Pavese, M., Fino, P. (2014). Direct Fabrication of Joints based on Direct Metal Laser Sintering in Aluminum and Titanium Alloys. Procedia CIRP, 21, 129-132. doi:10.1016/j.procir.2014.03.155

[21] Su, X., Yang, Y., Wang, D., Chen, Y. (2013). Digital assembly and direct fabrication of mechanism based on selective laser melting. Rapid Prototyping Journal, 19(3), 166-172. doi:10.1108/13552541311312157

[22] Laurentis, K. J., Mavroidis, C. (2004). Rapid fabrication of a non-assembly robotic hand with embedded components. Assembly Automation, 24(4), 394-405. doi:10.1108/01445150410562606

[23] Chen, Y., Zhezheng, C. (2011). Joint analysis in rapid fabrication of non-assembly mechanisms. Rapid Prototyping Journal, 17(6), 408- 417. doi:10.1108/13552541111184134

[24] Kruth, J. (2004). Selective laser melting of iron-based powder. Journal of Materials Processing Technology. doi:10.1016/s0924- 0136(04)00220-1

[25] J.P. Kruth, J. Vandenbroucke, J. Van Vaerenbergh, P. Mercelis. Benchmarking of different SLS/SLM processes as rapid manufacturing techniques. Int. Conf. Polymers Moulds Innovations (PMI), Gent, Belgium, 2005.

[26] Yadroitsev, I. , Pavlov, M.,Bertrand, P.,Smurov, I.(2009) Mechanical properties of samples fabricated by selective laser melting, 14Asmes Assises EuropA c ennes du Prototypages Fabrication Rapide, Paris.

[27] Abe, F., Osakada, K., Shiomi, M., Uematsu, K., Matsumoto, M. (2001). The manufacturing of hard tools from metallic powders by selective laser melting. Journal of Materials Processing Technology, 111(1-3), 210-213. doi:10.1016/s0924-0136(01)00522-2

[28] Hao, L., Dadbakhsh, S., Seaman, O., Felstead, M. (2009). Selective laser melting of a stainless steel and hydroxyapatite composite for load-bearing implant development. Journal of Materials Processing Technology, 209(17), 5793-5801.doi:10.1016/j.jmatprotec.2009.06.012

[29] Calignano, F. (2014). Design optimization of supports for overhanging structures in aluminum and titanium alloys by selective laser melting. Materials Design, 64, 203-213. doi:10.1016/j.matdes.2014.07.043

[30] Yadroitsava, I., Grewar, S., Hattingh, D., Yadroitsev, I. (2015). Residual Stress in SLM Ti6Al4V Alloy Specimens. Materials Science Forum, 828-829, 305-310. doi:10.4028/www.scientific.net/msf.828-829.305

[31] Yadroitsev, I., Thivillon, L., Bertrand, P., Smurov, I. (2007). Strategy of manufacturing components with designed internal structure by selective laser melting of metallic powder. Applied Surface Science, 254(4), 980-983. doi:10.1016/j.apsusc.2007.08.046

[32] Su, X., Yang, Y., Xiao, D., Luo, Z. (2012). An investigation into direct fabrication of fine-structured components by selective laser melting. The International Journal of Advanced Manufacturing Technology, 64(9-12), 1231-1238. doi:10.1007/s00170-012-4081-8

[33] Thijs, L., Verhaeghe, F., Craeghs, T., Humbeeck, J. V., Kruth, J. (2010). A study of the microstructural evolution during selective laser melting of Tia6Ala4V. Acta Materialia, 58(9), 3303-3312. doi:10.1016/j.actamat.2010.02.004

[34] Liu, Y., Zhang, J., Yang, Y., Li, J., Chen, J. (2017).Study on the influence of process parameters on the clearance feature in non-assembly mechanism manufactured by selective laser melting. Journal of Manufacturing Processes, 27, 98-107. doi:10.1016/j.jmapro.2017.04.005

[35] Yang, Y., Su, X., Wang, D., Chen, Y. (2011). Rapid fabrication of metallic mechanism joints by selective laser melting. Proceedings of the Institution of Mechanical Engineers, Part B: Journal of Engineering Manufacture, 225(12), 2249-2256. doi:10.1177/0954405411407997

[36] Fu, C. H., Guo, Y. B. (2014). 3-DIMENSIONAL FINITE ELEMENT MODELING OF SELECTIVE LASER MELTING TI-6AL- 4V ALLOY. 25th Annual International Solid Freeform Fabrication Symposium

[37] Leary, M. (2017). Surface roughness optimization for selective laser melting (SLM). Laser Additive Manufacturing, 99-118. doi:10.1016/b978-0-08-100433-3.00004-x

[38] Yadroitsev, I., Gusarov, A., Yadroitsava, I., Smurov, I. (2010). Single track formation in selective laser melting of metal powders. Journal of Materials Processing Technology, 210(12), 1624-1631. doi:10.1016/j.jmatprotec.2010.05.010

[39] Kruth JP, Mercelis P, Van Vaerenbergh J, Craeghs T, Bartolo PJ, et al. Feedback Control Select Laser Melt 2008:521a7.

[40] Agarwala,M.,Bourell,D.,Beaman,J.,Marcus, H.,Barlow,J.(1995) Direct selective laser

[41] Zaeh, M. F., Branner, G. (2009). Investigations on residual stresses and deformations in selective laser melting. Production Engineering, 4(1), 35-45. doi:10.1007/s11740-009-0192-y

[42] Karapatis,N.P. (2001) A sub-process approach of selective laser sintering, Ph.D. Thesis, Ecole Polytechnique Federal de Lausanne

[43] Flores, P., Lankarani, H. M. (2011). Dynamic Response of Multibody Systems With Multiple Clearance Joints. Volume 4: 8th International Conference on Multibody Systems, Nonlinear Dynamics, and Control, Parts A and B. doi:10.1115/detc2011-47224

[44] Megahed, S., Haroun, A. (2012). Analysis of the Dynamic Behavioral Performance of Mechanical Systems With MultiaClearance Joints. Journal of Computational and Nonlinear Dynamics, 7(1), 011002. doi:10.1115/1.4004263

[45] Chen, Y. H., Chen, Z. Z. (2010). Major Factors in Rapid Prototyping of Mechanisms. Key Engineering Materials, 443, 516-521. doi:10.4028/www.scientific.net/kem.443.516

[46] Frank, D., Fadel, G. (1995). Expert system-based selection of the preferred direction of build for rapid prototyping processes. Journal of Intelligent Manufacturing, 6(5), 339-345. doi:10.1007/bf00124677

[47] Alexander, P., Allen, S., Dutta, D. (1998). Part orientation and build cost determination in layered manufacturing. Computer-Aided Design, 30(5), 343-356. doi:10.1016/s0010-4485(97)00083-3

[48] Vaithilingam, J., Goodridge, R. D., Hague, R. J., Christie, S. D., Edmondson, S. (2016). The effect of laser remelting on the surface chemistry of Ti6al4V components fabricated by selective laser melting. Journal of Materials Processing Technology, 232, 1-8. doi:10.1016/j.jmatprotec.2016.01.022

[49] Orthoload-Loading of Orthopaedic Implants (n.d.) Retrieved from https://orthoload.com/test-loads/standard-loads-hip-joint/

[50] Breedveld, P., Herder, J. L., Tomiyama, T., 2. (2011). proceedings of IASDR: Diversity and Unity. Delft, The Netherlands: TUDelft.

[51] Osborn, A.F (1953) Applied Imagination- Principles and Procedures of Creative Thinking. Scribner, New York. ISBN:0684162563

[52] Gummer, A., Sauer, B. (2012). Influence of Contact Geometry on Local Friction Energy and Stiffness of Revolute Joints. Journal of Tribology, 134(2), 021402. doi:10.1115/1.4006248

[53] Mavroidis, C., Delaurentis, K. J., Won, J., Alam, M. (2001). Fabrication of Non-Assembly Mechanisms and Robotic Systems Using Rapid Prototyping. Journal of Mechanical Design, 123(4), 516. doi:10.1115/1.1415034

[54] Mechanics of Materials: Bending Normal Stress Mechanics of Slender Structures — Boston University. (n.d.). Retrieved from https://www.bu.edu/moss/mechanics-of-materials-bending-normal-stress

[55] Won,J.,Delaurentis,K., Mavroidis,C.(2000). Rapid Prototyping of Robotics Systems, in proceedings of the 2000 IEEE International Conference on Robotics Automation, San Fransicco, CA,pp.3077a3082.

[56] Cali, J., Calian, D. A., Amati, C., Kleinberger, R., Steed, A., Kautz, J., Weyrich, T. (2012). 3D-printing of non-assembly, articulated models. ACM Transactions on Graphics, 31(6), 1. doi:10.1145/2366145.2366149

[57] Li, Y., Chen, Y. (2017). Physical Rigging for Physical Models and Posable Joint Designs Based on Additive Manufacturing Technology. Procedia Manufacturing, 11, 2235-2242. doi:10.1016/j.promfg.2017.07.371

[58] Scuderi, G. R., Tria, A. J. (2006). Knee arthroplasty handbook techniques in total knee and revision arthroplasty. New York, NY: Springer.

[59] Nieminen, J., Pakarinen, T., Laitinen, M. (2013). Orthopaedic Reconstruction of Complex Pelvic Bone Defects. Evaluation of Various Treatment Methods. Scandinavian Journal of Surgery, 102(1), 36-41. doi:10.1177/145749691310200108

[60] Your 3D content on web, mobile, AR, and VR. (n.d.). Retrieved from https://sketchfab.com/?utm-campaign=brandutm-medium=cpcutm-source=adwordsgclid=CjwKCAiAz7TfBRAKEiwAz8fKOPEG9dsC69BBQ9y4ySOPfPy1Ec-7sOcMMahqRMt66u-kghMzsWU4OhoCmwMQAvD-BwE

[61] MeshLab. (n.d.). Retrieved from http://www.meshlab.net/

[62] Rhino 6 for Windows. (n.d.). Retrieved from https://www.rhino3d.com/

[63] Rombouts, M., Kruth, J., Froyen, L., Mercelis, P. (2006). Fundamentals of Selective Laser Melting of alloyed steel powders. CIRP Annals, 55(1), 187-192. doi:10.1016/s0007-8506(07)60395-3

[64] Zhang, L., Attar, H. (2015). Selective Laser Melting of Titanium Alloys and Titanium Matrix Composites for Biomedical Applications: A Reviewa. Advanced Engineering Materials, 18(4), 463-475. doi:10.1002/adem.201500419

[65] Santos, E. C., Osakada, K., Shiomi, M., Kitamura, Y., Abe, F. (2004). Microstructure and mechanical properties of pure titanium models fabricated by selective laser melting. Proceedings of the Institution of Mechanical Engineers, Part C: Journal of Mechanical Engineering Science, 218(7), 711-719. doi:10.1243/0954406041319545

[66] Gibson, I., Rosen, D. W., Stucker, B. (2016). Additive manufacturing technologies: 3D printing, rapid prototyping, and direct digital manufacturing. New York: Springer.

[67] Dizon, J. R., Espera, A. H., Chen, Q., Advincula, R. C. (2018). Mechanical characterization of 3D-printed polymers. Additive Manufacturing, 20, 44-67. doi:10.1016/j.addma.2017.12.002

[68] THINK OUT OF THE BOX! (n.d.). Retrieved from https://www.scaninabox.com/index.php

[69] (n.d.). Retrieved from https://www.danielgm.net/cc/

[70] Popovi, Z. B., Thomas, J. D. (2017). Assessing observer variability: A users guide. Cardiovascular Diagnosis and Therapy, 7(3), 317-324. doi:10.21037/cdt.2017.03.12

[71] Chen, Y., Lu, J. (2011). Minimize joint clearance in rapid fabrication of non-assembly mechanisms. International Journal of Computer Integrated Manufacturing, 24(8), 726-734. doi:10.1080/0951192x.2011.592995

[72] Break Strength Testing. (n.d.). Retrieved from https://www.ametektest.com/learningzone/testtypes/break-strength-testing

[73] Alam, M., Mavroidis, C., Langrana, N., & Bidaud, P.(1999). Mechanism Design using Rapid Prototyping. Proceedings of the 10th World Congress on the Theory of machines and mechanisms, Oulu, Finland

[74] Wang, X., Xu, S., Zhou, S., Xu, W., Leary, M., Choong, P., Xie, Y. M. (2016). Topological design and additive manufacturing of porous metals for bone scaffolds and orthopaedic implants: A review. Biomaterials, 83, 127-141. doi:10.1016/j.biomaterials.2016.01.012

Previous Successful Attempts in Rapid Fabrication of Joints

Table A.1: **Successfully printed non-assembly parts**

Author	Year	Reference Number	Type of joint or mechanism	Method	Material	Clearance size(mm)	Orientation angle (degrees)
Alam	1999	[73]	Revolute, spherical, joint	SLA	SL 5170 resin	0.5, 0.5, 0.3	90º for all, no information for the revolute
Won	2000	[53], [55]	Universal, spherical	SLS	Polyamide	0.5, 0.5	90º for all
Won	2000	[55]	Robotic Finger	SLS	Polyamide	-	-
Mavroidis	2001	[53]	Three-legged parallel manipulator, 5-DOF hand	SLA	SL 5170 resin	-	-
Mavroidis	2001	[53]	4-DOF finger	SLS	Polyamide	-	-
Yang	2010	[35]	Universal joint	SLM	stainless steel	0.2	90º
Chen	2011	[71]	Universal joint	SLM	stainless steel	0.3	-
Chen	2011	[71]	Universal joint	Objet Eden 350V	Fullcure 720	0.1	-
Chen	2011	[71]	crank-slider mechanism	Objet Eden 350V	Fullcure 721	no information	-
Chen	2011	[71]	artificial knee joint	Objet Eden 350V	Fullcure 722	no information	
Su	2011	[16]	slider-rocker mechanism	SLM	316L stainless steel	0.2	Tilted orientation
Cali	2012	[56]	Arm and hand articulated models	SLS, SLA	-	-	-
Su	2013	[21]	crank-rocker mechanism, universal joint	SLM	316L stainless steel	0.2	Tilted orientation of 45º
Calignano	2014	[20]	a simple drum-shaped pin joint	DSLS	titanium alloy		90º
Calignano	2014	[29]	gear train	DSLS	aluminum alloy	0.08	90º
Luthria	2016	[17]	hexagonal pin-hole	FDM	ABS plastic	-	0º, 30º, 60º and 90º
Liu	2017	[34]	collapsible abacus	SLM	316L stainless steel	-	Tilted orientation of 45º
Li	2017	[57]	humanoid model with ball-socket joints	EOS Formiga P110, Objet EDEN 351	Nylon PA 2200 , Veroclear RGD810	0.1, 0.2	-

Detailed Dimensions of Designs

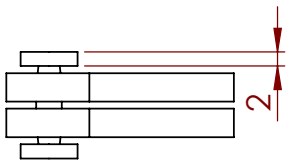

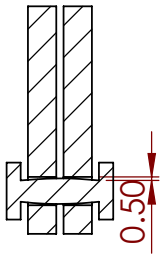

SECTION A-A
SCALE 1 : 1

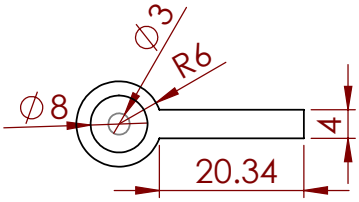

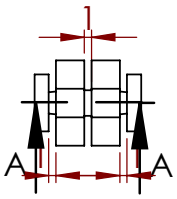

UNLESS OTHERWISE SPECIFIED: DIMENSIONS ARE IN MILLIMETERS SURFACE FINISH: TOLERANCES: LINEAR: ANGULAR:	FINISH:	DEBURR AND BREAK SHARP EDGES	DO NOT SCALE DRAWING / REVISION

	NAME	SIGNATURE	DATE
DRAWN			
CHK'D			
APPV'D			
MFG			
Q.A			

TITLE: Revolute Joint

MATERIAL:

DWG NO. 1

A4

WEIGHT:

SCALE:2:1

SHEET 1 OF 1

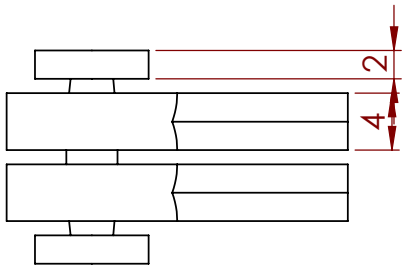

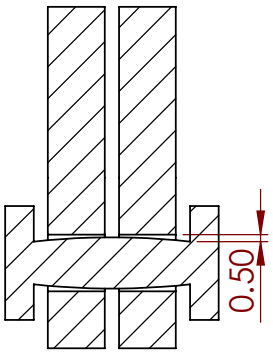

SECTION A-A

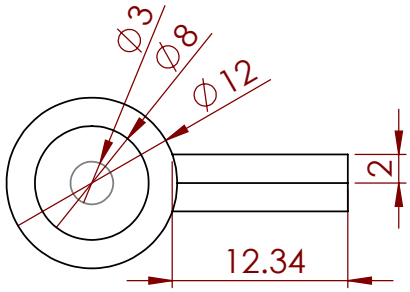

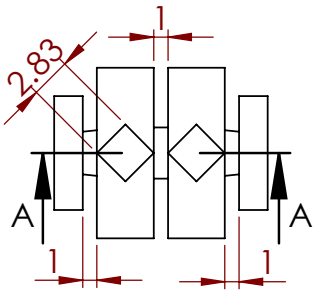

UNLESS OTHERWISE SPECIFIED: DIMENSIONS ARE IN MILLIMETERS SURFACE FINISH: TOLERANCES: LINEAR: ANGULAR:	FINISH:		DEBURR AND BREAK SHARP EDGES	DO NOT SCALE DRAWING	REVISION	
	NAME	SIGNATURE	DATE	TITLE:		
DRAWN				Modified Revolute		
CHK'D						
APPV'D						
MFG						
Q.A				MATERIAL:	DWG NO. 2	A4
				WEIGHT:	SCALE:2:1	SHEET 1 OF 1

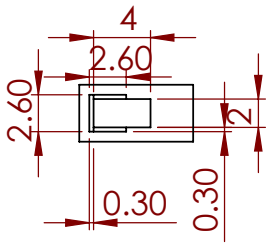

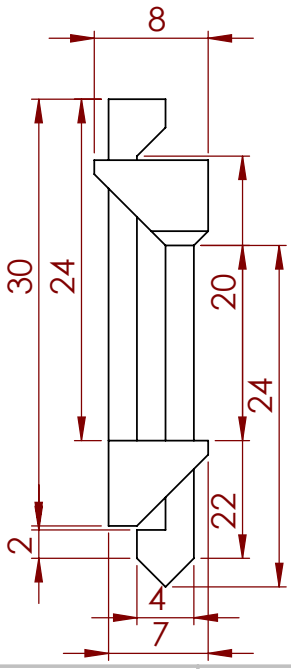

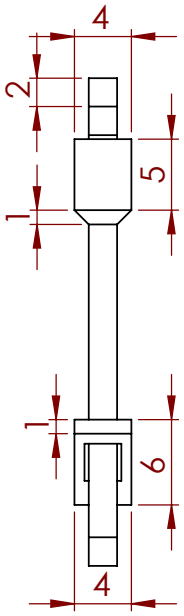

UNLESS OTHERWISE SPECIFIED: DIMENSIONS ARE IN MILLIMETERS SURFACE FINISH: TOLERANCES: LINEAR: ANGULAR:	FINISH:	DEBURR AND BREAK SHARP EDGES	DO NOT SCALE DRAWING / REVISION

	NAME	SIGNATURE	DATE
DRAWN			
CHK'D			
APPV'D			
MFG			
Q.A			

TITLE:

Prismatic_Assembly

MATERIAL:

DWG NO. 3

A4

WEIGHT:

SCALE:2:1

SHEET 1 OF 1

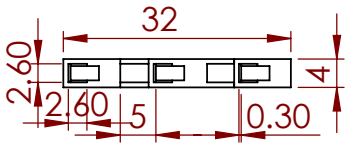

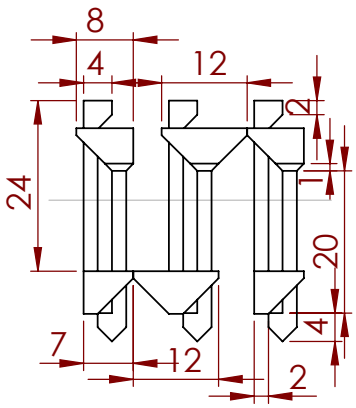

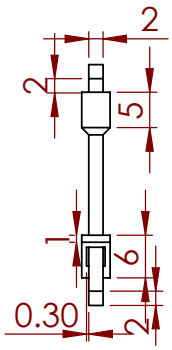

UNLESS OTHERWISE SPECIFIED: DIMENSIONS ARE IN MILLIMETERS SURFACE FINISH: TOLERANCES: LINEAR: ANGULAR:	FINISH:	DEBURR AND BREAK SHARP EDGES	DO NOT SCALE DRAWING / REVISION

	NAME	SIGNATURE	DATE
DRAWN			
CHK'D			
APPV'D			
MFG			
Q.A			

TITLE: Prismatic_Connectors

MATERIAL:

DWG NO. 4

A4

WEIGHT:

SCALE:2:1

SHEET 1 OF 1

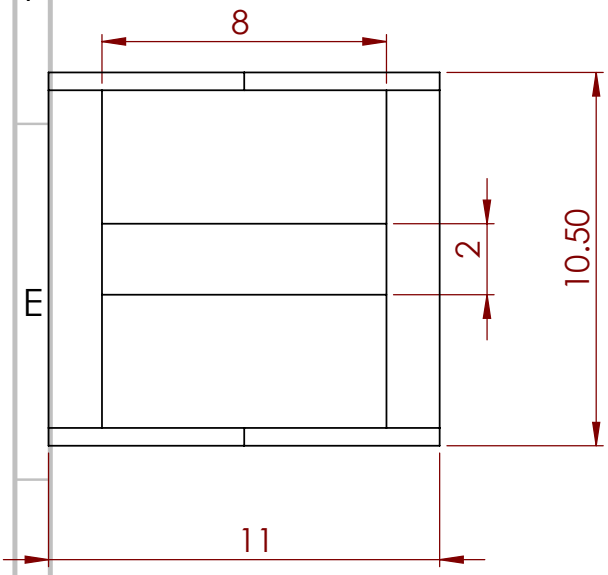

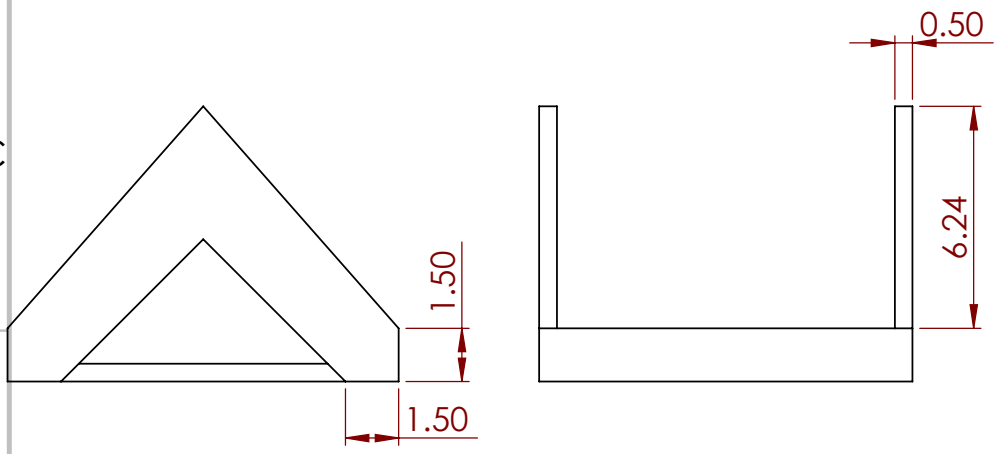

UNLESS OTHERWISE SPECIFIED: DIMENSIONS ARE IN MILLIMETERS SURFACE FINISH: TOLERANCES: LINEAR: ANGULAR:	FINISH:	DEBURR AND BREAK SHARP EDGES	DO NOT SCALE DRAWING / REVISION

	NAME	SIGNATURE	DATE
DRAWN			
CHK'D			
APPV'D			
MFG			
Q.A			

TITLE: Horizontal_"Prismatic"

MATERIAL:

DWG NO. 5

A4

WEIGHT:

SCALE:5:1

SHEET 1 OF 1

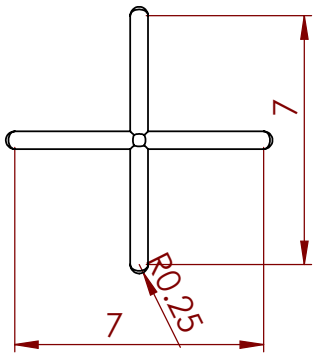

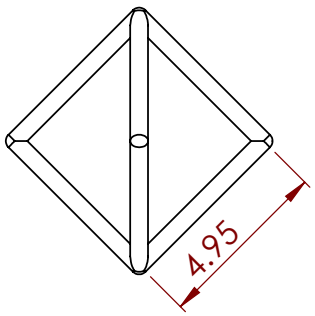

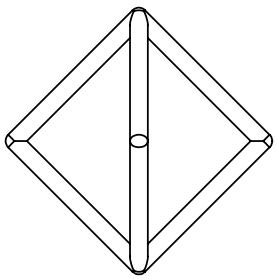

UNLESS OTHERWISE SPECIFIED: DIMENSIONS ARE IN MILLIMETERS SURFACE FINISH: TOLERANCES: LINEAR: ANGULAR:	FINISH:	DEBURR AND BREAK SHARP EDGES	DO NOT SCALE DRAWING / REVISION

	NAME	SIGNATURE	DATE
DRAWN			
CHK'D			
APPV'D			
MFG			
Q.A			

TITLE: rombus_unit_cell

MATERIAL:

DWG NO. 6

A4

WEIGHT:

SCALE:5:1

SHEET 1 OF 1

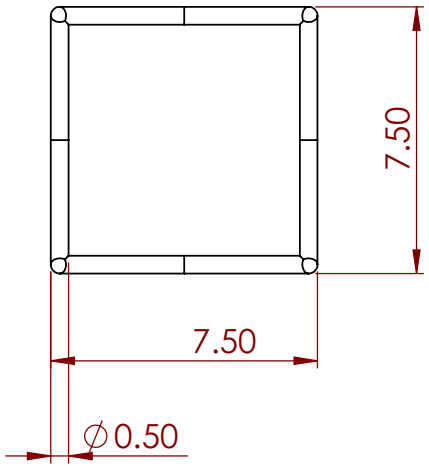

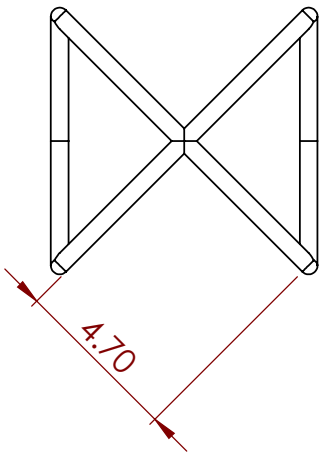

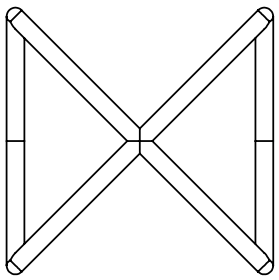

UNLESS OTHERWISE SPECIFIED: DIMENSIONS ARE IN MILLIMETERS SURFACE FINISH: TOLERANCES: LINEAR: ANGULAR:	FINISH:	DEBURR AND BREAK SHARP EDGES	DO NOT SCALE DRAWING / REVISION

	NAME	SIGNATURE	DATE
DRAWN			
CHK'D			
APPV'D			
MFG			
Q.A			

TITLE: Fccz_Connector

MATERIAL:

DWG NO. 7

A4

WEIGHT:

SCALE:5:1

SHEET 1 OF 1

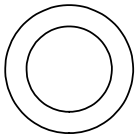

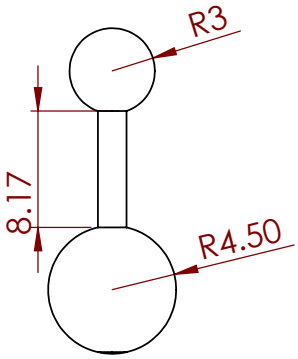

UNLESS OTHERWISE SPECIFIED: DIMENSIONS ARE IN MILLIMETERS SURFACE FINISH: TOLERANCES: LINEAR: ANGULAR:	FINISH:	DEBURR AND BREAK SHARP EDGES	DO NOT SCALE DRAWING / REVISION

	NAME	SIGNATURE	DATE
DRAWN			
CHK'D			
APPV'D			
MFG			
Q.A			

TITLE:

ball_official

MATERIAL:

DWG NO.

8

A4

WEIGHT:

SCALE:5:1

SHEET 1 OF 1

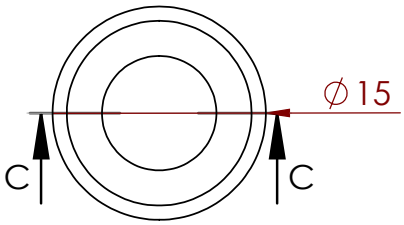

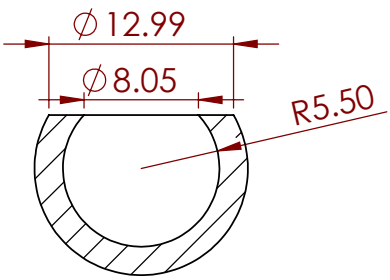

SECTION C-C

UNLESS OTHERWISE SPECIFIED: DIMENSIONS ARE IN MILLIMETERS SURFACE FINISH: TOLERANCES: LINEAR: ANGULAR:	FINISH:	DEBURR AND BREAK SHARP EDGES	DO NOT SCALE DRAWING / REVISION

	NAME	SIGNATURE	DATE
DRAWN			
CHK'D			
APPV'D			
MFG			
Q.A			

TITLE: socket_official

MATERIAL:

DWG NO. 9

A4

WEIGHT:

SCALE:2:1

SHEET 1 OF 1

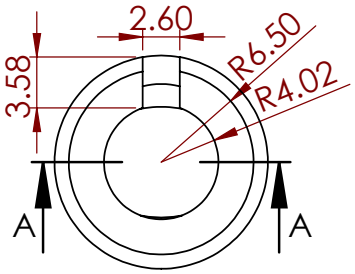

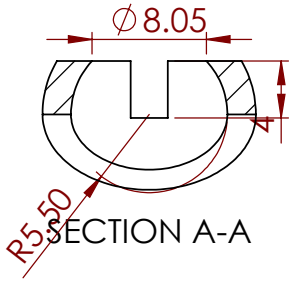

SECTION A-A

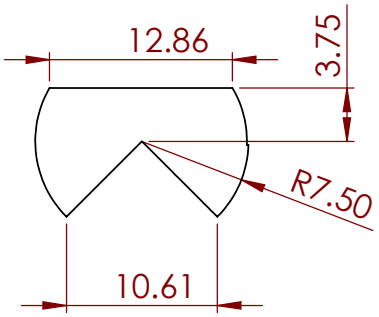

UNLESS OTHERWISE SPECIFIED: DIMENSIONS ARE IN MILLIMETERS SURFACE FINISH: TOLERANCES: LINEAR: ANGULAR:	FINISH:	DEBURR AND BREAK SHARP EDGES	DO NOT SCALE DRAWING / REVISION

	NAME	SIGNATURE	DATE
DRAWN			
CHK'D			
APPV'D			
MFG			
Q.A			

TITLE:

Socket's Openings

MATERIAL:

DWG NO. 10

A4

WEIGHT:

SCALE:2:1

SHEET 1 OF 1

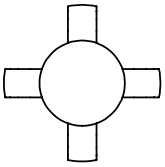

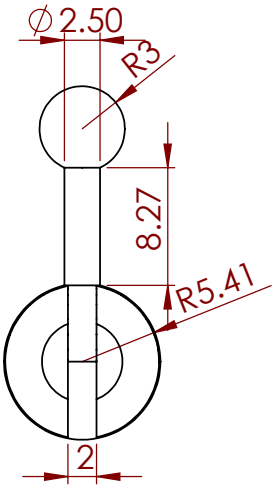

UNLESS OTHERWISE SPECIFIED: DIMENSIONS ARE IN MILLIMETERS SURFACE FINISH: TOLERANCES: LINEAR: ANGULAR:	FINISH:	DEBURR AND BREAK SHARP EDGES	DO NOT SCALE DRAWING / REVISION

	NAME	SIGNATURE	DATE
DRAWN			
CHK'D			
APPV'D			
MFG			
Q.A			

TITLE:

Ball with Cavities

MATERIAL:

DWG NO. 11

A4

WEIGHT:

SCALE:2:1

SHEET 1 OF 1

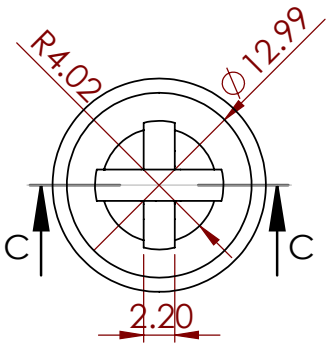

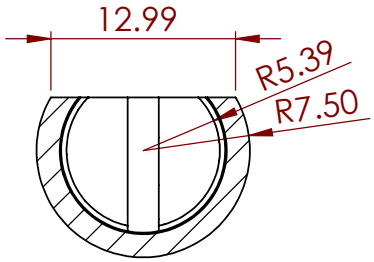

SECTION C-C

UNLESS OTHERWISE SPECIFIED: DIMENSIONS ARE IN MILLIMETERS SURFACE FINISH: TOLERANCES: LINEAR: ANGULAR:		FINISH:		DEBURR AND BREAK SHARP EDGES		DO NOT SCALE DRAWING	REVISION
	NAME	SIGNATURE	DATE			TITLE:	
DRAWN						Socket with Cavities	
CHK'D							
APPV'D							
MFG							
Q.A				MATERIAL:		DWG NO. 12	A4
				WEIGHT:		SCALE:2:1	SHEET 1 OF 1

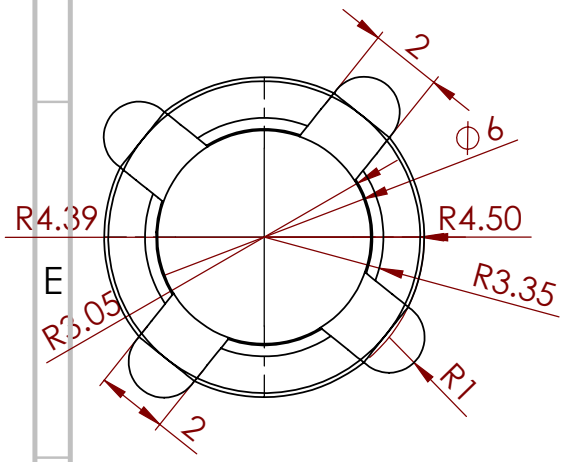

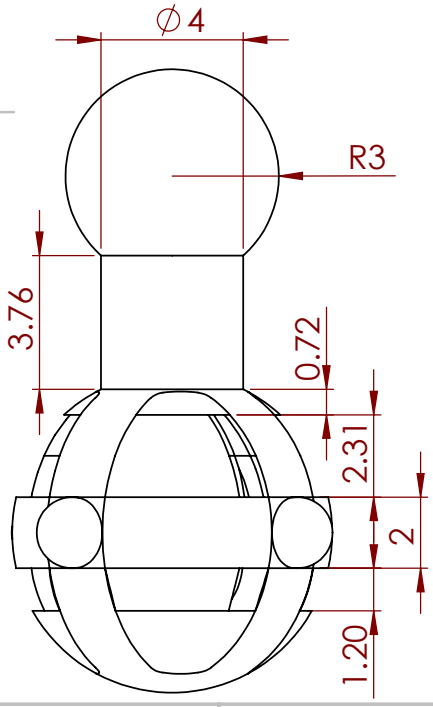

UNLESS OTHERWISE SPECIFIED: DIMENSIONS ARE IN MILLIMETERS SURFACE FINISH: TOLERANCES: LINEAR: ANGULAR:	FINISH:	DEBURR AND BREAK SHARP EDGES	DO NOT SCALE DRAWING / REVISION

	NAME	SIGNATURE	DATE
DRAWN			
CHK'D			
APPV'D			
MFG			
Q.A			

TITLE:

Modified Ball with Lattice Structure

MATERIAL:

DWG NO. 13

A4

WEIGHT:

SCALE:5:1

SHEET 1 OF 1

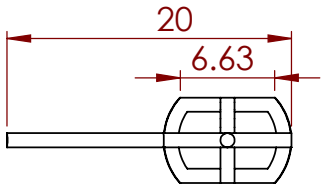

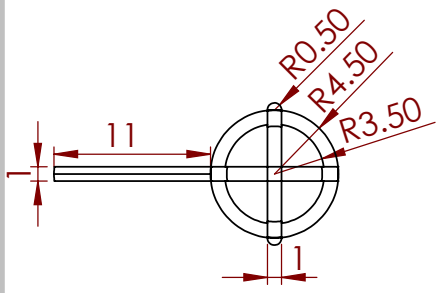

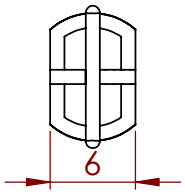

UNLESS OTHERWISE SPECIFIED: DIMENSIONS ARE IN MILLIMETERS SURFACE FINISH: TOLERANCES: LINEAR: ANGULAR:	FINISH:	DEBURR AND BREAK SHARP EDGES	DO NOT SCALE DRAWING / REVISION

	NAME	SIGNATURE	DATE
DRAWN			
CHK'D			
APPV'D			
MFG			
Q.A			

TITLE:

Cut Ball with Cavities

MATERIAL:

DWG NO. 14

A4

WEIGHT:

SCALE:2:1

SHEET 1 OF 1

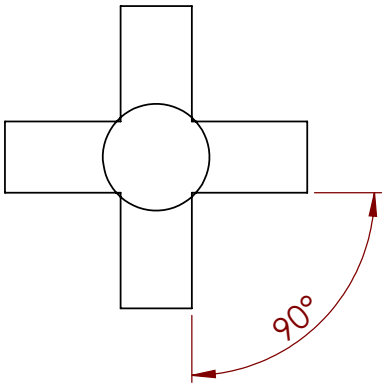

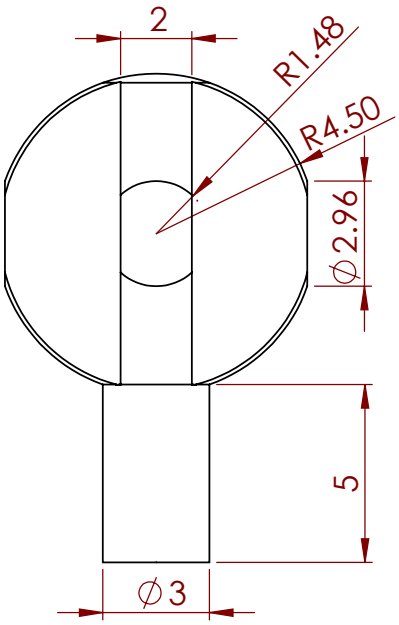

UNLESS OTHERWISE SPECIFIED: DIMENSIONS ARE IN MILLIMETERS SURFACE FINISH: TOLERANCES: LINEAR: ANGULAR:	FINISH:	DEBURR AND BREAK SHARP EDGES	DO NOT SCALE DRAWING / REVISION

	NAME	SIGNATURE	DATE
DRAWN			
CHK'D			
APPV'D			
MFG			
Q.A			

TITLE: Proposed Ball

MATERIAL:

DWG NO. 15

A4

WEIGHT:

SCALE:5:1

SHEET 1 OF 1

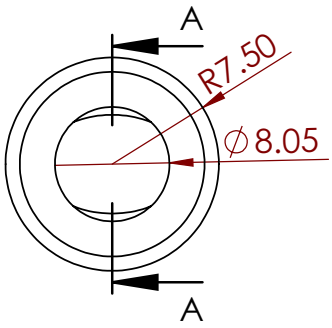

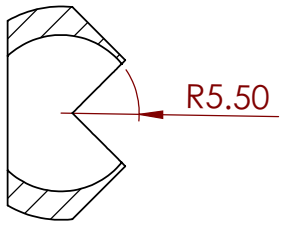

SECTION A-A

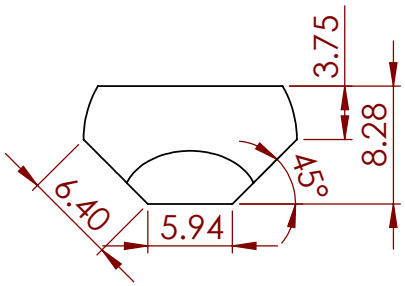

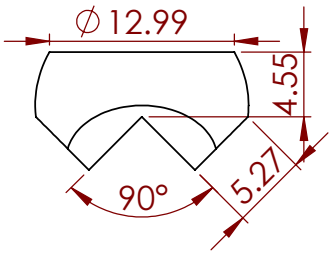

UNLESS OTHERWISE SPECIFIED: DIMENSIONS ARE IN MILLIMETERS SURFACE FINISH: TOLERANCES: LINEAR: ANGULAR:	FINISH:	DEBURR AND BREAK SHARP EDGES	DO NOT SCALE DRAWING / REVISION

	NAME	SIGNATURE	DATE
DRAWN			
CHK'D			
APPV'D			
MFG			
Q.A			

TITLE: Proposed Socket

MATERIAL:

DWG NO. 16

A4

WEIGHT:

SCALE:2:1

SHEET 1 OF 1

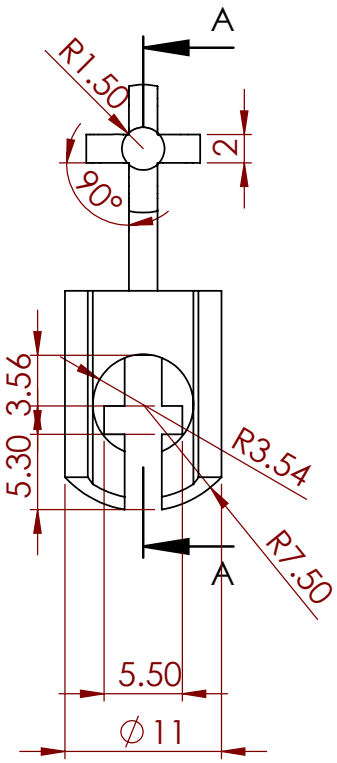

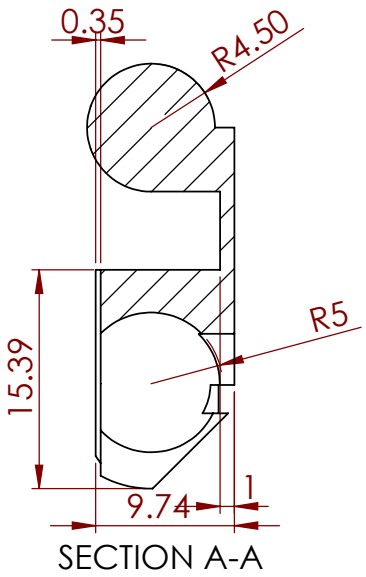

SECTION A-A

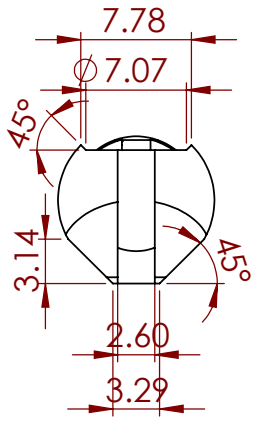

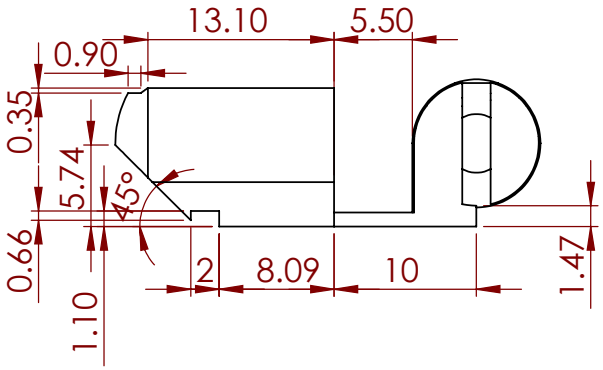

UNLESS OTHERWISE SPECIFIED: DIMENSIONS ARE IN MILLIMETERS SURFACE FINISH: TOLERANCES: LINEAR: ANGULAR:	FINISH:	DEBURR AND BREAK SHARP EDGES	DO NOT SCALE DRAWING / REVISION

	NAME	SIGNATURE	DATE
DRAWN			
CHK'D			
APPV'D			
MFG			
Q.A			

TITLE:

Caterpillar Chain

MATERIAL:	DWG NO. 17	A4
WEIGHT:	SCALE:2:1	SHEET 1 OF 1